POLITECNICO

MILANO 1863

SCUOLA DI INGEGNERIA INDUSTRIALE
E DELL'INFORMAZIONE

Data-Driven Modeling of the Flow Field Between Two PWR Surrogate Bundles Under Seismic Conditions Using Bagging-Optimized Dynamic Mode Decomposition (BOP-DMD)

TESI DI LAUREA MAGISTRALE IN
NUCLEAR ENGINEERING - INGEGNERIA NUCLEARE

Author: **Haidy Ibrahim**

Student ID: 970948
Advisor: Prof. Antonio Cammi
Co-advisors: Carolina Introini, Roberto Capanna
Academic Year: 2022-23

I dedicate this thesis work to my family. A special feeling of gratitude to my loving parents, Muhammad and Nihal whose words of encouragement kept me going. To my sister Sandy, and my brothers Youssef and Ziad who have never left my side and are very special. Finally, to the love of my life, Loai, I couldn't have made it without your support. Thank you.

Declaration

I certify that all the material used in this thesis which is not my own work has been identified and that no material is included for which a degree has previously been conferred on me.

Eng. Haidy Ibrahim

Signature

....

We specify that we have read the present work and that in our opinion it is fully adequate in scope and quality as a thesis towards the fulfillment of the requirements of the master's degree in Nuclear Engineering From Politecnico di Milano University (Polimi) - School of Industrial and Information Engineering,

Date: 18th of July 2023

Supervisor

Antonio Cammi

Signature

....

Examiner	Examiner	Examiner
....	....	....
Signature	Signature	Signature
....	....	....

Abstract

The safe operation of nuclear reactors under accidental operating conditions is a mandatory requirement for any plant design. One of the most challenging conditions is represented by earthquakes: however, works of literature discussing the response of reactor core bundles and their interaction with the moderator under seismic conditions are limited. Direct measuring techniques of flow field parameters are highly complicated and extremely expensive, hence fluid-structure interaction models are proposed to solve such problems. However, these models still have some limitations, for example, high computational costs and systematic uncertainty. As such, data-driven modeling as a data analysis technique can be used to reduce computational costs whilst obtaining results of high enough accuracy. In this work, we use Bagging-Optimized Dynamic Mode Decomposition (BOP-DMD) to provide stable forecasting of flow field parameters of coolant flow around PWR surrogate bundles under seismic conditions with spatial and temporal uncertainty quantification. This equation-free Model Order Reduction technique (MOR), which we have built using MATLAB through the use of experimental data, is suitable for future data prediction with large accuracy limits and low computational time. The benchmark of this work is the ICARE experimental facility, which is an experimental facility that studies the coolant flow between two PWR surrogate bundles under seismic conditions. Data used in this work for the training and validation of the model are obtained from 2D experimental measurements of flow velocity fields around PWR surrogate bundles under seismic conditions using the Particle Image Velocimetry technique (PIV). The study confirms the validity of the BOP-DMD method to provide field reconstruction of complex flow fields up to high certainty levels.

Keywords: PIV, BOP-DMD, PWR, Rod bundles, Seismic conditions

Estratto in lingua italiana

Il funzionamento in sicurezza dei reattori nucleari sia in condizioni nominali che accidentali è un requisito obbligatorio per la progettazione di qualsiasi impianto nucleare. In particulare, una delle condizioni accidentali più critiche è rappresentata dai terremoti: tuttavia, i lavori di letteratura che discutono la risposta degli elementi di combustibile nel nocciolo del reattore e come interagiscono con il fluido moderatore in condizioni sismiche sono limitati. Le tecniche di misurazione diretta dei parametri del campo di flusso sono molto complicate ed estremamente costose: per studiare questi fenomeni, lo stato dell'arte è usare modelli di interazione fluido-struttura. Tuttavia, questi modelli presentano alcune limitazioni, come gli elevati costi computazionali e l'incertezza sistematica. Per questo motivo, la modellazione guidata dai dati (*data-driven modelling* come tecnica di analisi può essere utilizzata per ridurre i costi computazionali e ottenere risultati sufficientemente accurati per il campo nucleare. In questo lavoro, utilizziamo la Bagging-Optimized Dynamic Mode Decomposition (BOP-DMD) per fornire previsioni accurate dei parametri del campo di flusso del refrigerante intorno a elementi di combustibile surrogati (rappresentativi di quelli di un PWR) in condizioni sismiche, quantificando inoltre l'incertezza spaziale e temporale. Questa tecnica di riduzione d'ordine (MOR) non richiede l'implementazione delle equazioni fisiche del modello, ma richiede solo la presenza di un insieme di dati di qualsiasi provenienza: in particolare, nel nostro lavoro usiamo dati sperimentali provenienti dall'impianto ICARE, ovvero misure sperimentali dei campi di velocità 2D del flusso, ottenute usando la tecnica della Particle Image Velocimetry (PIV). Abbiamo sviluppato l'algoritmo BOP-DMD in MATLAB, confermando la validità del metodo BOP-DMD per la ricostruzione di campi di flusso complessi e per la predizione del comportamento futuro del sistema con livelli di accuratezza elevati e bassi tempi di calcolo.

Parole chiave: PIV, BOP-DMD, PWR, Rod bundles, Condizioni sismiche

Contents

1 | Introduction

1.1. Pressurised Water Reactors

PWRs (Pressurized Water Reactors) are a specific kind of commercial nuclear reactors, extensively used to generate electric power. Because of their efficiency and dependability, they are essential to many countries' power generation systems. PWRs use the energy created by nuclear fission to generate heat, which is subsequently transformed into electrical energy using a steam turbine system. A typical Pressurized Water Reactor (PWR) core is composed of several fuel assemblies around which water flows to moderate the neutron flux and cool down the fuel assemblies. Disturbances to the nominal fluid flow patterns, for example, due to natural catastrophes such as earthquakes, could highly affect the reactor core's criticality and its safe operation.

1.1.1. Reactor specifications

A PWR core is composed of fuel assemblies, which typically comprise uranium dioxide pellets enriched in uranium-235. Within the reactor vessel, these fuel assemblies are surrounded by high-pressure coolant to avoid boiling in the primary loop even at high temperatures. Water performs two functions: it acts as a moderator, slowing down the neutrons produced during fission, and as a coolant and thermal carrier. A heat exchanger transfers heat generated in the core to a secondary loop, in which steam is produced to power the turbine-generator system. This design maintains a distinct boundary between the radioactive primary loop and the non-radioactive secondary loop, improving safety and efficiency. A typical PWR is shown in figure 1.1 [30].
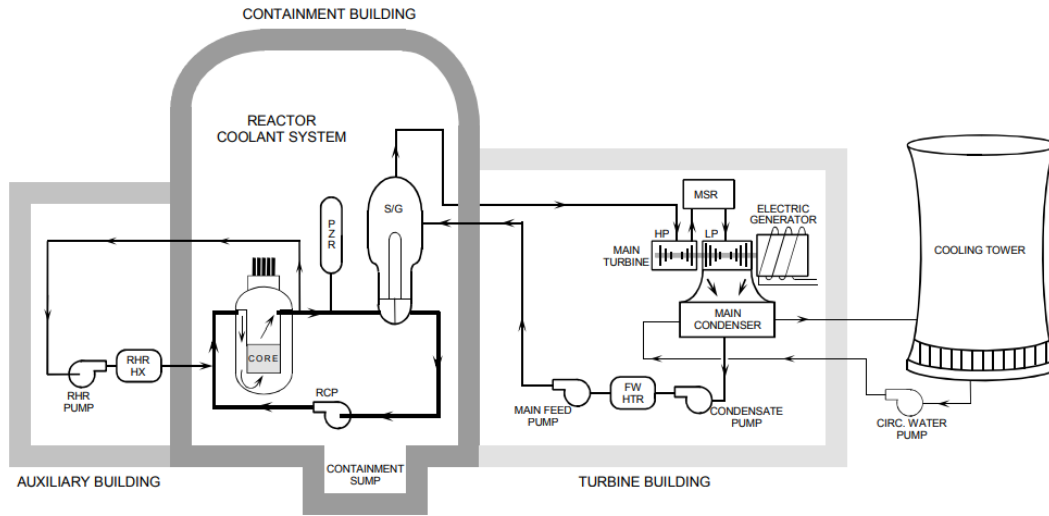
Figure 1.1: Typical PWR systems scheme (taken from [30].

The PWR system contains a number of safety features designed to avoid accidents and reduce potential dangers. Control rods, which are placed into the core to absorb excess neutrons and manage the nuclear chain reaction, are among these safety mechanisms. Coolant pumps and emergency core cooling systems are engaged in the case of an emergency to protect the reactor integrity and prevent overheating and thus fuel melting.

1.1.2.   PWR Under Seismic Conditions

Pressurized Water Reactors (PWRs) are built to resist seismic disturbances and assure the nuclear power plant's safety even in such circumstances. Seismic design considerations are critical in earthquake-prone areas to limit the influence of ground motion on the reactor's structural integrity and functionality. Indeed, before constructing any reactor, a thorough site selection process is carried out to assess the region's seismic hazard characteristics. To identify probable earthquake sources and quantify ground motion parameters at the site, geological surveys and seismic hazard assessments are carried out. The structural integrity of the reactor building and supplementary infrastructure is the primary focus of seismic design for PWRs. Even during an earthquake, the reactor structure must endure considerable ground motion and keep radioactive materials contained. To provide strength and flexibility, the structural design uses strong building elements such as reinforced concrete and steel. Key components, notably the containment structure, are designed with special care to withstand seismic forces.

Advanced computer-based seismic modeling and simulation techniques are used prior to

construction to examine the fluid and solid movements in the PWR under various seismic scenarios. These assessments aid in identifying potential risks and guiding the design to meet seismic design standards. The investigation of flow field patterns and fluid-structure interactions (FSI) under seismic situations becomes critical to ensuring the reactor's safe operation even in these extreme settings, as well as understanding the fluid's behavior and interaction with the reactor's structural components to maintain cooling efficiency, minimizing fuel rod damage, and avoiding any safety issues. In particular, maintaining the nominal distance between reactor fuel rods in each assembly, which is around 3 mm, is crucial in sustaining a nuclear reactor's safe functioning. The vibrations caused by ground motion during an earthquake can cause considerable structural motions and deformations, causing the fuel rods to come into contact with each other, thus disrupting the usual flow of the coolant. As such, flow field pattern analysis, which includes examining the velocity distribution, pressure gradients, and turbulence properties of the moderator fluid during seismic occurrences, becomes a key tool to ensure the reactor's safety even under seismic conditions.

Computational fluid dynamics (CFD) simulations, specific design codes, and experimental research are typically used to shed light on flow patterns by identifying probable locations of flow disruption or stalling induced by fuel rod interactions [17] [46]. CFD codes are based on the deterministic solution of the main governing equations to fluid motion (*ex, Navier-Stokes*). While those 1D codes exhibit some limitations when studying local effects and disturbances, CFD codes are quite accurate but very expensive from the modeling and computational point of view. Experimental measuring techniques commonly used include Laser Doppler Velocimetry (LDV), which was for example used to validate the CFD model of a 3-by-3 bundle flow with a grid spacer [52], or rod-embedded Fiber LDV to measure velocity in fuel rod bundles as in [15]. Other techniques include Imaging Flow Velocimetry (IFM) [10] and Particle Image Velocimetry (PIV) [54] [5].

Among these techniques, PIV has shown many advantages, among which are its usability between fuel bundles in tight geometries, its capability of resolving the velocity field into its components, and its relatively low computational cost. The key working principle is to make the fluid motion visible, which involves three major steps: 1) feed the flow with seed particles that are light reflecting; 2) illuminate the flow with a light sheet (typically a laser sheet); 3) record particle movements using cameras [2]. Time-resolved PIV between two PWR surrogate bundles is the technique with which the data that will be used in this thesis work were obtained, with the final goal to achieve domain-wide field reconstruction and forecasting. Such measurements are interpreted using a cross-correlation algorithm and stored in high-dimensional arrays [2] [36] [31]. However, those high-dimensional data

arrays are not easy to be analyzed: as such, in this thesis work, we integrate the use of model-order reduction techniques (MOR) to reduce the dimensionality of the data and to extract their key features, with the time-resolved PIV as an experimental measuring technique.

When modeling complex systems, is useful to reduce them to a computationally cheap form i.e. achieve low dimensionality [47]. This is usually done through the use of model-based reduction algorithms that relies on the projection onto low-dimensional sub-spaces of the system's governing equations. However, in situations where these governing equations are not known or not well formulated, or when experimental data are available, the use of Data-Driven Models (DDM) is preferred [42]. An example of such an approach is Dynamic Mode Decomposition (DMD) [39]. To model a system using DMD the only requirement is to have a series of snapshots, either coming from high-fidelity models or directly from experimental data, of the system's variables of interest, dense enough to resolve the transient dynamics of interest [19]. The algorithm decomposes this dataset into low-dimensional dynamic modes which capture its key features, which can then be used to map the entire system and for future data prediction.

Another possibility to provide efficient visualization (solution) of complex fluid fields, which is not discussed in this thesis work, is to combine both deterministic approaches with MOR techniques to reduce the computational cost and achieve acceptable results. Such an approach could include the integration of CFD simulations with DDM as DMD to provide stable forecasts of simulated complex fields. A comparative study between the application of DMD to experimental or CFD analysis is found in the work of Luong and Wang (see [24])

1.2. Thesis Objectives

The main objective of this thesis study is to investigate the behavior of PWR flow fields under seismic situations. As was previously mentioned, the usual space between reactor fuel rods in each assembly is around 3 mm, leaving little room for movement. During an earthquake, the vibrations might cause fuel rod contact, disrupting the axial flow of the moderator. This phenomenon poses a serious obstacle to the reactor's safe operation under seismic conditions. As a result, the key goal of this research is to study the flow field patterns and fluid-structure interactions (FSI) in PWRs subjected to seismic events. This is done by achieving a list of specific objectives, listed below.

1. Examine the difficulties related to dealing with high-dimensional data in the context of measurement noise: experimental data inevitably contain noise, which can

impair analysis accuracy. As such, the first goal is to understand the limitations of the typical Dynamic Mode Decomposition (DMD) algorithm in dealing with noisy velocity fields measurements of coolant flow around PWR bundles under seismic conditions, as well as the influence of increasing noise levels field on its ability to capture system dynamics.

2. Following the first goal, investigate the use of Bagging-Optimized Dynamic Mode Decomposition (BOP-DMD) as an improvement to the precise DMD algorithm: BOP-DMD is a modified version of DMD that tries to eliminate noise bias and increase algorithm performance with high-noise data. The goal is to assess BOP-DMD's performance in resolving the issues associated with noisy high-dimensional data obtained from the PIV measurements mentioned above.

3. Apply the BOP-DMD method to velocity fields for reconstruction and forecasting: velocity fields are complex and three-dimensional, and they require accurate reconstruction and forecasting for a variety of applications. The goal is to use the BOP-DMD algorithm to reconstruct the velocity fields and test its capacity to accurately forecast the future behavior of the system.

4. Compare the findings of BOP-DMD to those of the exact DMD algorithm: a comparison of BOP-DMD and the conventional DMD algorithm is performed to assess the performance and effectiveness of BOP-DMD in dealing with noisy data and producing credible reconstructions and forecasts.

5. Investigate the effect of noise on field reconstruction: the study also involves the analysis of the reconstructed fields in the presence of noise and after applying denoising techniques, with the goal of understanding the impact of noise on reconstruction quality and evaluating the benefits of noise filtering methods in improving the accuracy of the results.

6. Confirm the BOP-DMD technique dependability in reconstructing and forecasting the behavior of high-dimensional fields: the ultimate goal of this thesis work is to test the BOP-DMD algorithm's efficacy and dependability in the reconstruction and future prediction of complex fields, especially in the presence of noise.

To the author's knowledge, applying BOP-DMD to a dynamical flow field between two PWR surrogate bundles is a first of a kind and the outcome of such analysis could be valuable to both data science and thermal hydraulics community, especially in the field of nuclear reactors' thermal hydraulics for safe reactor operation.

1.3.   Thesis Structure

The thesis is divided into chapters, each of which addresses a different aspect of the study topic.

The first chapter provides an introduction to the thesis. It opens with a review of Pressurized Water Reactors (PWR) and their specifications, emphasizing their importance in the realm of nuclear energy. The chapter delves more into the behavior of PWRs under seismic conditions, highlighting the importance of studying flow field patterns and fluid-structure interactions (FSI) to assure reactor safety during earthquakes. The thesis objectives are next presented, detailing the particular goals and objectives of the research. Finally, the chapter finishes by explaining the overall structure and organization of the thesis, laying the groundwork for the following chapters.

The second chapter dives into the theoretical basis required to comprehend the research approach. It begins with an overview of Data-Driven Modeling, covering fundamental concepts and approaches used in this subject. Dynamic Mode Decomposition (DMD), a common data-driven modeling technique, is the topic of this chapter. It describes in full DMD's architecture, methodology, and applications in numerous disciplines. Traditional DMD's limitations are also emphasized, paving the way for the introduction of an improved version known as Bagging-Optimized Dynamic Mode Decomposition (BOP-DMD). The chapter finishes with a synopsis of the principles and the overall conclusion based on the theoretical foundation.

The experimental design is the focus of Chapter 3. It begins by introducing Particle Image Velocimetry (PIV), the study's non-intrusive flow measurement technology. The basics of PIV are presented, including measurement considerations and flow velocity evaluation. The experimental setup is detailed in-depth, including information on the equipment and techniques used to collect data. The chapter also includes the experimental results, highlighting the flow field patterns seen under the given conditions. Finally, a conclusion summarizing the experimental design's findings and implications is drawn.

The fourth chapter focuses on the research approach. It starts by outlining the data gathering and treatment method and any pretreatment processes needed for the analysis. The DMD code implementation is presented, with emphasis on the methodological aspects involved. The handling of noisy fields in DMD and the issues caused by growing noise levels receive special consideration. The BOP-DMD algorithm is then presented, with details on parameter selection, optimization, and application to field reconstruction and validation. The chapter also goes through various denoising techniques used to improve

the accuracy of the results.

The results and discussions obtained from the analysis are presented in Chapter 5. The analysis involved flow field reconstruction using both exact DMD and BOP-DMD. Results from both approaches are compared, with a focus on the effect of noise on the adopted approach with some viable denoising techniques presented. The analysis was extended to include the reconstruction of the complex vorticity field which provided some valuable insights into the dynamics and behavior of the flow field.

Overall, the thesis structure follows a natural path, beginning with the introduction and background material, then the experimental design and technique, and finally the results and discussions. This structured method enables the reader to understand the study process, theoretical concepts, and findings in a clear and systematic manner.

2 | Theoretical Background

Abstract

Models based on the mathematical description of the physics of the system being modeled were widely used in science and engineering. However, in the last decade, and with the abundance of experimental data, the use of *data-driven modeling*(DDM) techniques became of great use. This chapter is a preface to data-driven modeling techniques and briefly overviews its most popular applications. It also identifies the technique applied in this study, *Dynamic Mode Decomposition* (DMD).

2.1.   Introduction to Data-Driven Modeling

Scientific models of a system can either be physical, mathematical, or empirical. The first two rely on scientific laws and equations that could be very complex and imposes slow system prediction. The latter, however, relies on mathematical equations that were not derived from the physics of the system, but rather on the collection of a series of time-dependent measurements. Data-driven modeling (DDM) is an empirical approach to modeling that doesn't rely on the physical behavior of the system it models, in fact, it only relies on the use of machine learning (ML) techniques to overcome the need for such sophisticated "equation-based" models [12] [16]. In DDM, the analysis of the system is done by finding a relation between system inputs and outputs without the need for governing equations which could be, sometimes, either unknown or too complex to be of use. In a field like fluid dynamics, to properly model fluid motion, the use of Navier-Stokes equations (NSE) is a must. Such equations are nonlinear and very complex, and hence, require tremendous efforts to be solved. DDM overcomes the challenges imposed by physical models, such a modeling approach is intended to achieve low dimensionality, solve numerical prediction problems, and reconstruct highly non-linear systems [41] [42].

2.1.1.   Key Concepts

DDM relies on many overlapping fields of science like data mining, machine learning (ML), computational intelligence (CI), and many others. Data mining and knowledge discovery in databases (KDD) are wide concepts that have been applied in fields like engineering, economics, telecommunication, etc. The idea of data mining is to navigate through a large set of data to find patterns and connections between those data that can be put to use in an application of some sort. Data mining uses ML which is an area of computer science, or in other words, a sub-area of artificial intelligence (AI) that mainly applies the concept of deep learning. Most data-driven models rely on computational intelligence (CI) and machine learning (ML) algorithms to find a relationship between the input and output of the system under study. This is achieved through the use of a relatively large data set to train and validate the model, whilst achieving the desired accuracy [41].

Data-driven models could be built by following certain general steps: 1) study and identify the phenomena/variable to be modeled; 2) collect the data (it should be noted that DDM requires the collection of a relatively large dataset to model the system under study up to an acceptable level of accuracy); 3) feed the dataset to the chosen model structure to train the model; 4) test and validate the model through iterations [16]. The process of DDM is shown in 2.1 where the input data is fed to the model where the training process (*series of iterations*) starts until a desired output is obtained [42].
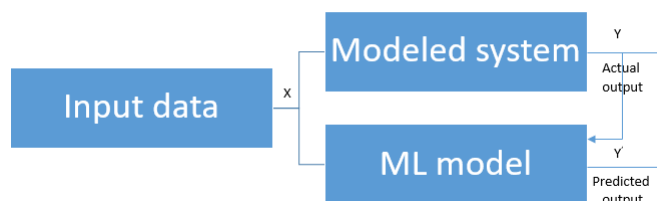

Figure 2.1: Learning in data-driven modeling.

The word data, when used here, refers to a set of measurements (X) over some time steps (K), and the idea of the model is to find a relationship (mapping function) between the input (X) and the output (Y) where $Y = F(X)$. This is known as *training*, once the mapping function (F) is found, it could be used for data predictions or uncertainty calculations.

Limitations to DDM should also be mentioned [29], one of the most important limitations is the problem of overfitting which affects the model uncertainty. Such a problem is a

methodological issue, in the sense that during the process of model training, we should find a technique (e.g. Eigen modes decomposition) through which we can choose the number of modes up to which we can fit our data to achieve the model generalization and simultaneously avoid overfitting problems. Another limitation is error propagation: systemic errors could be captured during the data measurement process and hence affect the model accuracy. Such limitation imposes the use of error filtering techniques (e.g. fast Fourier transform) to the original data set.

2.1.2. Data-Driven Modeling Techniques

With the great advancements in fields like ML and DL, and with the wide availability of databases, DDM techniques have been improved greatly in the past few years. In this section, we will discuss some of those techniques, their advantages, limitations, and some of their applications.

Artificial Neural Networks

Artificial Neural Networks (ANN) is a DDM technique that is widely used in many fields of science. The technique itself dates back to the 1940s, and it is inspired by the human brain's neural network. Just like any other DDM technique, ANN is based on the idea of feeding a set of inputs to a model that maps those inputs into an output, however, the mapping (or training) is done through a network that finds the underlying relationships in the input data.

The structure of ANN is as follows, a first layer of interconnected nodes (neurons) known as *input layer* where input data are fed to those nodes either externally or from another node. The nodes then pass the inputs forward through connections to successive hidden layers of more nodes. Finally, the output is received from the output layer as a weighted sum of the inputs. The hidden layer is where the training of data is performed, it is essential to the network as it allows the NN to learn the connections between the data. Each neuron in the structure represents a processing unit where inputs are treated, and weights are associated with those inputs where at the final node they are added together to produce an output. This is known as the Feed Forward (FF) structure, for other ANN structures, see [28].

ANNs show great advancements over computers or physics-based models, for example, ANNs do not require an explicit description of the system under study, they do not require tedious programming, they possess the ability to generalize and handle incomplete data, and finally, they can relate data to system solutions showing the capability of future

predictions. Limitation to ANNs is however presented in the choice of the training, validation, and test data sets where all three must possess the same statistical properties (e.g. same mean square error) [41].

ANNs have many applications, in the field of hydrology, ANNs have been used to model the rainfall-runoff processes see [13] and to build a controller for real-time control of water levels in the channels of polders see [23]. Also, in medicine, ANNs have been applied to medical imaging and signal processing see [26]. Moreover, ANNs have been used in industry to optimize the manufacturing process see [6].

Fuzzy Rule-Based Systems (FRBS)

Another widely known DDM technique is Fuzzy Rule-Based Systems (FRBS), the main concept behind FRBSs is to use fuzzy logic for reasoning, the method was first developed in 1965 by Zadeh, see [53]. The fuzzy set theory imposes a binary set membership that has been stretched to include any membership between 0 and 1 [53]. FRBSs have the advantage of directly modeling uncertainties, generally, the mapping between inputs and outputs is performed through a set of IF-THEN rules which could be either set by a human expert or drawn from the historical data set. For a detailed description of FRBSs see [37].

Like any DDM, FRBS has some limitations that are worth mentioning, first of all, there is an exponential relation between the variables studied and the fuzzy sets, which can lead to model complications. Another limitation is that FRBS requires optimization by an external method like neural networks. However, such limitations did not affect the usability of the technique, in fact, FRBS has lots of applications, especially in control theory see [42]. Furthermore, FRBS was used for drought assessment see [16], for the estimation of soil hydraulic conductivity see [34], and also for the control of water levels in polder areas see [23].

Chaos Theory and Non-Linear Dynamics

The theory of nonlinear dynamics or also known as *Chaos Theory* treats deterministic or random data sets, hence the term "nonlinear". Nonlinear dynamics DDMs are, in return, the DDMs which are able to treat dynamically changing random data and find a mapping relation from the inputs to outputs [41]. The main idea is to represent the system measurements by a state-space matrix and find its trajectory in the phase space. A similar approach is adopted in this study and will be explained in detail in later sections.

Applications to such technique include the prediction of the surge water level in the North

Sea close to the Hook of Holland by Solomatine et al. (2000) and Velickov et al. (2003) [40], for load forecasting in Greece by K Stergiou, and TE Karakasidis [43], and for sports performance prediction by W Sun [44].

Other DDM Techniques

In addition to the abovementioned techniques, there are other DDM approaches that are worth mentioning. Although these techniques are less commonly used than, for instance, ANN, however, they are a recent topic of research for many data scientists. Among those approaches is *Genetic programming* (GP), the method was developed in 1992 [41], its main concept is to take many mathematical building blocks for evolving equations and grouping them into a single expression. A similar approach is *Evolutionary regression* with the main goal of finding a regression equation with coefficients found through an evolutionary approach [41]. Here we should mention the concept of *Classification*, which is the concept of dividing the data set into classes and then associating some data vectors to those classes. This is done to obtain a model that is a class label and not a real number (obtained in regression models) [41]. The *instance-based learning* (IBL) method is used for both classification and prediction, this is achieved through combining observations from the set of the training data [41]. A more relatively recent approach is *Support vector machines* (SVM), the method is based on the concept of identifying a surface that separates two classes in classification, or even solving forecasting problems [41].

2.1.3. Data Driven Modeling Applications

DDM has been widely used in many applications since its basic concept is to disregard the system underlying physical phenomena and treat all data points alike, allowing it to be applied almost to all fields of science. In the field of mechanical engineering and material science, DDM has been used to model solids, perform multiscale analysis of heterogeneous materials, and in biomechanics for soft tissue characterization. In industrial engineering, DDM has shown promising results in monitoring and prediction applications. Many other applications are discussed in the work of Montáns (see [27]).

In this study, our attention is drawn to DDM applications in the field of fluid and particle dynamics. DDM has been applied to fluid field systems to improve the accuracy of simulations when simulating turbulent and transitional flow [27]. An article by Jan Heiland discusses the application of NN for low-dimensional linear parameter varying approximations of Navier-Stokes equations (see [12]). Another application of DDM in the field of fluid dynamics is the work of Zhang [55] where a technique named *dynamic mode*

decomposition (DMD) is applied to a fluid field, the study included the evaluation of the technique's accuracy which is shown to be encouraging. Also, a fast DMD was proposed for online evaluations. In this study, we are using an adjustment to DMD known as *bagging optimized DMD* for better forecasting performance, hence it is crucial to introduce both in detail.

2.2. Dynamic Mode Decomposition

One of the most recent data-driven modeling techniques is dynamic mode decomposition (DMD), which can be considered as a combination in its formulation of the proper-orthogonal decomposition (POD) [1], and Fourier-transform [19]. The former is a spatial reduction technique while the latter is a transform in the time domain. In this section, we will try to briefly explain the basics of DMD and the algorithm followed [19, 22].

2.2.1. Introduction

Data-based models are intended to simplify systems modeling, they are applied to explore, mimic, and control complex systems, however, their main goal would remain to achieve low dimensionality of complicated high-dimensional systems. Dynamic mode decomposition (DMD) provides complex data decomposition into a group of dynamic modes through the exploitation of low dimensionality, the technique originated in the field of fluid dynamics by Schmid and Sesterhenn [19] to initially decompose complex fields into their simple spatiotemporal coherent basis, allowing the interpretation of such complex fields. Since fluid fields are dynamical systems that are characterized by their high dimensionality and nonlinearity, DMD was needed to deal with such fields to provide future state prediction and control [19]. DMD, being an equation-free DDM technique in its formulation, is capable of performing accurate decomposition of any complex system state into its much simple spatiotemporal structure allowing for; future states prediction, system control, and diagnostics. The popularity of DMD as a DDM technique has grown over the years due to the great developments that data science has witnessed in the last decades. The wide expansion in data mining, data resources, and improved machine learning algorithms have laid the ground for a vast development in DDM techniques, including DMD.

DMD can be looked at as an extension of nonlinear dynamics with a special connection to Koopman operator theory [19]. The method performs computation on collected experimental data from a nonlinear dynamical system and then provides a combination of low dimensional linear dynamic modes of the system. The collected experimental data are a

---

[1]POD is a numerical method used for extracting spatial structures of complex systems.

series of measurements collected over fixed time periods (*Snapshots*). As was previously mentioned, DMD is considered a combination of POD that allows for spatial dimensionality reduction, and FT in time. Therefore, DMD produces spatial modes of a system associated with their corresponding temporal modes permitting the future prediction of future system states. The advantage of such a technique lies in its simplicity, DMD as any DDM does not make any assumption about the modeled system, is easy to execute, and does not require tedious variables optimization. Also, it can provide future states of the system at any time point.

The DDM technique is intended to perform three major tasks; system diagnostics, system control, and system state prediction.

1. **Diagnostics**: The DMD method was initially developed as a diagnostic tool since it poses the capability of extracting low-rank spatiotemporal modes from complex systems of high dimensionality. The output modes are easy to interpret and explore.

2. **System Control**: This is the most complicated application for DMD. Having the capability of controlling the future states of a system, and allowing a data-driven approach to control theory is the ultimate goals of DMD. A detailed explanation of DMD with control can be found in the work of Kutz and Brunton [33].

3. **System State Prediction**: An advanced application of DMD is to predict the future states of a system, of course, this is drawn from its capability of producing temporal (dynamical) modes to the system understudy. Those temporal modes allow the anticipation of the future system states even in the absence of experimental data at those future states.

2.2.2.   DMD Architecture

The architecture of the DMD method simply starts with data extraction. The word "data" here describes snapshots of a measurement in time. Here we should define N to be the number of spatial points recorded per snapshot, and M to be the number of snapshots. DMD imposes a constrain on the snapshots' time intervals are regularly spaced, collection time can be expressed as

$$t_{k-1} = t_k + \Delta t \tag{2.1}$$

Where Δt is the time spacing between two snapshots, and the sampling time starts at t_1 and ends at t_M.

The collected data is stored in a matrix X that is $N \times M$ in dimensions. The DMD method could be considered as computing the eigenvalues and eigenvectors from the measured

experimental data of a linear model that is an approximation of the system (nonlinear) dynamics. Hence, as a first approximation, we describe our system as a linear dynamical system where

$$dX/dt = AX \tag{2.2}$$

and its solution can be obtained with a simple knowledge of the initial condition X_0

$$X(t) = \sum_{k=1}^{n} \phi_k \exp(\omega_k t) b_k = \Phi \exp(\Omega t) b \tag{2.3}$$

where ϕ_k and ω_k are the eigenvectors and eigenvalues of the matrix A, and b_k is the loading of the initial X_0. Mathematically speaking, the architecture of the DMD is based on finding the operator that maps our data matrix X from a current state in time to its future projection, such that

$$X_{k+1} = \mathcal{A}X_k \tag{2.4}$$

$\mathcal{A}$ is the mapping matrix, it is a linear time-independent operator having the same dimensions of the data matrix X, and it has the capability of mapping matrix X from a current state K to a future state $K+1$ Where

$$\mathcal{A} = \exp(A\Delta t) \tag{2.5}$$

and the solution to the system can be expressed in terms of the eigenvalues λ_k and the eigenvectors ϕ_k of the mapping matrix $\mathcal{A}$ as

$$X_k = \sum_{j=1}^{r} \phi_j \lambda_j^k b_j = \Phi \Omega^k b \tag{2.6}$$

Such that the first mode can be expressed as $X_1 = \Phi b$. Hence, the DMD algorithm finds a mapping matrix that maintains a least square fit

$$||X_{k+1} - \mathcal{A}X_K||_2 \tag{2.7}$$

A full description of the DMD architecture can be found in the book of *Dynamic Mode Decomposition* by Kutz [19].

2.2.3. DMD Algorithm

One major challenge when treating a dynamical system is its high dimensionality, as mentioned before, the data matrix X is an N by M matrix, accordingly matrix A is a

high dimensional matrix too, hence a technique is to be used to reduce the matrix to a low rank, this is done by following the single value decomposition (SVD) approximation see A.

First, we take the SVD of matrix X

$$X \approx U\Sigma V^* \tag{2.8}$$

where V^* is the conjugate transpose of V, $U \in \mathcal{C}^{n \times r}$, $\Sigma \in \mathcal{C}^{r \times r}$, $V \in \mathcal{C}^{m \times r}$, $n = 1...N$, $m = 1...M$, and r is the rank to which matrix X will be reduced. The SVD of matrix X means simply truncating the matrix to a lower rank, further details on SVD can be found in [18].

Then, matrix $\mathcal{A}$ can be found by solving equation 2.4 after the substitution of the reduced matrix X

$$\mathcal{A} = X'V\Sigma^{-1}U^* \tag{2.9}$$

It should be noted here that it is more convenient to treat the $r \times r$ projection of matrix $\mathcal{A}$, and this is obtained through

$$\widehat{A} = U^*\mathcal{A}U = U^*X'V\Sigma^{-1} \tag{2.10}$$

This reduced matrix also satisfies the eigenvalue problem

$$\widehat{A}W = W\Lambda \tag{2.11}$$

where W is the eigenvector and Λ is the matrix containing the eigenvalues λ_k. These eigenvectors and values can be related back to the original mapping matrix to reconstruct the DMD modes.

Finally, the eigenvalues and vectors of $\mathcal{A}$ are used to obtain the DMD modes through

$$\Phi = X'V\Sigma^{-1}W \tag{2.12}$$

It should be noted here that equation 2.12 is the same as equation $\Phi = UW$ if and only if matrix X and X^{-1} have the same column spaces.

Equation 2.12 gives the *exact DMD modes* since they are the exact eigenvectors of $\mathcal{A}$. However, the modes of $\Phi = UW$ are the *projected DMD modes*, and the approximate solution at any time incident is given by equation 2.6. For deeper details on the DMD algorithm see [19] and [18].

2.2.4. Simple example

This is a simple example intended for demonstration purposes, it is presented in the book by Kutz, see [19]. The example shows how the DMD algorithm is structured and some of the DMD method capabilities.

Imagine having a spatiotemporal signal that is a mix of two other spatiotemporal signals, also imagine having two frequencies for that signal $\omega_1 = 2.3$ and $\omega_2 = 2.8$. For the sake of simplicity, assume that our signal takes the following shape

$$f(x,t) = f_1(x,t) + f_2(x,t) = \operatorname{sech}(x+3)\exp(i2.3t) + 2\operatorname{sech}(x)\tanh(x)\exp(i2.8t)$$

$$(2.13)$$

To build the algorithm shown in 2.2, MATLAB was used where the mixed signal f was created, moving forward, the algorithm was able to decompose the signal into its components. It was also able to reconstruct the signal back from its dynamic modes.

```
1
2      %Defining domain
3
4 -    xi=linspace(-10,10,400);
5 -    t=linspace(0.4*pi,200);
6 -    dt=t(2)-t(1);
7 -    [Xgrid, T]=meshgrid(xi,t);
8
9      % creating two spatio-temporal patterns
10
11 -   f1=sech(Xgrid+3).*(1*exp(1i*2.3*T));
12 -   f2=(sech(Xgrid).*tanh(Xgrid)).*(2*exp(1i*2.8*T));
13 -   f=f1+f2;
14     %SVD f to reduce it
15 -   [u,s,v]=svd(f.');
16
17     % Start of DMD
18 -   X=f.';
19 -   X1=X(:,1:end-1);
20 -   X2=X(:,2:end);
21
22     %Rank truncation
23 -   r=2;
24 -   [U,S,V]=svd(X1, 'econ');
25 -   Ur=U(:,1:r);
26 -   Sr=S(1:r, 1:r);
27 -   Vr= V(:,1:r);

29     %building A tilde
30
31 -   Atilde=Ur'*X2*Vr/Sr;
32
33     %eigen decomp
34 -   [W,D]=eig(Atilde);
35
36     % DMD modes
37 -   phi=X2*Vr/Sr*W;
38 -   lambda=diag(D);
39 -   omega=log(lambda)/dt;
40
41     %Reconstruction in time
42 -   X1= X(:,1);
43 -   b=phi\X1;
44
45     %time dynamics
46 -   time_dynamics=zeros(r,length(t));
47 -   for iter=1:length(t)
48 -       time_dynamics(:,iter)=(b.*exp(omega*t(iter)));
49 -   end
50 -   X_DMD=phi*time_dynamics;
51
```

Figure 2.2: DMD Algorithm

Figure 2.3 shows the signal f, its two separate components f_1 and f_2, and the reconstructed signal from the dynamic modes of the original signal. This example highlights the core of the DMD method.
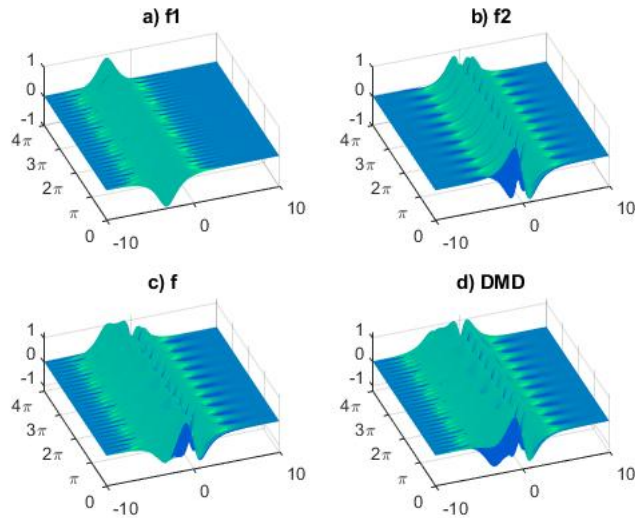
Figure 2.3: An example of spatiotemporal dynamics of two signals(a) $f_1(\text{x, t})$ and (b)f_2(x, t) that are mixed in (c) f (x, t) = f_1 (x, t) + f_2(x, t) and the (d) Reconstructed signal.

It is evident here that the reconstructed field agrees to a great extent with the original signal. This emphasizes the DMD's ability to diagnose fields, decompose them into their dynamic modes, and reconstruct them again. Of course here, we solved a very simple example, in reality, dynamic fields are much more complex and usually are accompanied by noise. This imposes some sort of a challenge on the DMD method and shall be discussed in detail in one of the coming sections.

2.2.5. DMD Applications

The DMD method has proven itself as a robust DDM technique and found its way into many fields of applications, the work of Zhang [55] mentioned earlier is one of many applications found in the literature. Also, in the work of Weiner and Semaan [51] DMD was applied to a flow under a transonic shock buffet the technique was tested for its robustness and showed promising results. Another example is the work of Zhengxiao [25] where a combination of DMD algorithms and NN are used for forecasting a laminar flow around a 2D cylinder and a turbulent flow around a 3D SD7003 airfoil. Finally, in the work of Di Ronco and Intorini [7] DMD was applied to a Molten Salt Fast Reactor (MSFR) for stability analysis.

2.2.6.   DMD Limitations

As has been discussed in the precedent section(s), DMD is a technique that is able to perfectly treat dynamic spatiotemporal signals. However, some limitations of the technique are due noting. First of all, DMD fails when treating low-rank translational or rotational signals [19]. This comes from the fact that the method is based on the SVD method which is naturally translational-rotational invariant [18]. Another limitation, the most important to our application, is that the technique fails when treating high-rank transitional data. Naturally, complex fluid fields are transitional, hence, DMD partially fails to treat such fields [19]. An adjustment to the technique is to be made to enable it to treat such fields. This is discussed in the next section.

2.3.   Bagging-Optimised Dynamic Mode Decomposition

The field of data-driven modeling is moving forward with many adjustments against the limitations imposed by complex fields. Since fluid field measurements could be highly noisy, the use of regular DMD is not much reliable, as it has shown a biased behavior towards noise which makes accurate data reconstruction impossible. One of those adjustments to the DMD [49] algorithm to make it capable of the analysis of noisy fields, is bagging-optimized dynamic mode decomposition (BOP-DMD) providing a strong forecasting algorithm.

2.3.1.   Key Concepts

The exact DMD discussed earlier2.2 is a data-driven architecture that is intended to provide best-fit models for dynamical systems, the method however simple it is to be applied, still exhibits series limitations. The *exact DMD* technique is seriously biased to noise, it shows a limited performance when analyzing fields drawn from actual experimental measures, and it fails to capture the system dynamics, limiting its application in literature to solely diagnostic purposes [19] [18]. The method is best used on numerical data that exhibits a noise-free behavior, DMD is then capable of reconstructing and forecasting accurate solutions.

Bop-DMD is a data-driven modeling technique that depends on the statistical method of bagging which improves the forecasting accuracy of DMD even in the presence of noise and provides uncertainty quantification for the reconstructed fields. Following [38] the algorithm was developed by Sashidhar and Kutz as a modification to a previously de-

veloped one *optimized DMD* [3]. The optimized DMD method was developed to achieve debiasing towards noise for a given signal. This is achieved through nonlinear optimization which is done by some variable projection techniques [3]. Opt-DMD yields very accurate DMD modes and eigenvalues to a great extent, even for highly noisy fields. However, the technique shows a failure of convergence of variable projection [38]. This was solved by BOP-DMD, the method features three additional characteristics: 1) initialization procedure to stabilize the variables projection algorithm; 2) statistical bagging scheme to reduce variance and stabilize the models; 3) uncertainty quantification for temporal and spatial profiles. These three features make BOP-DMD a successful DDM for highly noisy data and high-dimensional fields.

Bagging, which is known in the field of statistical analysis as *boot strap aggregation*, is a statistical approach that can be applied to any regression method to enhance its prediction capabilities [4]. The method produces an ensemble of models that reduces their variance and accordingly put an end to over-fitting by design [45]. The idea behind bagging is simple, first of all, a number of bootstrap samples are randomly drawn from the original data, then the prediction method is applied to each sample separately, and finally, all the results are grouped and an average is produced which is the final prediction. This averaging process highly reduces the variance, allowing better performance. Bagging was applied to many DDM techniques including *deep* NN and showed a huge performance enhancement [11] [38].

Bop-DMD is an enhancement to the exact DMD in the sense that it is not only a diagnostic technique but also capable of reconstructing and forecasting complex dynamical signals. Following Sashidhar and Kutz [38], both OPt-DMD and BOP-DMD were applied to different fields and the results were shown for comparison. Bop-DMD shows a noticeably better performance than OPt-DMD, the error between the mean of the eigenvalues and the true ones is relatively smaller in the case of BOP-DMD. This error also reduces with the batch size increase (number of randomly selected samples) until an optimal value. This is a great advantage of the BOP-DMD over both *exact* DMD and OPt-DMD, making it the technique of choice in this study.

2.3.2. BOP-DMD Algorithm

In the BOP-DMD algorithm, an initial guess is accounted for to provide a provide an acceptable solution to linear models, while using the regression architecture of OPt-DMD highlighted in [3]. The architecture of the algorithm is shown in table 2.1.

BOP-DMD Algorithm

Inputs	Data matrix $\mathbf{X}$, number of trials $\mathbf{K}$, randomly selected indices $\mathbf{P}$.
Procedures	1- Compute ϕ_0, Ω_0, b_0, Perform Opt-DMD regression. 2- Compute K OPt-DMD modes ϕ_k, Ω_k, b_k for k $\in \{1, 2, ..., K\}$. 3- Choose p out of n snapshots; p $<$ n and perform bagging. 4- ϕ_0, Ω_0, b_0 are used as a seed for BOP-DMD, initialize and update.
Output	eigenvalues, eigenvectors, and their loadings (Φ, Ω, b)

Table 2.1: Bagging Optimized DMD algorithm architecture

The input for the BOP-DMD algorithm is the original data matrix X, the number of trials k, and the randomly selected indices p. First, the Opt-DMD algorithm is run on the full data matrix to get the eigenvalues $\lambda_{K_o}pt$ which will be used as the initial conditions for the BOP-DMD algorithm. Using this initial condition, the algorithm is run for k trials to obtain subsets of the original data matrix X_k which are generated by choosing p randomly selected column indices of the original data matrix X. At this point, bagging is introduced and the obtained eigenvalues λ_k, DMD modes ϕ_k, and their loadings b_k are used as initial conditions [38]. Once the final eigenvalues, DMD modes, and their loadings are obtained, the algorithm proceeds similarly to that of the exact DMD discussed in 2.2.

2.3.3. BOP-DMD Applications

The applications found in the literature for BOP-DMD are very limited being a newly developed technique. However, in the work of Sashidhar and Kutz [38], BOP-DMD was applied to two hypothetical fields to demonstrate the capabilities of the technique. The first field represents a simple fluid flow around a cylinder, the field was created using numerical simulation. The results show the ability of BOP-DMD to stabilize the predicted DMD modes and eigenvalues. The second field or set of data is the sea surface temperature

data over a number of years. The method was used for the purpose of forecasting and proves itself as a pioneering technique in the area of future data prediction. The technique is also discussed in the work of Kutz and Nachbin [21] where DMD has been applied to the pilot wave hydrodynamic system for characterization.

2.4. Conclusion

In conclusion, *Data-Driven Modeling* is the go-to approach when treating complex nonlinear dynamical systems, or when the physical equation is either unknown or very complex to be solved. There are a number of DDM techniques that one can use, the choice of the technique might depend on the application or mostly on the technique's limitations. In this study, our technique of choice is BOP-DMD, a newly developed technique in the field of data science. We intend to test the BOP-DMD method for its capabilities, this is shown in the following section(s).

3 | Experimental Design

Abstract

The safe operation of nuclear reactors under normal and extreme conditions will always be a top priority for scientists and engineers. Among those extreme conditions are earthquakes; an inevitable natural phenomena that require special care from the point of view of nuclear reactor operation. The field of research and experiments on nuclear reactors operating under earthquake (seismic conditions) is unlimited. Among those experiments is one performed at the *ICARE* experimental facility in France, which studies the coolant flow between two PWR surrogate bundles under seismic conditions, and will be the focus of this chapter.

3.1.   Introduction

The study of a nuclear reactor's thermal hydraulics is crucial for safe, stable reactor operation. A Pressurised Water nuclear Reactor (PWR) is the most common nuclear reactor type, according to the report recently published by IAEA [1] on nuclear reactors in the world, there is a total of 303 operational PWR and 48 more under construction, which makes it the most common nuclear reactor type in the whole world. Such abundance in the number of PWRs in the world draws great attention to it. A PWR core, as previously introduced in 1.1, is composed of a number of fuel assemblies where coolant flows from an inlet, moving through the entire core, then to an outlet taking away the core residual heat, that would be later on put to use (ex. electric power generation). The concept of *safe operation* applies to both normal and accidental conditions, this, of course, involves reactor operation under severe natural phenomena like earthquakes. A PWR should be designed to withstand such conditions, hence, the study of the effects of such phenomena on reactor operation is crucial. In the case of an earthquake, there are a number of factors to be taken into consideration from a reactor operation point of view, among which, are coolant flow under seismic conditions and fluid-structure interaction

---

[1]International Agency of Atomic Energy

(FSI).

Unfortunately, works of literature in this area are limited to the study of fuel assemblies under similar conditions[5], hence an investigation of the flow field between two fuel bundles under seismic conditions was of high value. This was achieved by Capanna and Longo [5] where a time-resolved particle image velocimetry (TR-PIV) technique was applied to two dummy PWR bundles under a mimic condition to an earthquake to study fluid flow in between bundles, and fluid-structure interaction (FSI). This thesis work is based on the analysis of the experimental data obtained by Capanna and Longo [5], hence it is only relevant to dedicate this chapter to gain a perspective on the executed experiment and the outcomes.

3.2. Particle Image Velocimetry

Before getting to the experiment, an introduction to the technique applied is necessary. This section briefly discusses the key concepts of *Particle Image Velocimetry* with a special focus on some relevant aspects of the experimental study discussed in this chapter.

3.2.1. Introduction to particle image velocimetry

Particle Image Velocimetry (PIV) is a measurement method (technique) that emerged in 1980_s and has established itself as a leading measurement technique in many fields of science and engineering [35]. The technique is a high-speed measuring technique that is used to record velocity fields for any type of flow. It can be looked at as a method that allows for the visualization of flow fields through the use of illumination and *seed particles*. PIV has undergone many enhancements since it was first introduced in the 1980_s, allowing for better accuracy, enhanced spatial and temporal resolution, and dynamic velocity range. Today, PIV has become capable of recording velocity vectors up to their three components for a flow field within a volume almost at no time with an optimal spatial and temporal resolution [32]. The PIV technique is deployed in many applications also for both analysis and validation purposes [32], for many fields of science and engineering including, fluid dynamics, aerodynamics, oceanography, hydroinformatics, and many more. In this section, we will introduce the working principle of PIV, measurement techniques, image evaluation, and recent applications.

3.2.2.   Principle of Particle Image Velocimetry

Generally, the measurement of an object's velocity is simply recording the distance covered by the object over a certain interval of time. However, calculating the velocity of a certain flow field is much more complicated since the flow field does not contain a visible moving object to calculate its displacement. Before applying direct measuring techniques similar to PIV, the velocity of a given flow was derived from other measurables (ex. pressure) using physical relations. However, such indirect measuring techniques have a set of drawbacks, for one instance they may change field properties incorporating measuring errors. Also, they are limited to deriving velocity at a single location, hence emerged the need for direct optical measuring techniques, and hence the need for PIV [35].

Working Principle: The working principle behind PIV is relatively simple. Imagine having a flow within a volume, since the visualization of this flow is limited, an aiding agent known as *seeding* or *tracer* is used. Typically the tracer is smoke for gaseous fields and a light-reflecting particle (ex. glass beds) for liquid fields. After loading the flow with the seeding particles, a light source, *typically a LASER source*, is used to illuminate the system allowing for flow visualization. A camera is then used to record the motion of the particles that are, in some sense, representative of the fluid motion. Particle motion is recorded by recording the light scattered by the particle on two separate frames (double exposure) or on a number of consecutive frames. Then, a calibration is performed to obtain a relation between image displacement and particle displacement. Once the displacement of the particle is obtained, a post-processing stage starts where invalid measurements are eliminated.

Figure 3.1 shows the typical PIV setup [35]. Seeding particles are added to the non-disturbed flow around a certain plain of interest where the flow is illuminated using a laser sheet two times, between each laser pulse there is a delay time given by Δt, and the choice of this delay time is controlled by the flow velocity and the imaging *magnification* that shall be discussed later. Assuming that the seeding particles move at the local flow velocity, the scattered light by the particles is recorded using a very high-quality lens at two separate frames of a customized *cross-corelation* camera, and the output is recorded on a computer. The recordings are divided into smaller subareas known as *interogation areas* and the local displacement vector for the recorded images of both illuminations is determined for each sub-area through some statistical methods, this is done for all sub-areas of the recordings.
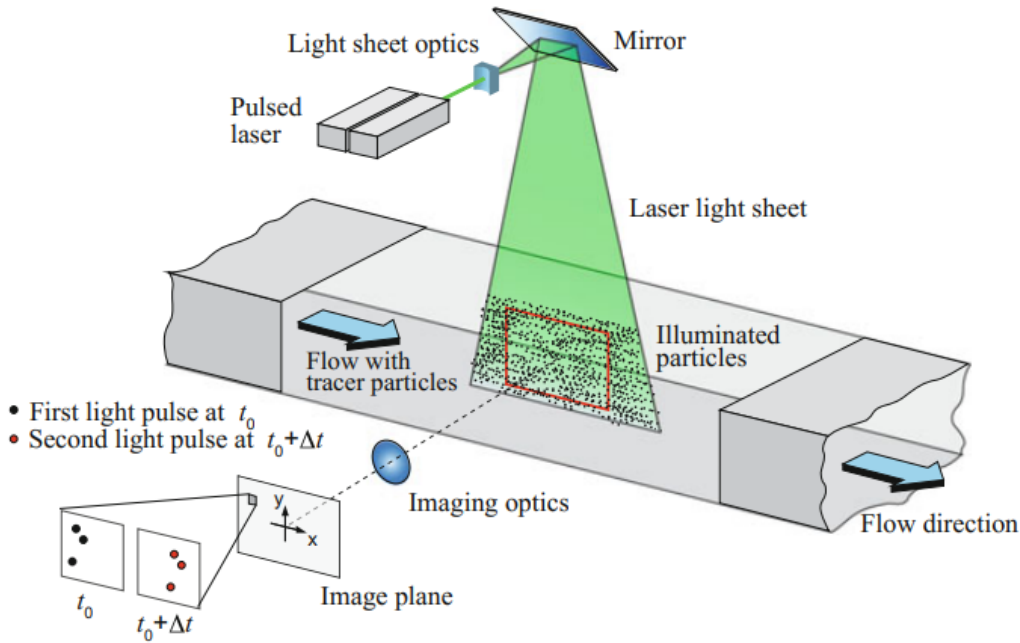
Figure 3.1: Typical PIV setup [35].

PIV is a high-speed measuring technique in the sense that images are recorded at a frequency in the range of KHz and the evaluation time of one PIV recording of many velocity vectors (components) is in the range of one second, such high speed allows for online measurements.

3.2.3.   Measuring considerations

Seeding particles: Tracers are light-reflecting particles that are designed to be large enough to allow for proper light reflection, but also small enough to be easily disbursed in the flow. The distribution of the particles should be homogenous and also the field should pose a uniform density for high-quality measurements. The density of recorded particles per image determines the type of evaluation, for low-density particles per image, evaluation through particle tracing is performed, however, for high-density particles per image evaluation of speckles (clusters of particles) is performed [35] [48].

Light source: Typically lasers in the form of sheets are used during the deployment of PIV. Specifically, Nd:YAG [2] due to its high light intensity. However, since pulsed lasers take time to load pulses, which is usually different from the delay time Δt between two frames, a two-cavity laser configuration is applied and it is shown in figure 3.2. Also, the

---
[2]Neodymium Yttrium Aluminum Garnet

wavelength λ of the emitted light from the Nd:YAG laser is in the infrared range, which is incompatible with the used cameras, hence the wavelength is altered to fall in the range detectable by the cameras [48].
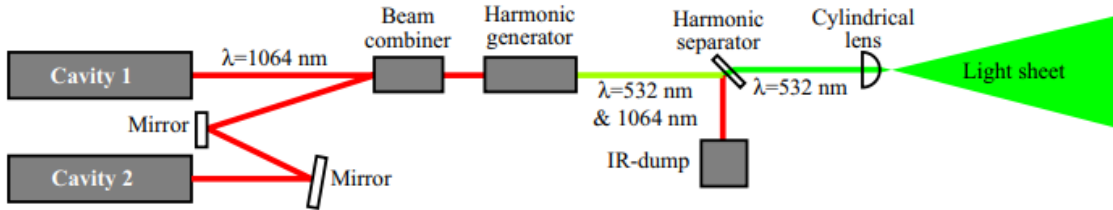
Figure 3.2: Double cavity Nd:YAG PIV-laser [48].

Cameras: The constraints on the used cameras increases with the complexity of the measurement. For high-velocity complex fields or if the recorded area and seed particles are small, advanced cameras are needed. Usually, images are taken within a small Δt, therefore, cameras with short exposure time (or high shutter speed) are required. Today's high-speed cameras' exposure time is in the range of μs. Alternatively, cameras with progressive scan architecture are used for exposure time less than 1 μs. Constraints on PIV cameras are discussed in detail in [48] [35].

3.2.4. Flow velocity evaluation

The main purpose of PIV as mentioned before is to obtain the distance covered by the particle during the delay time Δt and then convert this to a velocity of some sort. This process is known as *Cross-Correlation* [48]. Generally, the relation between the seeding particle velocity and its displacement is given by

$$V = \frac{d}{M\Delta t} \tag{3.1}$$

where V is the velocity, d is the displacement, and M is the image magnification [35]. Cross-correlation functions are used to calculate velocity vectors, they are calculated over each subarea (IA) of the image. This could be explained as selecting which IA displacement can yield the best pattern match and then this displacement would be proportional to the average velocity of the subarea as in 3.1.

The cross-correlation functions (CCF) given in 3.2 are the unbiased one-dimensional CCF for the $M \times N$ point samples A(m,n) and B(m,n); x< M and y<N

$$R_{A,B}(x,y) = \begin{cases} \frac{1}{(M-|x|)(N-|y|)} \sum_{n=1}^{M-x} \sum_{n=1}^{N-y} A(m,n)B(m+x,n+y), & \text{if } x,y \geq 0. \\ \frac{1}{(M-|x|)(N-|y|)} \sum_{m=1}^{M+x} \sum_{n=1}^{N-y} A(m-x,n)B(m,n+y), & \text{if } x < 0, y \geq 0. \\ \frac{1}{(M-|x|)(N-|y|)} \sum_{m=1}^{M+x} \sum_{n=1}^{N+y} A(m-x,n-y)B(m,n), & \text{if } x,y < 0. \end{cases}$$

$$(3.2)$$

Of course, this direct method given in 3.2 becomes less reliable when dealing with larger data sets, hence *Fast Fourier Transform* FFT is used [48]. FFTs allow for a great reduction in the operations from $\mathcal{O}[N^4]$ to $\mathcal{O}[N^2 \log_2 N]$ for two-dimensional correlations [35]. This is helpful when applying CT[3] shown in

$$R_{AB} \Leftrightarrow \hat{A} \cdot \hat{B}^* \tag{3.3}$$

where $\hat{A}$ and $\hat{B}$ are the Fourier transforms of A and B, and $\hat{B}^*$ is the CC[4] of $\hat{B}$. To conclude the discussion on the velocity evaluation, another important concept should be taken into consideration. An actual measurement of the seeding particles' displacement is performed by specifying the location of the highest correlation peak [48]. This is treated through what is called "*subpixel interpolation*". The reason why interpolation is applied is that there is some uncertainty in the detection of peak location in terms of pixels. Subpixel interpolation is performed using a three-point estimator [35]. Imagine the maximum peak is detected at $[i, j]$, also imagine the peak to be Gaussian following 3.4, displacements are calculated as given by 3.5

$$f(x) = C \exp[-(x_o - x)^2/k] \tag{3.4}$$

$$\begin{aligned} x_o &= i + \frac{\ln R_{(i-1,j)} - \ln R_{(i+1,j)}}{2\ln R_{(i-1,j)} - 4\ln R_{(i,j)} + 2\ln R_{(i+1,j)}} \\ y_o &= j + \frac{\ln R_{(i,j-1)} - \ln R_{(i,j+1)}}{2\ln R_{(i,j-1)} - 4\ln R_{(i,j)} + 2\ln R_{(i,j+1)}} \end{aligned} \tag{3.5}$$

---

[3]Correlation Theorem: cross-correlation of two functions is equivalent to a complex conjugate multiplication of their Fourier transforms

[4]Complex Conjugate

3.2.5. PIV Applications

PIV has proven itself as a leading technique among all other direct measuring techniques. Naturally, the technique has undergone a number of enhancements since its development in 1980 improving its accuracy and expanding its capabilities allowing its application in a great number of fields of science and engineering. Following [8] an integration of PIV and DDM techniques was executed for the purpose of systematic data-clustering analysis of a highly complex fluid field. Another study (see [50]) involved applying the analysis of axial flow around a nuclear fuel assembly under seismic conditions.

The comprehensive book on PIV by Raffel and others [35] includes many applications for PIV like applying PIV to transonic flows allowing the execution of non-intrusive measurements. Also, more applications include applying PIV to boundary layers, different flow fields at different temperatures, aeroacoustic and pressure measurements, and much more (see [35] for further details). The experiment on which this chapter is based is another application to PIV and shall be discussed in the next sections.

3.3. Experimental setup

The experiment was performed at the ICARE[5] experimental facility in France, the facility scheme is shown below in figure 3.3. A closed loop of water is driven by a centrifugal pump of 90 KW. The loop's essential components are the test section, a compensation tank, a heat exchanger, temperature and pressure sensors, a hydraulic jack, position sensors, and a flow meter.

The *test section* is a cuboid with a square basis ($22.5 \times 22.5 \ cm^2$) and holds up to four fuel assemblies in a square lattice. The test section is adjusted according to the experiment in hand. It could either be set to a large confinement configuration leaving a space of 8 mm between fuel assemblies and the section walls, or between assemblies. Another possibility is the small confinement leaving a gap of 4 mm. Also the assemblies under testing could be set to one, two, or four assemblies. The *compensation tank* and the *heat exchanger* are both intended to maintain a constant flow temperature throughout the period of the experiment. The *pressure sensors* and the *flow meter* are mainly used to monitor the flow. The *hydraulic jack* is intended to excite one of the assemblies, while the LDTV[6] position sensors record bundle displacement. To permit optical access to the test section, a number of viewports of acrylic are applied[5].

---

[5]ICARE webpage: https://icare.cnrs.fr/
[6]Linear Variable Differential Transformers.
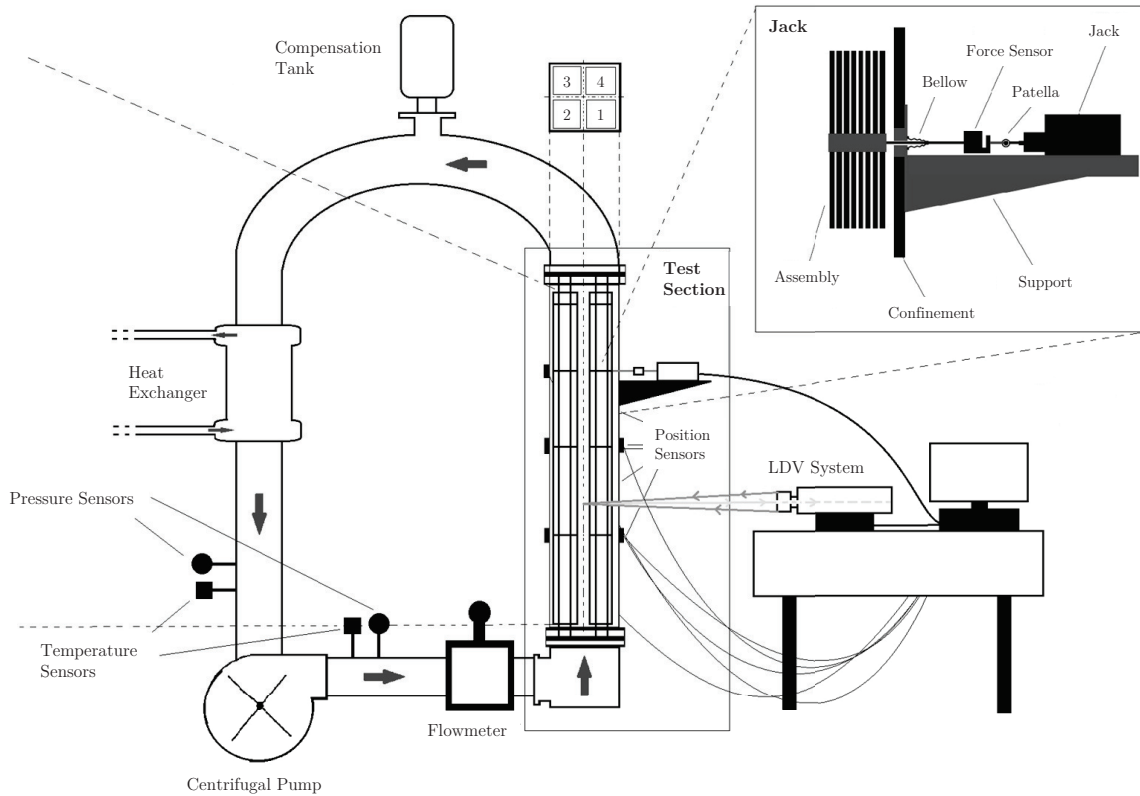
Figure 3.3: ICARE experimental setup.

Depending on the used pump, the flow velocity is kept around 5 m/s to mimic a PWR's typical coolant flow velocity. The test section represents a typical PWR assembly, each sub-bundle is 2.75 m long (almost half that of the typical PWR) and is a square lattice of 8×8 rods. Each lattice includes 60 acrylic[7] rods and 4 stainless steel rods that are welded to 5 spacer grids and nozzles. The rods are 9 mm in diameter (0.5 mm less than a typical PWR rod) and arranged with a pitch-to-diameter ratio of 1.33.

3.4. Experimental procedures

Following the experimental setup described in 3.3, the flow was loaded with high florescent seeding particles with the consideration of seeding particles mentioned in 3.2.3 taken into account, silver hollow glass spheres were used that are $10\mu m$ in diameter. The Illumination source was selected to be a very thin laser sheet. However, some of the present limitations were that if the light source was administrated between fuel bundles, it would interfere with acrylic rods resulting in an unwanted glare recorded on the camera

---

[7]poly-methyl-methacrylate

due to the difference between the refractive indices of acrylic and water. Hence, it was only necessary to, with great care, administrate the light sheet in the test section to avoid interfering with acrylic rods. To achieve this geometric and Gaussian optics theories were applied to obtain a laser beam width that is smaller than the gap between rods [5]. Given the below relations;

$$\frac{f}{W_o} = \frac{2n_{water}}{P - D}$$
$$h_{gap} = \frac{P - D}{2}$$

(3.6)

such that W_o is the initial beam half waist before the focusing of the lens, f is the lens (spherical) focal point, n is the medium refractive index, and h_{gap} is the gap width.

The beam spot size at the converging lens focal point will be finite and will stay within a fraction from this section known as *Raleigh range* Z_R, both are given by

$$W_f = M^2 A \frac{f\lambda}{W_o}$$
$$Z_R = \frac{\pi W_f{}^2}{AM^2\lambda}$$

(3.7)

this implies that the beam width after the focal point of the lens W_f will depend on the focal length f, the beam quality M^2, and the aberrations A imposed by the lens. To apply a safety margin the gap between the bundles is to be set to twice the Raleigh range [5].

Given the relations above, the experiment involved the optimization of both f and W_o. Here it should be noted that since the beam is not perfectly collimated, hence a ray transfer matrix (ABCD) was also included in the calculations (See [5] for further details). Finally, a lens with $f = 200mm$ was chosen and it was tested in air yielding a $W_f = 350\mu m$ that will correspond to a $W_f = 460\mu m$ in the test section [5].

The laser sheet was a typical Nd:YAG (10 W CW frequency-doubled laser) with a vertical $M^2 = 4$ and horizontal $M^2 = 2.6$, high divergence less than 2 mrad. The used camera was a high-speed CMOS with an exposure time between 15 to 30 μs allowing a frame rate of 500 Hz with a resolution of 544 W $\times$ 504 H pixels recording continuously for 2s. The exposure was intended to be short to limit (or even prevent) motion blur for raw images. The used lens was a Nikon 60 mm micro lens with an $\{-stop$ of 4 installed to a 27.5 mm extension achieving a magnification of $M \approx 1.5$. The optical access of the camera was situated between the bundles and the viewports to limit any distortions. After loading the system with seeding particles, the light source illuminates the system and the camera

records the images. The runs are repeated to maximize the number of forcing cycles and achieve acceptable statistical convergence of the averaged data. The PIV cross-correlation algorithm is DAVIS 10.3 from LaVision, Inc. with an interrogation window of 32 by 32 pixels allowing a spatial resolution of 0.4 mm. It should be noted here that there is a level of uncertainty in the obtained data from the lack of use of a calibration target and hence, the results obtained from the experiment are treated as qualitative [5].

3.5. Results

It is essential for this study to discuss the results of this experiment that will lay the ground for the analysis conducted in the following chapters. The time-resolved PIV allowed for the measurement of some important flow parameters such as; flow velocity, vorticity, and turbulent kinetic energy TKE. As previously mentioned, the flow maintained an average velocity of 1 m/s with Reynold's number of $R_e \approx 10^4$. Measurements were carried out mainly below the midplane at around 6 cm in depth from the leading plane of the assembly. The bundles are excited using the hydraulic jack at a 5 Hz frequency with an excitation amplitude of 1.7 mm, resulting in fluctuations in the velocity field due to bundle movement. Following [5], the axial velocity (average) exhibits a profile shown below in Figure 3.4. Those fluctuations are introduced by the bundle displacements introduced by the conditions simulating an earthquake. It can be noted that the severity of the fluctuations depends on the excitation phase. Other physical properties were also analyzed, for example, turbulent kinetic energy (TKE) was calculated using Matlab, which is a good measure of the effect of bundle excitation on the flow, following [5] it is proven that the excitation of one fuel bundle can create some modulations of the axial flow turbulence. It should be noted that the results obtained here are only qualitative, hence a level of uncertainty in the results exists. Quantitative analysis requires the use of spatial calibration targets which was not permitted by the facility design.
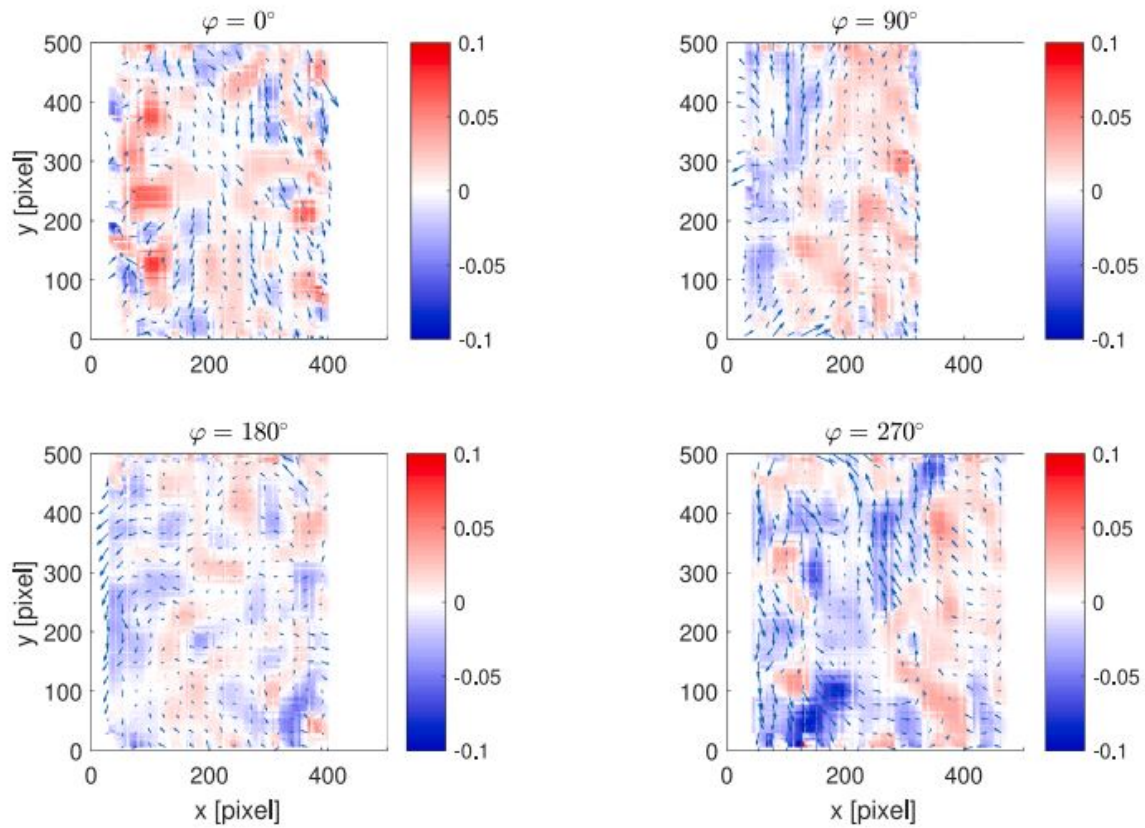
Figure 3.4: Velocity fluctuation field with vorticity background for different oscillation phases [5].

3.6. Conclusion

It is clearly evident that PIV is a leading technique in many applications but specifically in identifying flow structures. The study of PWR hydraulics under different conditions is of great importance in the fields of reactor safety and reactor operations. The ICARE facility hosts a test section that is a replica of a typical PWR assembly and simulates earthquake conditions. The use of PIV in such a configuration allowed for the identification of flow structure and its analysis, it also allowed for the study of the effect of bundle excitations (typical to that of an earthquake) on the turbulence of the flow. The analysis of data obtained from this experiment is used in our analysis and shall be discussed in the following chapter(s).

4 | Methodology

Abstract

This chapter provides an overview of the methodology employed in this study aiming at the investigation of complex fluid field measurements through the use of some DDM techniques. The research design, data acquisition, data treatment, and research considerations utilized in this research work are described to offer some insight into the approaches adopted to reconstruct complex fields. We exploit the advantages of DDM discussed earlier to treat complex fluid measurements to obtain forecasted and accurate field values.

4.1. Data Acquisition and Treatment

The rigorous experiment that produced the analyzed data used in this study has been thoroughly described and laid out in the preceding chapter. The primary source of data for the current study was this experiment, which also served as the basis for the subsequent data analysis. The experimental setup involved careful planning and adjustments to ensure accurate and reliable results. The researchers devised PIV to obtain some insight into the behavior of coolant flow around a typical PWR bundle under seismic conditions, specifically focusing on the effects of excitation amplitudes and frequencies on the behavior of such a complex flow field. These parameters were chosen based on their known significance in influencing the system's response and behavior. Four separate trials, each with a distinct set of excitation amplitudes and frequencies, were conducted to begin the study. These parameters' modifications were carefully chosen to provide a wide variety of potential outcomes and represent the complete range of the system's response. The first experiment used an excitation frequency of 3 Hz and an amplitude of 0.5 mm. This specific setup was chosen to examine the system's reaction to stimulation with a moderate frequency and a relatively low amplitude. By applying this specific oscillation setup, the behavior of the system was observed. In the second setup, the stimulation amplitude stayed fixed at 0.5 mm, but the frequency was increased to 8.06 Hz, in order to test how the system responds to a faster oscillation by increasing the frequency while

keeping the amplitude constant. Moving on to the third setup, the stimulation amplitude was increased to 1.7 mm while the frequency was reduced to 1 Hz. This particular combination allowed the effects of a higher amplitude stimulation at a lower frequency to be investigated. With an intention to test how the system responds to greater input and slower oscillation by changing these parameters. The analysis was most likely focused on understanding the system's ability to sustain greater amplitudes and any potential non-linearities that could occur at this amplitude range. Finally, the fourth experiment had an excitation amplitude of 1.7 mm and a frequency of 14 Hz. The goal of this experiment was to evaluate the system's response to both a larger amplitude and a higher frequency at the same time. It was intended to test how the system behaved under more intense and fast stimulation settings. The analysis of such data would allow for determining the system's stability, analyzing any potential resonance phenomena, and examining the system's dynamic reaction to this amplitude and frequency combination. Overall, these four experiments provided a thorough examination of the system's behavior under a variety of excitation settings. Analysis of the system's dynamic properties, stability bounds, and potential nonlinear reactions by systematically adjusting the excitation amplitude and frequency contributes to a broader understanding of the system and its performance under various operating conditions, allowing for more informed decision-making in practical applications or future refinements.

The obtained experimental measurements were saved as a 3D matrix with dimensions defined by the x-coordinate, y-coordinate, and time steps. The matrix was $46 \times 42 \times 12812$, implying that there were 46 grid points along the x-coordinate, 42 grid points along the y-coordinate, and 12812 recorded time steps. This matrix form allows for the storage and organizing of the domain's measured parameters. The measured data included many velocity field-related characteristics. Each cell in the domain and each time step had these parameters recorded. The parameters were as follows for the four experimental setups:

1. **Instantaneous transversal velocity**: At a particular position and time, this refers to the velocity component perpendicular to the axial direction. It indicates the lateral movement or cross-stream velocity of the flow.

2. **Instantaneous axial velocity**: This is the velocity component in the axial direction, which is parallel to the flow's primary direction. It represents the velocity along the flow's streamlines.

3. **Transversal velocity unaveraged**: This is the instantaneous transversal velocity with no averaging. It provides a more thorough perspective of the flow field's lateral velocity fluctuations.

4. **Axial velocity unaveraged**: This metric, like the transversal velocity unaveraged, captures the immediate axial velocity without any averaging. It enables detailed velocity fluctuations in the streamwise direction to be analyzed.

5. **Vorticity of the velocity field**: The local rotation or swirling motion of fluid components is measured by vorticity. It quantifies the velocity vector's local curl at each point in the flow field. This parameter offers information on the flow's vortical shapes and behavior.

6. **Turbulent Kinetic Energy (TKE)**: The energy associated with turbulent fluctuations in the flow is represented by TKE. It quantifies turbulent motion and offers information about the turbulent features of the flow. TKE is frequently employed as a measure of turbulence intensity and is critical in turbulent flow studies.

The axial velocity field from the first experiment, which featured an excitation of 0.5 mm at 3 Hz, was the primary focus of the investigation. This decision was made to ensure brevity while also allowing for a more in-depth investigation of a given parameter and experimental condition. However, results from the other fields (instantaneous transversal velocity, transversal velocity unaveraged, axial velocity unaveraged, vorticity, and TKE) were also used for comparison. These additional findings enabled us to examine and compare the behavior of numerous parameters across trials, resulting in a full understanding of flow dynamics under diverse excitation circumstances.

In the data treatment stage of the analysis, two techniques were applied to the previously described data matrices: exact dynamic mode decomposition (DMD) and bagging optimized DMD (BOP-DMD). These techniques were employed to compare their effectiveness and to highlight the advancements offered by BOP-DMD over exact DMD. A prominent method for extracting coherent structures and dynamic patterns from complicated and high-dimensional data is the discussed earlier dynamic mode decomposition (DMD). It divides the data into spatial modes that correspond to distinct temporal dynamics. In this analysis, the data matrices were first subjected to exact DMD. Exact DMD seeks to determine the system's dominant modes without any additional modifications or enhancements. However, the bagging-optimized DMD (BOP-DMD) technique was also used to improve the accuracy and robustness of the study. BOP-DMD is an improved version of DMD that uses ensemble learning and bootstrap aggregation (bagging) to refine the results. Bagging entails resampling the data to create several subsets, applying DMD to each subset, and then aggregating the results. This ensemble method reduces the impacts of noise and uncertainty in the data, resulting in more dependable and precise mode identification. The analysis attempted to compare the performance of these techniques

and emphasize the advantages of BOP-DMD over exact DMD. BOP-DMD improves robustness against noise and uncertainty, as well as accuracy in recognizing the system's underlying dynamic modes. The use of BOP-DMD can provide more detailed insights into flow dynamics and allow for a better comprehension of the data's coherent structures and temporal patterns. The investigation aims to emphasize the importance of using more complex and sophisticated techniques in data treatment by highlighting the advancements of BOP-DMD over exact DMD. These developments have the potential to dramatically improve the accuracy and reliability of analysis results, resulting in a better knowledge of the system's behavior and useful insights for future study or practical applications.

4.2.   DMD Code Implementation

Following the data collection and treatment phases, the investigation began with the use of the exact Dynamic Mode Decomposition (DMD) algorithm, which was made possible by the creation of a custom MATLAB code, a widely established and frequently used programming language in the scientific world. DMD was chosen as the foundation for subsequent analysis because it is generally acknowledged as an effective tool for extracting dynamic patterns from complex data. DMD provides vital insights into the underlying dynamics of the system by decomposing the data matrix into its constituent modes. The first stage was to apply Singular Value Decomposition (SVD) to the data matrix, specifically the instantaneous transversal velocity data matrix, calling it V_y. SVD is a fundamental matrix factorization technique that aids in the identification of singular values, left singular vectors, and right singular vectors. The analysis intended to establish the ideal rank or a number of modes to which the system would be reduced by examining the singular values acquired by SVD. The singular values were important in calculating the rank because they quantified the relevance of each mode. The analysis attempted to determine the number of modes required to accurately depict the system's dynamics by examining the singular values in relation to their magnitudes. This decision was critical since it directed later studies and interpretations. Once the rank was determined, and following the DMD algorithm explained earlier in 2.2.3, the data matrix was subjected to the exact DMD technique. The data matrix was divided into two parts in this algorithm: the first half represented the current data matrix, marked as X, while the second half represented the future data matrix, denoted as X'. This split made it easier to compute the mapping matrix A, which would then be decomposed to get the eigenvalues and eigenvectors necessary to calculate the DMD modes. The computation of the DMD modes enabled the retrieval of the time dynamics of the system. Each mode indicated a unique temporal behavior inherent in the data, allowing the analysis to find hidden patterns

and coherent structures. The DMD modes provided a simple depiction of the system's dynamics, allowing for the identification of dominant modes and providing insights into the system's developing nature over time. Furthermore, the availability of DMD modes provided options for projecting the system's future states. It became possible to project the system's behavior beyond the existing data by using the temporal information contained in the modes. This forecasting skill had profound implications for domains ranging from fluid dynamics to climate modeling, allowing researchers and practitioners to make accurate forecasts and anticipate future system states. Specifically, applying DMD to our study, enabled us to gain some insights into the method. In the next section, we will discuss those insights.

4.2.1. Methodological considerations

Singular value decomposition: Singular Value Decomposition (SVD) is a sophisticated mathematical approach for decomposing matrices into their constituent components. It provides useful insights into the data's structure and relationships, making it a popular choice for a variety of applications. When it concerns 3D matrices, however, doing SVD explicitly in MATLAB presents some difficulties. Because MATLAB's integrated SVD function is intended to handle two-dimensional matrices, applying it straight to three-dimensional matrices is not supported. This restriction is due to the fundamental characteristics of SVD and its mathematical structure. Despite this constraint, researchers and practitioners have developed different techniques to overcome it and apply SVD to investigate 3D matrices. One popular method is to reshape the 3D matrix into a 2D matrix yet retain the spatial information. Concatenating or rearranging the dimensions of the 3D matrix to generate a 2D matrix with a different structure can accomplish this. By restructuring the data in this way, classic SVD methods meant for 2D matrices can be used. This is the approach followed in this thesis study. It is crucial to note, however, that converting a 3D matrix to a 2D matrix may present certain issues and considerations. The reshaping procedure must be carefully designed to preserve spatial linkages and consistency within the data. Furthermore, the reshaping operation may raise computational and memory demands, particularly for large-scale 3D matrices. Alternative decomposition algorithms that are better suited for higher-dimensional data might be favored over classic SVD in some instances. Tensor decomposition methods, such as Tucker decomposition or higher-order singular value decomposition (HOSVD), for example, are specifically developed to handle multi-dimensional data structures such as 3D matrices. These techniques take advantage of tensors' intrinsic structure to extract significant components and capture underlying patterns in data see [18]. Hence, while running SVD on

3D matrices directly within MATLAB is not supported, there are alternate methodologies and particular methods available to analyze and decompose such data structures. To handle higher-dimensional data, these approaches frequently include restructuring the 3D matrix into a suitable 2D form or applying tensor decomposition algorithms. Researchers can still get useful insights and extract relevant information from 3D datasets by exploiting these methodologies, allowing for further analysis and interpretation in a variety of disciplines.

Rank choice: A major aspect of establishing the dimensionality of the low-dimensional space is the energy content corresponding to each eigenmode of the matrix. One can make informed choices about the number of modes to retain for their analysis by analyzing the eigenmodes and their associated energy contributions. The associations between the eigenmodes and the inverse of their energy content are graphically shown in Figure 4.1. An eigenmode's energy content indicates the percentage of total energy or variability in the data recorded by that mode. Higher-energy modes contribute more to the overall dynamics, whereas lower-energy modes contribute less. As more modes are studied, the cumulative energy content can be calculated by studying the relative contributions of the eigenmodes. In the context of this study, an appropriate number of modes is defined by reaching an energy content of around 90%, ie, an inverse of 10%. This criterion was used to find a compromise between collecting a significant percentage of the data's variability and lowering the problem's complexity. One can acquire a compact depiction of the underlying dynamics while avoiding information loss by keeping modes that collectively account for a significant percentage of the energy content. The dimensionality of the low-dimensional space is determined by the precise value of 90% energy content. Once this level is achieved, additional modes may only contribute minimally to the overall energy content, making them less important for the investigation at hand. One can confidently identify the number of modes to retain by evaluating the eigenmodes in relation to their energy contributions, substantially lowering the complexity of the problem without surrendering critical information.
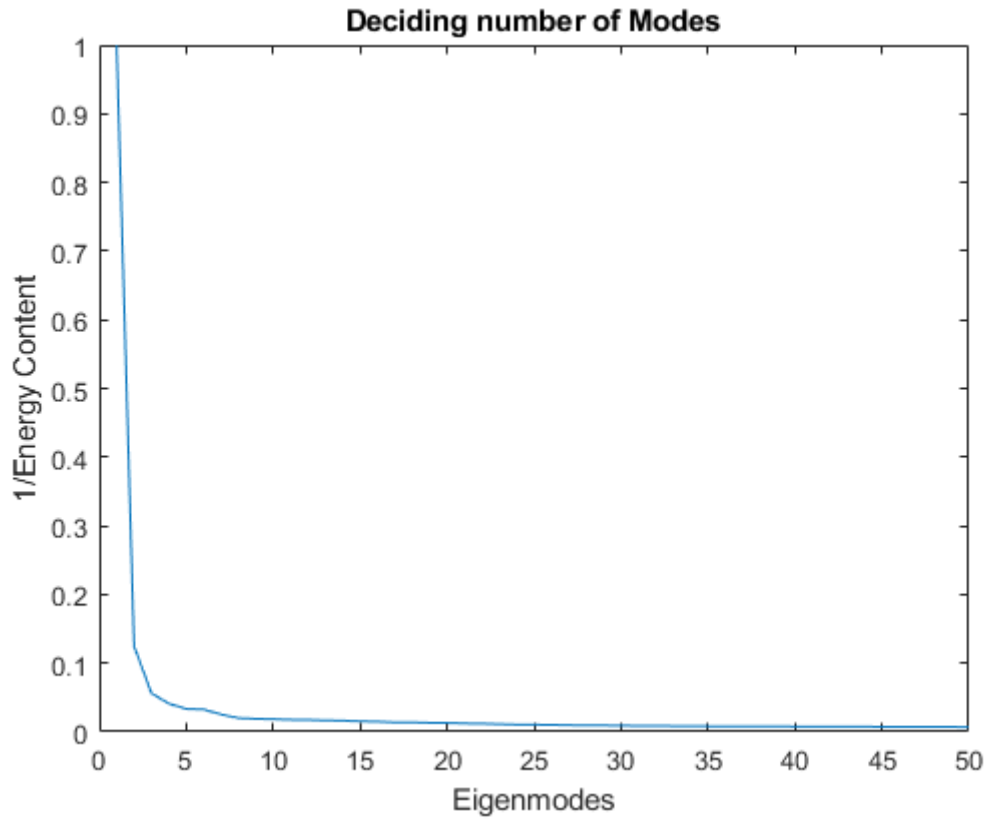
Figure 4.1: Eigenmodes of the instantaneous transversal velocity V_y V.s. the inverse of their energy content

It should be noted that the acceptable energy content level, such as 90%, may differ based on the individual application and the intended trade-off between dimensionality reduction and information retention. One may test multiple thresholds to determine the sensitivity of their study results and strike an optimal balance. In conclusion, by evaluating the matrix's eigenmodes and their related energy content, researchers can make informed selections about the number of modes to retain for their investigation. As illustrated in Figure 4.1, achieving roughly 90% energy content serves as a criterion for establishing the dimensionality of the low-dimensional space. This method effectively reduces dimensionality while keeping a considerable percentage of the data's variability, allowing for a more concise description of the underlying dynamics.

4.2.2. Dynamic mode decomposition of noisy fields

While Dynamic Mode Decomposition (DMD) is a useful method for evaluating dynamic systems, its limitations must be considered, especially when working with noisy data. Data that contains random or undesirable fluctuations, measurement errors, or disruptions

that can conceal the fundamental trends and dynamics of the system is referred to as noisy data. Noisy data can have a variety of impacts and issues in the context of DMD. One disadvantage of DMD is that it expects linear and noise-free data. This is a critical assumption for accurate mode decomposition and reconstruction. However, in real-world applications, different sources of noise, such as measurement errors, outside influences, or inherent system unpredictability, are pervasive. A high level of noise may cause problems with the recognition and extraction of the fundamental coherent structures and modes when noisy data is given into the DMD algorithm, resulting in erroneous findings. The data used in the current study are drawn from experimental measurements, and not numerical simulations, hence they are characterized by high noise which is uncontrollable.

The inclusion of noise in the data can produce false modes or distort the recognized modes, jeopardizing the analysis's credibility. These false modes may occur as a result of noise components being misidentified as coherent structures, leading to incorrect interpretations of the system's dynamics. Furthermore, noise can impair the accuracy of mode amplitudes, frequencies, and phase correlations, making it difficult to extract significant information from the DMD analysis see 3.5.

Several strategies can be used to reduce the impact of noise on DMD analysis. Pre-processing the data with noise reduction or filtering methods to lower the noise content while maintaining the relevant dynamics is a typical strategy. Signal smoothing, denoising methods, and adaptive filtering procedures are examples of these techniques. One can improve the accuracy and reliability of the DMD analysis by lowering the noise level. Two different denoising methods were followed in this study and will be discussed later.

Incorporating regularization techniques is another strategy for dealing with noisy data in DMD. Regularization approaches constrain the DMD algorithm in order to encourage smooth and physically relevant modes while suppressing noise. Regularization allows the method to distinguish between coherent modes and noise components, resulting in enhanced mode identification and reconstruction see [9]. It should be noted that, while noise reduction and regularization techniques can be advantageous, they should be used with caution. Over-filtering or excessive regularization of data might result in the loss of important dynamics and information. To guarantee accurate findings, the correct balance between noise reduction and keeping the system's features must be found. Furthermore, it is worth noting that DMD has intrinsic limits when dealing with nonlinear and non-Gaussian noise. Nonlinearities in the data might cause deviations from the linear assumptions of DMD, thereby impacting the mode decomposition's accuracy. Furthermore, non-Gaussian noise with heavy-tailed distributions can make estimating mode amplitudes and frequencies difficult.

To summarize, noisy data makes DMD application difficult. In real-world circumstances, the assumptions of linearity and noise-free data are violated, resulting in potential mistakes and false modes in the analysis. However, the impact of noise can be decreased by using proper noise reduction techniques, regularization procedures, and careful evaluation of the data's features, allowing for more reliable and accurate DMD analysis. To extract significant insights from the DMD analysis, it is critical to find a balance between noise reduction and keeping important dynamics.

4.3.   BOP-DMD Code Implementation

The use of the BOP-DMD code in this investigation demonstrated this study's commitment to using state-of-the-art data analysis methodologies and technologies. Compatibility, stability, and accessibility throughout the analysis process were assured by building the code in MATLAB similar to the exact DMD discussed earlier. The BOP-DMD code contained a wide range of capabilities that were specifically developed to use the strength of the BOP-DMD algorithm discussed earlier (see 2.3.2. The code used a modular framework that allowed for the easy integration of multiple procedures such as data pretreatment, dimensionality reduction, and mode extraction. This modular design provided flexibility and ease of customization, allowing us to tailor the code to the experimental setup in hand and the research goals. The ability of the BOP-DMD code to exploit the benefits of singular value decomposition (SVD) for dimensionality reduction was a critical feature. Similar to the exact DMD, the code efficiently decomposed the matrix into its constituent components by applying SVD on the data matrix V_y, capturing the most significant modes and lowering the dimensionality of the dataset. This step was critical in simplifying the following analysis and improving the results' interpretability. Similar to the exact DMD algorithm, the BOP-DMD code proceeded to determine the dimensionality of low-dimensional space. The algorithm proceeded with the seeding parameters obtained from the optimized-DMD code being initialized. These initial values were used to kick off the iterative process. The code adjusted the seeding parameters in each cycle depending on the current estimation of the DMD eigenvalues, modes, and loadings. The code was intended to converge toward a more accurate depiction of the system's behavior by continuously refining these parameters. The algorithm identified the ideal number of modes required to capture the system's key dynamics by analyzing the matrix's eigenmodes and their related energy content, allowing us to obtain a compact representation of the data while keeping the crucial information hidden within it.

The BOP-DMD code also provided the liberty of parameter selection, allowing us to fine-

tune the analysis depending on the individual objectives and limits of the study. The
number of cycles (trials) and randomly selected column indices (see 2.1) were chosen to
achieve a compromise between computational efficiency and capturing the main elements
of the data. We were able to optimize the algorithm's performance through an iterative
process of parameter adjustment, resulting in more robust and accurate findings.

4.3.1.   Parameter Selection and Optimization

To accomplish the most precise and effective analysis possible using the BOP-DMD
method, the parameters of the algorithm were carefully chosen and optimized. The num-
ber of cycles (trials) and the number of randomly selected column indices were two critical
characteristics thoroughly investigated in this study. The number of iterations conducted
during the BOP-DMD analysis is represented by the number of cycles k. It specifies
how many times the algorithm is run, allowing estimation of the dominant modes in the
data. The number of cycles in this investigation was set at 100. This value was chosen
through a trial and error approach in which different cycle values were tested repeatedly
and their impact was evaluated on the quality of the results. The goal was to achieve a
compromise between getting precise mode estimates and minimizing the computational
expense of running more cycles. Similarly, the number of randomly chosen column indices
p was critical in the analysis. These column indices indicate the randomly chosen spatial
positions in the data matrix for the BOP-DMD computations. The computing overhead
can be greatly decreased while still capturing the basic dynamics of the system by pick-
ing a subset of column indices. The number of randomly selected column indices in this
investigation was determined to be 50. Again, this decision was made iteratively, with
numerous numbers being examined and reviewed to obtain the best mix of accuracy and
computational efficiency. It is important to note that the values of these parameters may
differ based on the unique dataset, research aims, and computational resources available.
The selection process detailed in this study can be enhanced and optimized in future
investigations based on the specific qualities and limits of the data being evaluated.

4.3.2.   Handling Non-linearities in Data

Non-linearities must be considered when analyzing experimental data since they might
have a major impact on the accuracy of the results. Non-linearities are departures from
linear associations between variables in which the result does not vary in proportion to
the input. These non-linear effects might be caused by turbulence, boundary conditions,
or complex physical phenomena. Non-linearities in data must be handled carefully, as
ignoring them might lead to incorrect interpretations and predictions. It is crucial to

note, however, that the BOP-DMD algorithm used in this study is primarily intended for linear systems. As a result, it does not explicitly account for data non-linearities.

Some presumptions were made during the investigation to limit the potential impact of non-linearities. The most important assumption was that the non-linearities in the treated data would be ignored. This decision was made due to the emphasis on investigating the capabilities of the BOP-DMD algorithm and its performance in capturing the system's linear dynamics. The investigation attempted to provide insights into the algorithm's capability under simplified linear conditions by ignoring non-linear effects. This is known as *local linearity assumption* where DMD makes the assumption that the system's dynamics are locally linear between consecutive snapshots. The algorithm can nevertheless provide useful insights into the underlying dynamics of the non-linearities in the data that are not too high or if they can be locally approximated by linear behavior.

While the local linearity assumption appears to be a potential approach for dealing with non-linearities in DMD, further analysis and optimization are required in future studies. The algorithm's performance in capturing non-linear dynamics can be improved by integrating the local linearity assumption and segmenting the data into smaller sections, resulting in more accurate predictions and reconstructions.

4.3.3. Fields reconstruction and validation

The reconstructed field was obtained through the BOP-DMD algorithm discussed in 2.3.2. The reconstructed field approximates the original field of axial velocity. It captures the data's dominating spatial and temporal patterns, providing a description of the system's dynamics. Validation of the algorithm's performance can be accomplished by comparing the reconstructed field to the original field of axial velocity. The validation process entails evaluating the accuracy of the reconstructed field by comparing it numerically and qualitatively to the original field. To assess the level of agreement between the two domains, numerous indicators and visualization techniques can be used. Measures such as root mean square error (RMSE) (adopted in this analysis), correlation coefficients, and visual assessment of spatial and temporal patterns may be incorporated.

By comparing the reconstructed field to the original field, insights regarding the algorithm's capacity to capture the underlying dynamics and recreate the basic components of the data can be obtained. It allows for the evaluation of the reconstruction's quality and fidelity, which is critical for ensuring the dependability of following forecasting or analysis opportunities that depend on the reconstructed field. Validation results are discussed in the next chapter.

4.3.4.   BOP-DMD of noisy fields

BOP-DMD has been considered an improved variant of exact DMD, especially when dealing with noisy fields. Its improved noise handling capabilities originate from its ability to integrate randomization in data point selection and execute an iterative process to develop the DMD modes and eigenvalues. Despite the inherent noise robustness of BOP-DMD, additional noise filtering techniques were used in this analysis to improve the quality and accuracy of the results. Noise filtering techniques are critical in reducing the impact of noise on data and enhancing the quality of the reconstructed field. Before running the algorithm, noise filtering techniques (discussed in the next section) were applied to the data in the context of BOP-DMD. The goal was to limit the effect of noise on the DMD analysis, resulting in more accurate predictions and reconstructions. It should be noted here that while BOP-DMD provides inherent noise robustness, the use of noise filtering techniques is still advantageous, especially when dealing with highly noisy fields. The combination of BOP-DMD's noise resilience and noise filtering approaches results in a more robust and accurate analysis, especially when the noise level is high.

4.4.   Denoising approaches

When dealing with noisy datasets, noise filtering is a critical stage in data analysis and processing. Noise can produce spurious fluctuations and distortions that obscure the underlying signals and make accurate analysis difficult. To solve this difficulty, different noise filtering algorithms have been devised and implemented, with the goal of reducing noise while improving data quality and reliability. Two denoising approaches were followed in this analysis:

Fast Fourier Transform (FFT): The Fast Fourier Transform (FFT)-based de-noising method is a popular noise filtering technique. The FFT technique decomposes a signal into its frequency components, offering an understanding of the data's spectral characteristics. The FFT-based approach to noise filtering uses the frequency-domain structure of the data to detect and suppress noise components. The following steps are involved in the de-noising process. The noisy signal is first converted into the frequency domain by the FFT technique. The energy distribution across different frequency components is then revealed by computing the power spectrum. The noise components, which are often distinguished by their high-frequency content, are recognized based on their divergence from the underlying signal's expected spectral properties. These noise components are then muted or eliminated while the important signal components are preserved.

The noise in the processed data in this study can be attributed to two main sources: systematic noise from the measuring equipment and arbitrary noise from the lack of a calibration target during the experiment. Both sources add to the total noise level in the recorded data, as well as the introduction of spurious fluctuations and abnormalities. The FFT method, applied in this study, analyzes the frequency content of a signal, providing significant insights into the data's spectrum features. The presence of smaller peaks beside the dominant peak can be seen by inspecting the power spectral density (PSD) plot against the frequencies. These small peaks in the PSD graph correlate to data noise components. These noise components are often distinguished by their higher frequencies and can be linked to a variety of sources, including electrical interference, sensor noise, and other external influences. These minor peaks relating to noise were discovered and removed to reduce noise and improve the accuracy of the reconstructed fields. Figure 4.2 depicts the PSD plotted against frequencies as a visual representation of the noise in the data. Minor peaks representing noise can be seen alongside the center peak, which reflects the dominating signal.
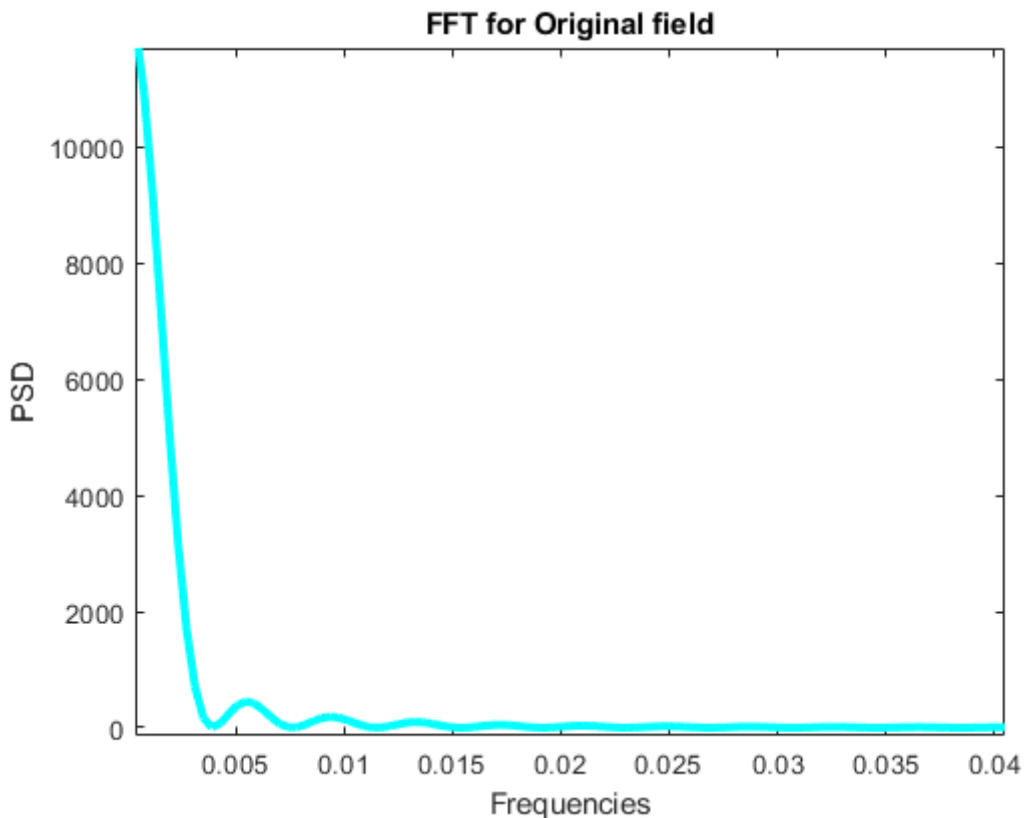
Figure 4.2: PSD vs. Frequencies for the axial velocity field

It is essential to note that the particular cut-off criterion for removing noise components

may differ depending on the data characteristics and the desired level of noise reduction. The thresholds or cutoff frequencies should be carefully selected based on the analysis's unique requirements and the nature of the noise in the data.

Figure 4.3 shows both reconstructed and original fields in the presence of noise and after de-noising; clearly, the reconstructed field shows better agreement with the original field after de-noising was done.
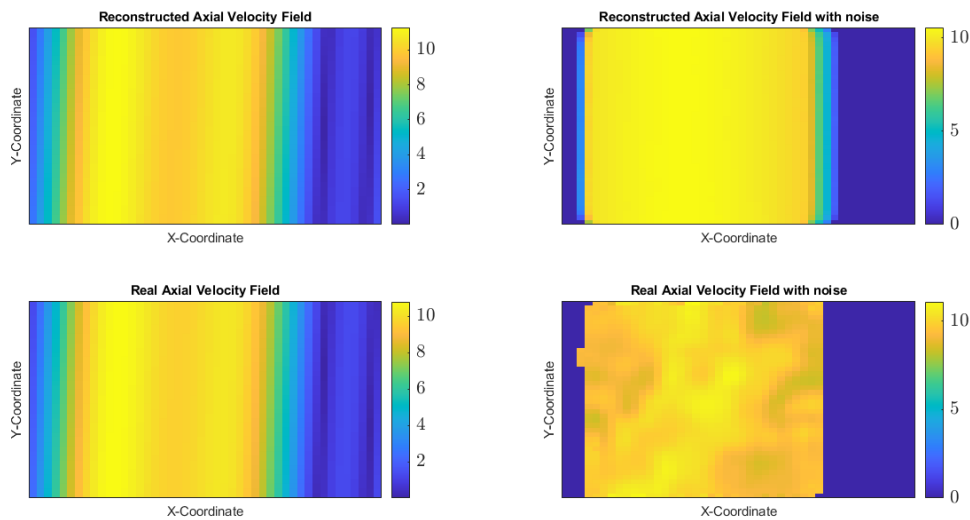
Figure 4.3: Reconstructed and original fields in the presence of noise (right) and after de-noising (left).

Wavelet analysis: In addition to the FFT-based de-noising technique, wavelet analysis was used to test and confirm the noise filtering results. Wavelet analysis is a strong tool that examines signals in both the time and frequency domains at the same time, making it especially effective for evaluating signals with non-stationary properties. Wavelet analysis works by decomposing a signal into a set of wavelet functions at various scales, allowing for the detection of localized characteristics and fluctuations in the signal at various temporal and frequency resolutions.

Figure 4.4 shows the wavelet analysis of the axial velocity field (one of the fields analyzed in this study), we can see here that it was suitable to approximate (decompose) the signal to a group of square-shaped functions known as *Haar wavelet*. The choice of the function to which the signal is approximated depends entirely on the signal itself.
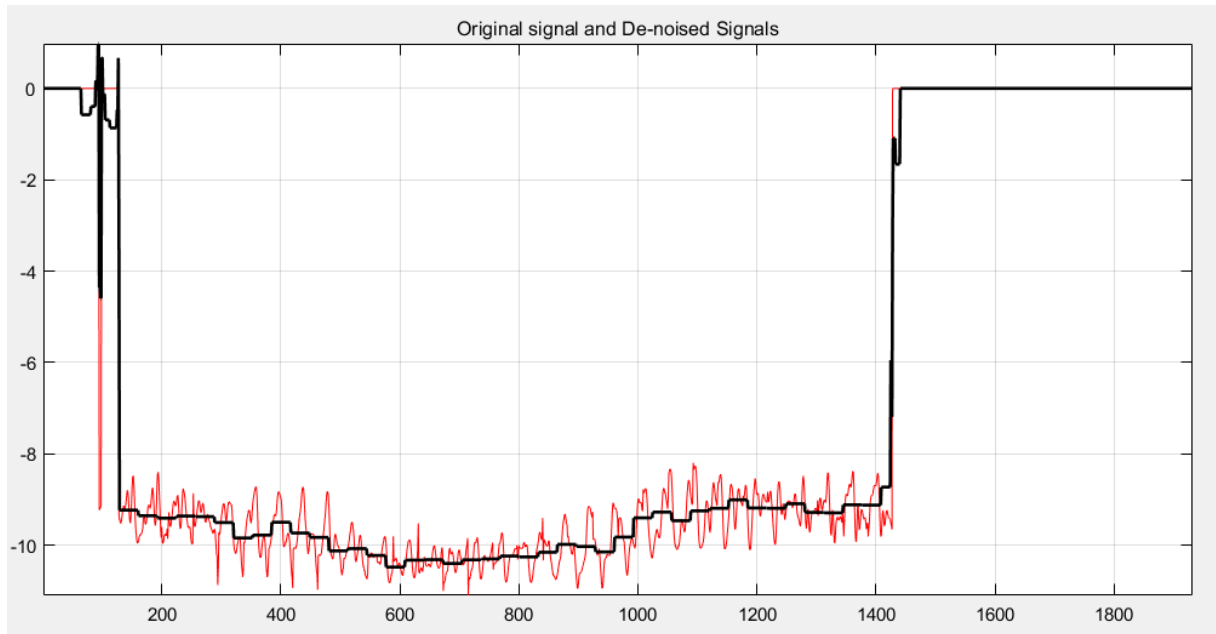
Figure 4.4: Wavelets Analysis.

Further insights into the noise characteristics and their impact on the data can be obtained by applying wavelet analysis to the reconstructed fields. The wavelet analysis gave more details about the noise content in the reconstructed fields. It gave a thorough picture of how the noise components are spread across different scales or frequencies, in particular. It was feasible to identify and quantify the contribution of noise at different degrees of resolution by studying the wavelet coefficients at different scales. The wavelet analysis supported the FFT-based de-noising technique by providing a distinct perspective on the noise in the data. The validity and reliability of the noise filtering procedure might be tested by comparing the results obtained from both approaches. Consistency between the two assessments would increase confidence in the success of the noise reduction strategies used. Results from both techniques are shown in the next chapter for comparison.

4.5. Conclusion

In this chapter, the approach used in this work to analyze and process experimental data was described. The DMD method, both exact DMD and BOP-DMD, provided useful insights into the dynamics of the system under study. The dimensionality of the low-dimensional space was calculated by applying SVD to the data matrices, allowing for a reduced issue formulation and enhanced fit. The BOP-DMD algorithm implementation provided considerable advantages over exact DMD, especially when dealing with noisy fields. The technique's iterative nature, along with the use of seeding parameters

from the optimized DMD algorithm, improved the accuracy and resilience of the results. Furthermore, noise filtering techniques like FFT-based de-noising increased the level of accuracy of the reconstructed fields, increasing the reliability of subsequent analyses. Overall, the methods offered in this chapter provide a thorough framework for interpreting experimental data and gaining significant insights into system dynamics. The use of DMD algorithms, noise filtering techniques, and a well-designed experimental setup enabled accurate data reconstruction, prediction, and analysis. These findings serve as the framework for the following chapters, in which the findings will be addressed in depth and compared to gain further insight.

5 | Results and discussion

Abstract

The study of the flow fields of a PWR under seismic conditions is the main objective of this thesis work. This is through adopting a progressive data-driven modeling approach known as BOP-DMD. To the author's knowledge, this is the first tested application to the newly established modeling technique, BOP-DMD. In this chapter, findings from applying both exact DMD and BOP-DMD are displayed and discussed in detail with the intention of highlighting the capabilities of both techniques. Also, all the obstacles faced while performing this analysis are discussed in order to gain a wider perspective on the proposed methodology of this study.

5.1.   Introduction

This chapter presents the results and analysis obtained from the application of the proposed methodology for the assessment and modeling of the axial velocity field (and others) in pressurized water reactors (PWRs) under seismic conditions, involving the exact Dynamic Mode Decomposition (DMD) and the Bagging-Optimized Dynamic Mode Decomposition (BOP-DMD). The constraints discovered in the classic DMD method when handling noisy data motivated the development of the enlarged BOP-DMD approach. The critical step of determining the proper rank for data reduction in DMD and BOP-DMD is described. The rank determination is critical in accurately capturing the system dynamics and ensuring the dimensionality of the reduced space is sufficient. The following sections of the chapter examine the axial velocity field using both DMD and BOP-DMD techniques. First, the precise DMD approach is used to reconstruct the field, displaying the reconstructed flow patterns. The limitations of such a technique are displayed along with some attempts to enhance the findings. The findings of applying BOP-DMD are then displayed and discussed, along with the denoising attempts and the effect of noise on the results.

Other fields than axial velocity are also analyzed and their results are displayed as an

assurance of the applicability of BOP-DMD on different data fields. Also, the analysis was extended to include the reconstruction of the vorticity field from the original velocity field, which further confirmed the capabilities of such a leading data-driven modeling technique.

A summary of the findings drawn from this thesis work is published in the NURETH-20 conference [1] [14].

5.2.   Analysis of the Axial Velocity

In this study, we chose the axial velocity field (V_y) obtained as a direct measurement from the experiment discussed in 3.1 of the first experimental setup (excitation at 0.5 mm and 3 Hz) as our primary field around which the analysis is centered, the field is used to test the proposed methodology (see 4). This field was particularly chosen as it was foreseen to achieve the best outcome possible in the matter of testing the methodology. As shown in figure 5.1 the axial velocity field yielded the lowest dimensionality upon reduction, and the reason for this is expected to be that the field incorporates the minimum percentage of noise components.
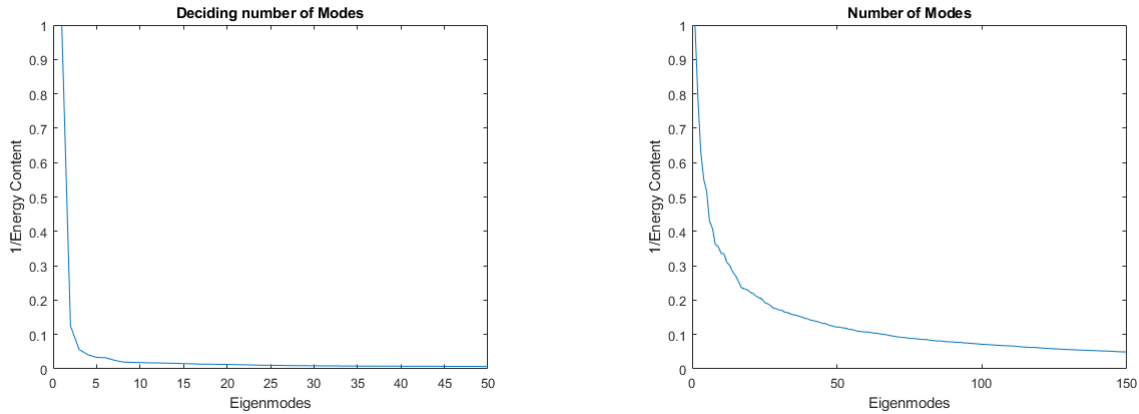
Figure 5.1: Rank choice of V_y (left) and V_x (right)

Figure 5.1 shows the eigenmodes plotted against the inverse of the energy content of both the axial velocity field V_y and the transversal velocity field V_x. As can be seen from the plot, the axial field reaches an energy content of 90% at 3 eigenmodes while the transversal field reaches the same value at almost 75 modes. This implies that the axial velocity field can be reduced to 3 essential modes whilst maintaining 90 % of the information it holds, while the transversal one needs almost 25 times more eigenmodes.

---

[1]Topical Meeting on Nuclear Reactor Thermal Hydraulics

Clearly, the axial velocity would be the field of choice since it compasses a significantly lower computational time and accordingly would greatly facilitate the analysis and the validation process. Figure 5.2 shows a 2D representation of both axial and transversal velocities taken at a fixed point in time (T=1), the figure clearly emphasizes the difference between both fields. For the axial velocity field, while keeping in mind that the flow is in the axial direction, The plot shows a null axial velocity field at the peripheral regions and then follows a decreasing behavior and then a semi-constant one at mid regions. The semi-constant behavior is quite reasonable since the plot was taken at an initial time point where the flow field wouldn't have acquired enough momentum to show variations in its axial velocity. On the other side, for the transversal velocity field, there is still a null value of the transversal component near the peripheral regions, however, for the mid-region, the fields exhibit random fluctuations, which is a clear measure of the turbulent characteristics carried by this component.
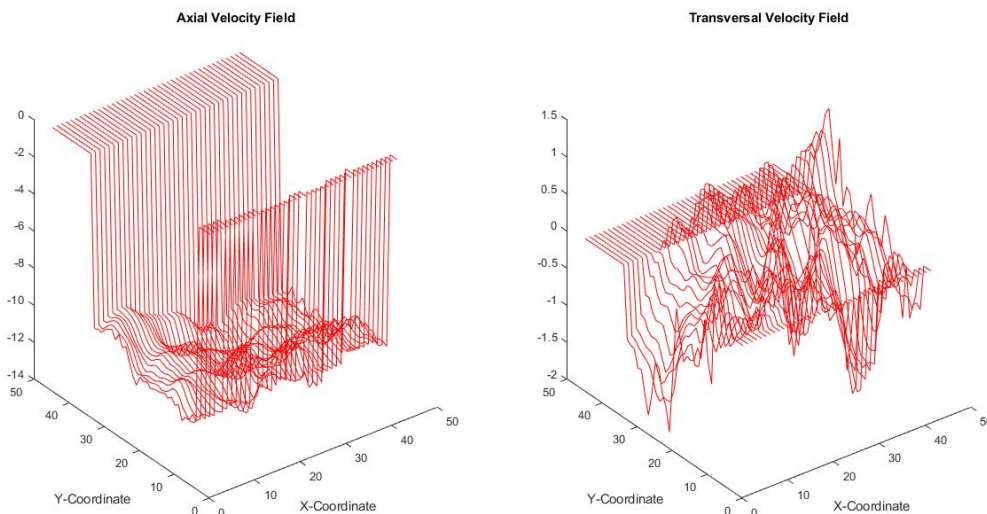
Figure 5.2: 2D Representation of the Axial and Transversal Velocity Fields (T=1).

Figure 5.3 is the same as figure 5.2 but taken at a later time point (T=1000), at this time step, it is clear that the flow has acquired enough momentum that even the axial velocity exhibits clear fluctuations, this is highlighted in the next section when closely studying the axial velocity field. For the transversal field, even stronger fluctuations are noted at such a time step.
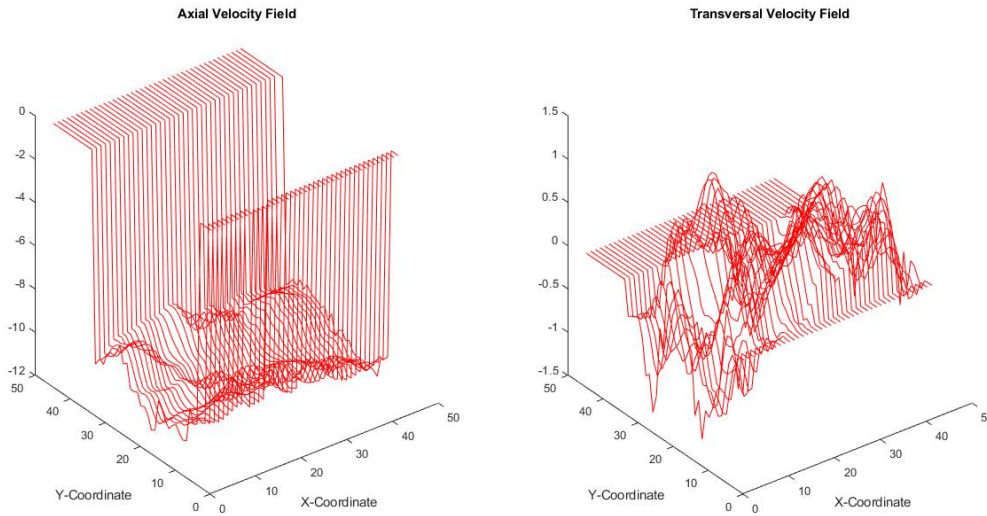
Figure 5.3: 2D Representation of the Axial and Transversal Velocity Fields (T=1000).

The relatively high number of modes obtained at 90 % energy content of the transversal velocity field (see figure 5.1) only means that the field exhibits a more random behavior, i.e. this is the velocity component that carries the turbulence characteristics of the flow, and it only makes sense, since the flow is in the axial direction. It should be noted here that the choice of such an acceptable value of energy content is purely optional, and it may depend on the application on hand. For example, a lower value may yield less accurate results, while a higher value only imposes a higher computational time and overfitting of the data, hence compromise is necessary. The analysis of complicated fields like the transversal velocity is still possible and is included in the study, results are shown near the end of the chapter.

5.2.1. Field Reconstruction Using DMD

The first stage of this analysis was to study the applicability of the DMD method described earlier, the technique shows a proven utility in literature, and it was only relevant to test it on the flow fields in hand. After landing on the axial velocity field as the field of choice, the analysis started with reducing the field to the low dimensional space and then proceeded with the production of the DMD modes and the reconstruction of the field. The reconstructed field was then compared to the original field for validation.
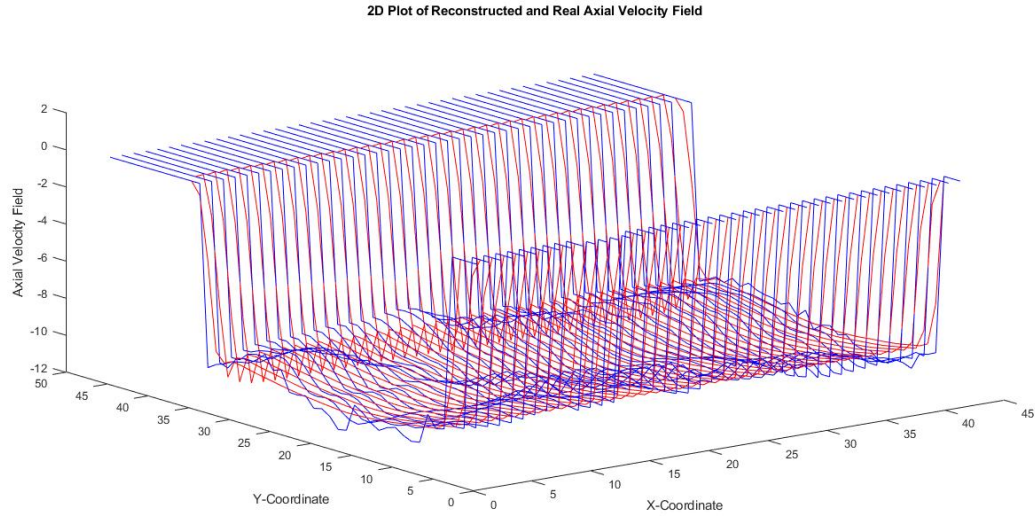
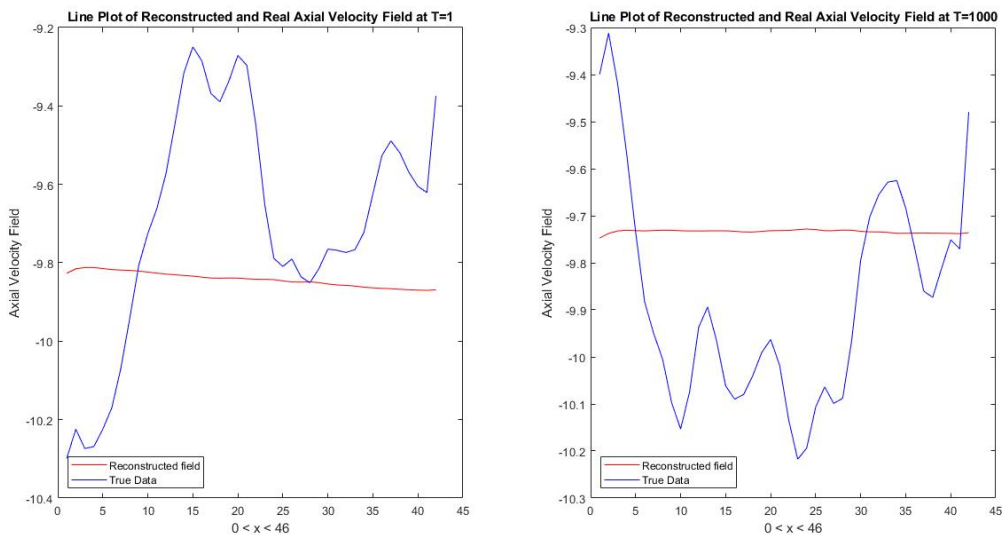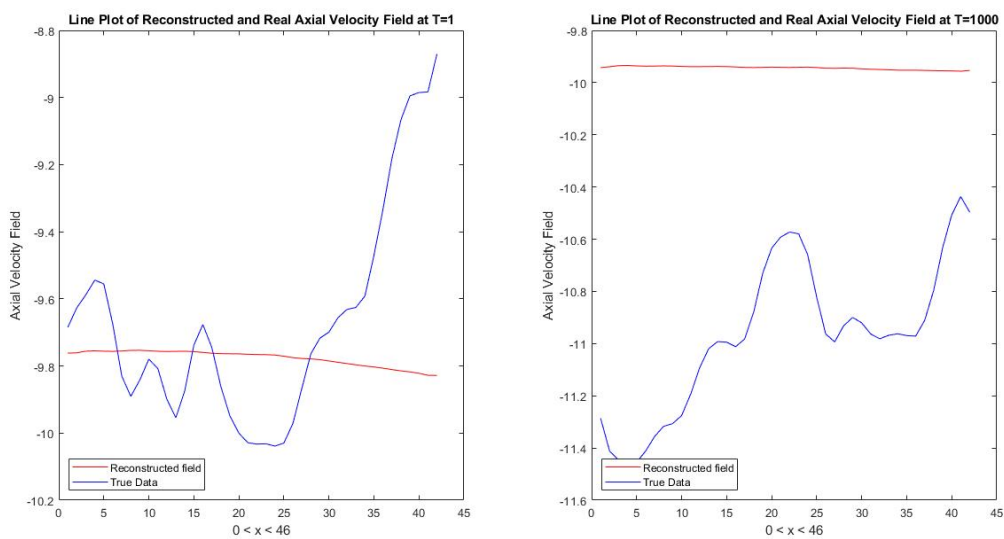Figure 5.4: 2D Representation of the Real Axial Velocity Field (Blue) and the Reconstructed one (Red) at T=1.

The comparison was performed in 2D and is shown in Figure 5.4. The figure shows the axial velocity field taken at a fixed time point (T=1). The blue lines represent the original data field, while the red lines represent the reconstructed one using the exact DMD method. It is clearly evident that there is a general agreement between both reconstructed and original fields. Also, figure 5.5 is the same as figure 5.4 but taken at a future time instant (T=1000), shows a great agreement between both fields even though the field is highly fluctuating at such time step as discussed earlier. However, at such a time step, we can see that the reconstructed field only shows an average behavior of the original field, which wouldn't be sufficient for applications like future predictions.
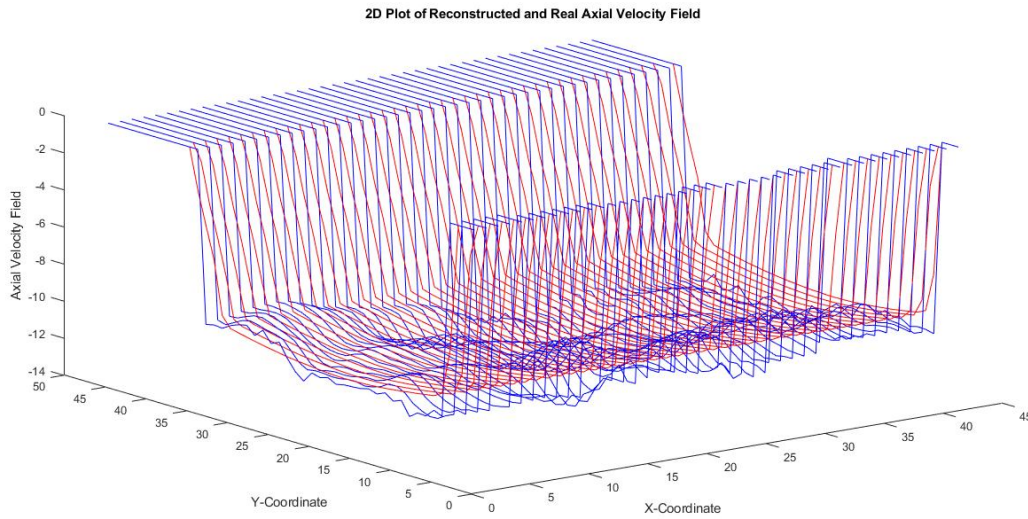
Figure 5.5: 2D Representation of the Real Axial Velocity Field (Blue) and the Reconstructed one (Red) at T=1000.

Although the 2D representation was sufficient to show the general agreement between both fields, a 1D representation was needed to closely study the reconstructed field at different positions and time instants. Figure 5.6 shows both reconstructed and original fields taken for all X, Y=1, and T=1. It is clear that the reconstructed field greatly agrees with the original in the general behavior, however, not all the system dynamics of the original field is captured by the reconstructed field.
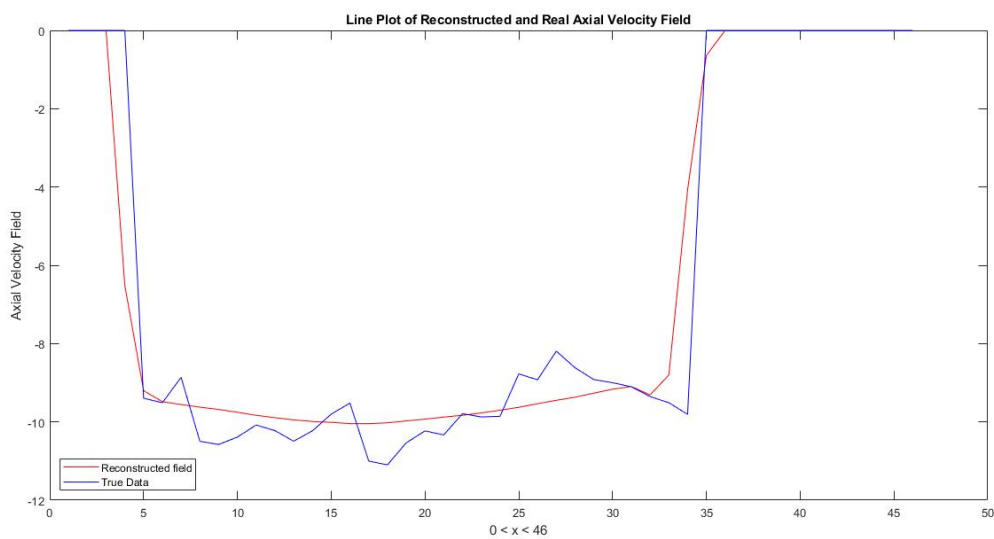
Figure 5.6: 1D Representation of the Real Axial Velocity Field (Blue) and the Reconstructed one (Red) at Y=1, T=1.

Looking at figure 5.7 that is showing both original and reconstructed axial velocity taken at the vicinity of the mid-axial plane (Y=20) at the initial time point (T=1), we can clearly see that the reconstructed field does not really capture field fluctuations. Also, there should be noted that at the right peripheral region, a false prediction of field values, that is a deviation from the general trend, is noted.
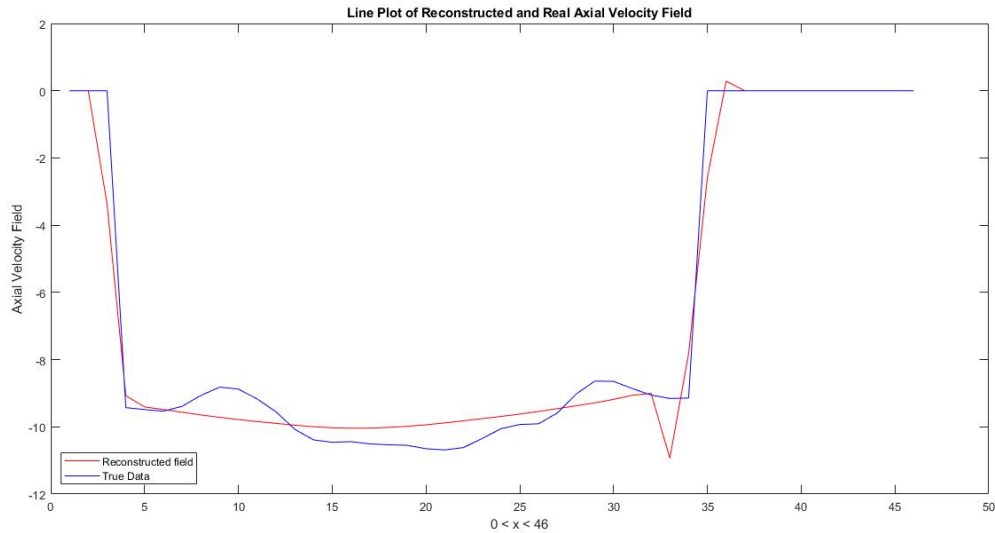
Figure 5.7: 1D Representation of the Real Axial Velocity Field (Blue) and the Reconstructed one (Red) at Y=20, T=1.

Seeing that the DMD method is only capable of the reconstruction of the average field behavior, it was only necessary to look at the field from the transversal direction. Figure 5.8 shows both reconstructed and original fields as seen from the mid-transversal plane (X=20) at T=1, this is a solid confirmation of the deducted conclusion; the DMD technique is only capable of capturing the average behavior of simple flow fields.
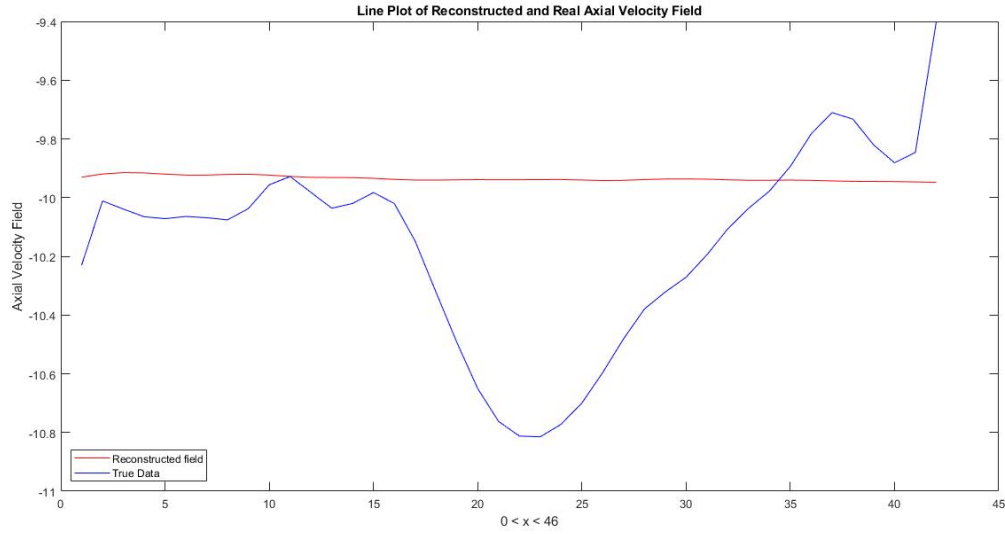
Figure 5.8: 1D Representation of the Real Axial Velocity Field (Blue) and the Reconstructed one (Red) at X=20, T=1.

To confirm the above findings, the analysis of the axial velocity field of the three remaining experimental setups was necessary. First, the axial velocity field from the second experimental setup was studied. At this setup, the shaking conditions are slightly changed, whilst maintaining a displacement of 0.5 mm, the shaking frequency was set at 8.06 Hz. Such higher frequency would naturally impose more disturbances to the flow field. Figure 5.9 shows both reconstructed and original fields taken at initial and later time points (T=1 and T=1200). The plot confirms how only the average behavior is captured by the reconstructed field, and the system dynamics are lost. However, it also shows a new finding, that the system time-dynamics are lost at future time points. The plot at T=1200 shows a clear deviation between both fields.
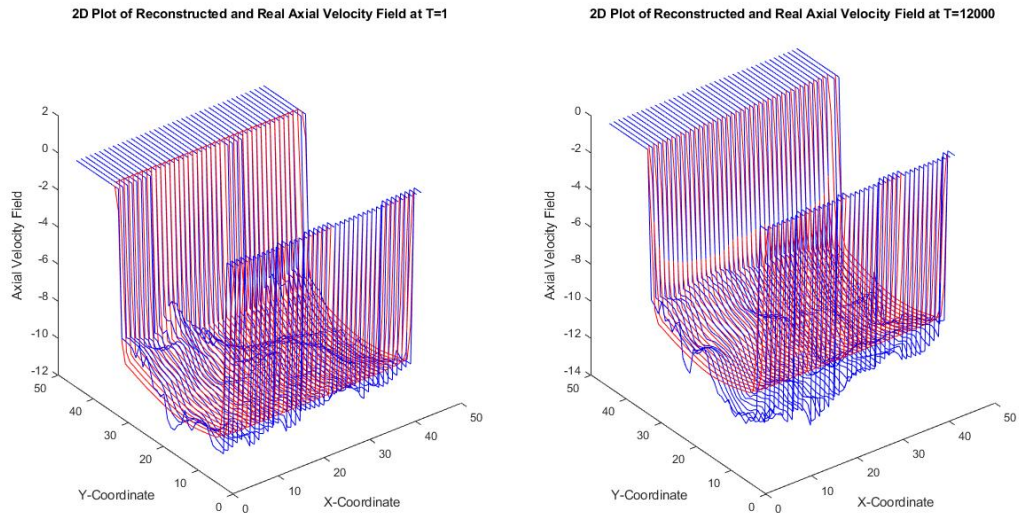
Figure 5.9: 2D Representation of the Real Axial Velocity Field (Blue) and the Reconstructed one (Red) at T=1, T=1200.
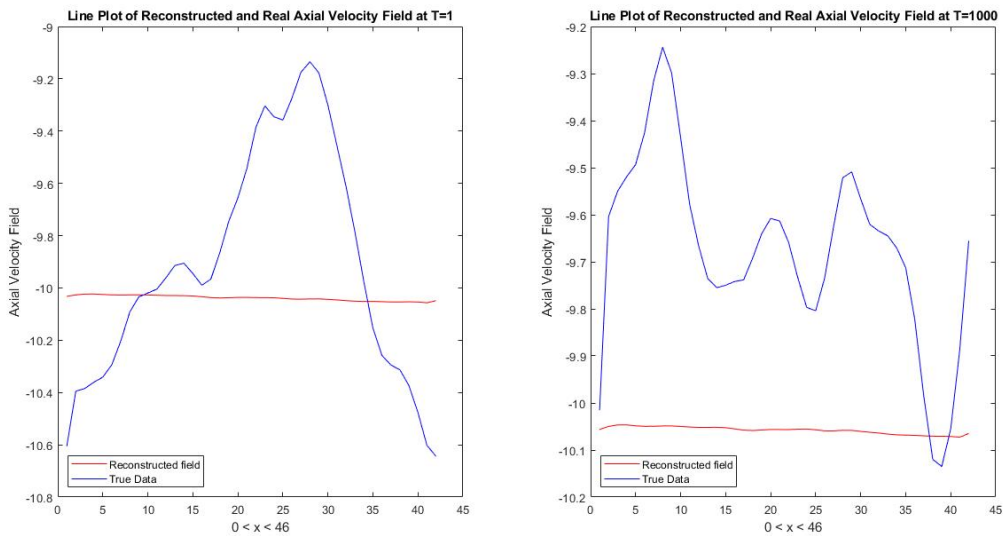
Figure 5.10: 1D Representation of the Real Axial Velocity Field (Blue) and the Reconstructed one (Red) at X=20 for T=1, T=1200.

Figure 5.10 shows a line plot of both fields at initial and later time points taken for X=20. At the initial time point, the average behavior is captured, however, with increasing fluctuations due to the higher shaking frequency, the average behavior is not even captured moving forward in time.

The third experimental setup imposed a higher excitation displacement (1.7 mm) with

a lower excitation frequency (1 Hz). At such conditions, spatial fluctuations are more dominant than temporal. Looking at figure 5.11 and figure 5.12 show that even though the reconstructed field highly deviates from the original one at future time points, the average behavior is still maintained.
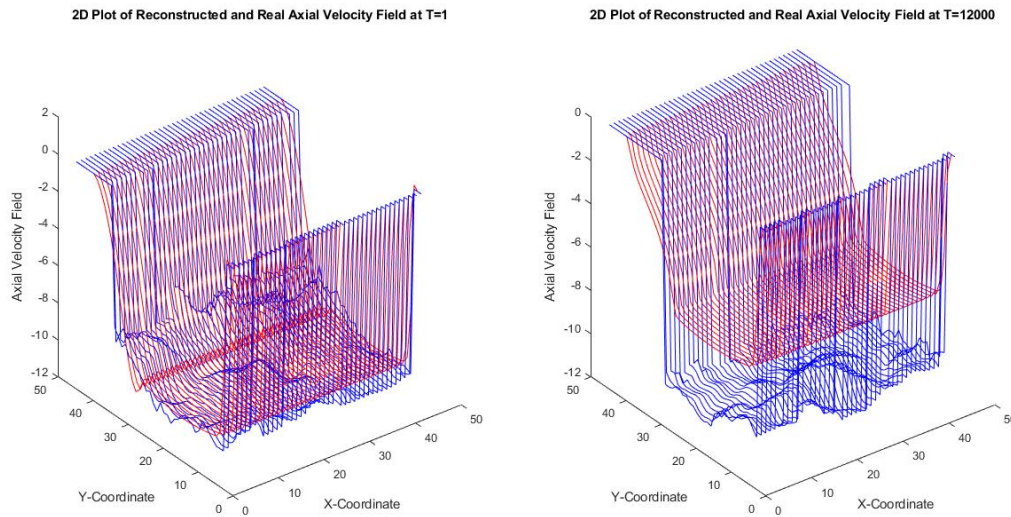
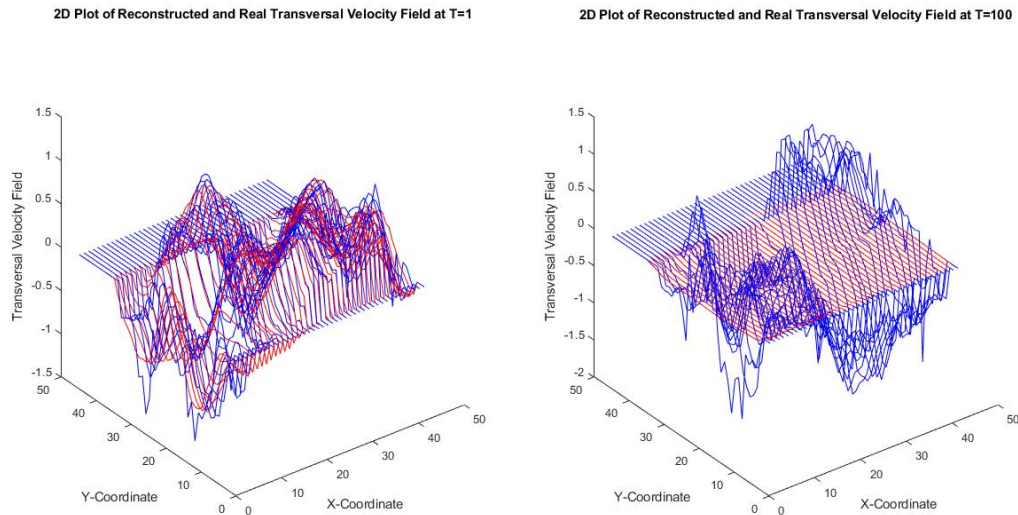

Figure 5.11: 2D Representation of the Real Axial Velocity Field (Blue) and the Reconstructed one (Red) at T=1, T=1200.

Figure 5.12: 1D Representation of the Real Axial Velocity Field (Blue) and the Reconstructed one (Red) at X=20 for T=1, T=1200.

The final experimental setup was performed at both high excitation displacement (1.7

mm) and high excitation frequency (14 Hz). Such severe conditions would result in a highly complex flow field. Testing the exact DMD method on such a special field was crucial. Figures 5.13 and 5.14 show both original axial velocity and reconstructed at different time points. Now at these strong excitation conditions, the DMD reconstructed field deviates from the original field even at the initial time step. Looking at the 1D plot, we can see that capturing the average behavior in such conditions becomes impossible.
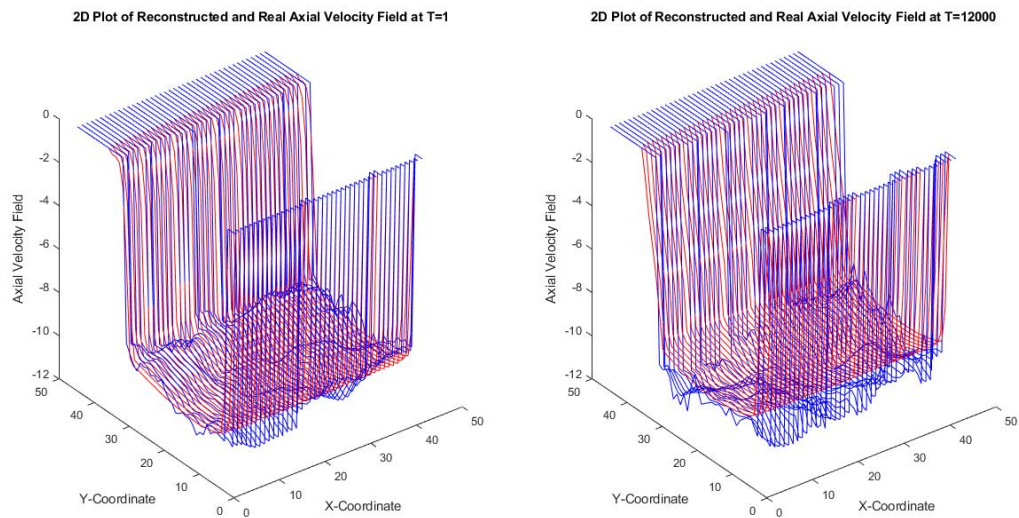
Figure 5.13: 2D Representation of the Real Axial Velocity Field (Blue) and the Reconstructed one (Red) at T=1, T=1200.
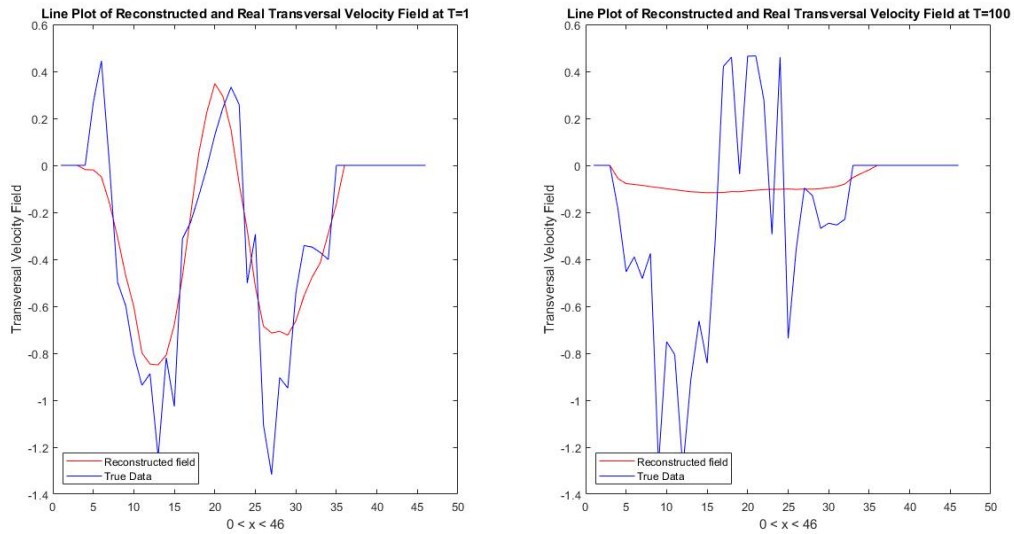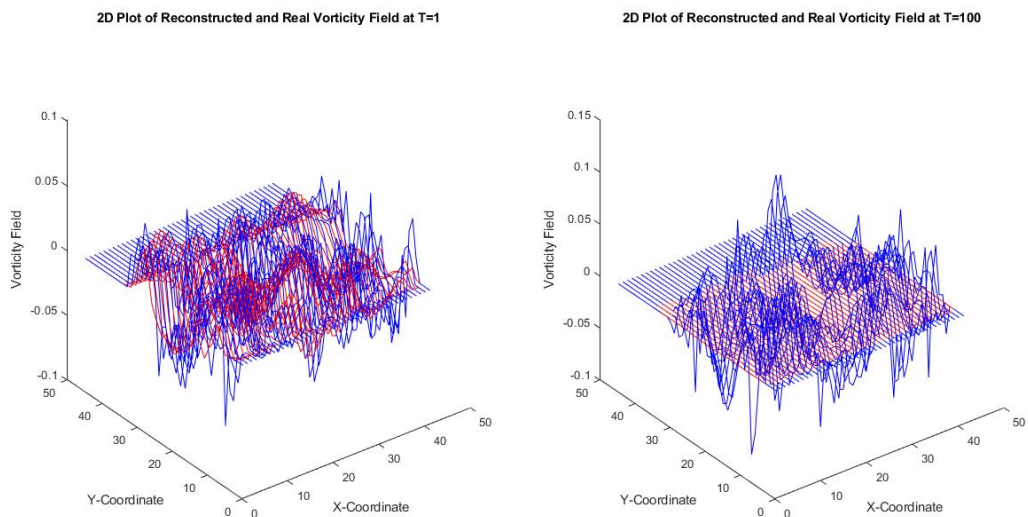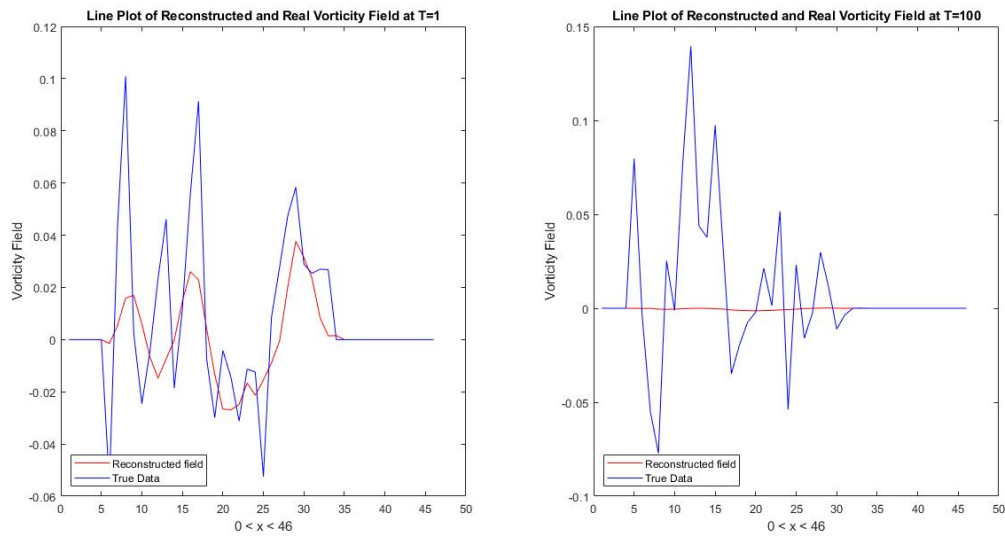

Figure 5.14: 1D Representation of the Real Axial Velocity Field (Blue) and the Reconstructed one (Red) at X=20 for T=1, T=1200.

The previous plots support the above-mentioned deduction, that is, with growing system dynamics (fluctuations) due to moderate to severe seismic conditions, the nature of the flow grows to be relatively complex, and the DMD method fails to capture the system's dynamics. This only confirms that the exact DMD method, as a data-driven method, is only insensitive to temporal fluctuations.

The word *deviation* was repeatedly mentioned above, and hence, an explanation is required. When dealing with a data reconstruction technique similar to DMD, during the validation process, it is important to find an acceptable level of agreement between the original data field and the fabricated one. If the agreement is only restricted to the general behavior of the field (increasing, decreasing .. etc.) the method is considered accurate, and if this agreement is in the exact values carried by the data points, the method is then considered precise. Of course, the level of agreement is quantified and studied closely to determine if the method is acceptably accurate or precise. In our case, a visual representation of the deviation of the reconstructed field from the original field was needed.
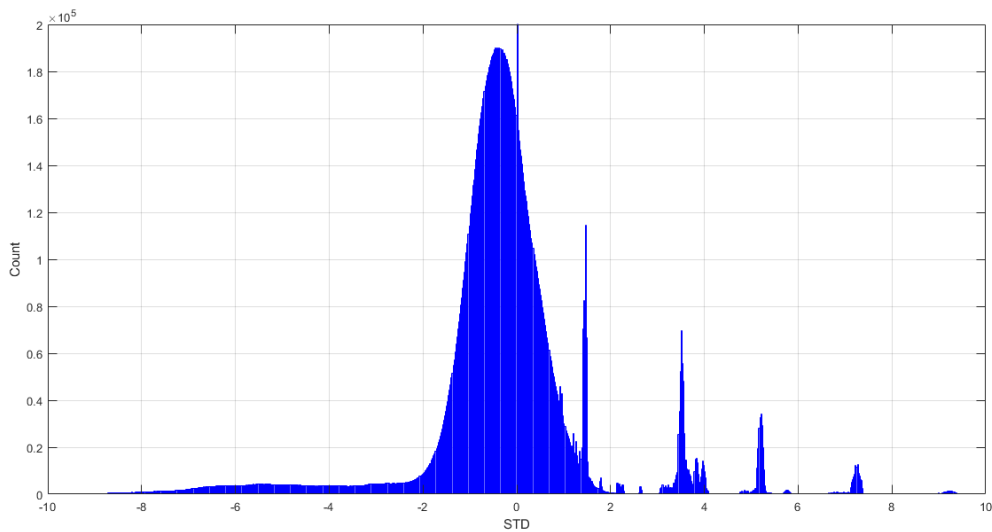
Figure 5.15: Standard Deviation of the Reconstructed Axial Velocity from the Original Field (first experimental setup).

Figure 5.15 shows the standard deviation of the axial velocity field of the first experimental setup (field of least fluctuations) from the original axial velocity field. Evaluating the standard deviation is crucial in assessing the accuracy of the exact DMD method. A low standard deviation corresponds to a more accurate and precise reconstructed field, while a large standard deviation value indicates that the technique is unreliable and needs modifications. In our case, it is evident that almost 90 % of the data lies in the vicinity

of an absolute standard deviation equal to 0.5, this only means that the majority of the data points deviate from the mean by 0.5 units. In a large data set similar to the axial velocity field, this value indicates an acceptable level of variability.

For fields of higher noise and data fluctuations, for example, axial velocity under the fourth experimental setup the situation definitely worsens. Figure 5.16 shows the standard deviation of the axial velocity field of the fourth experimental setup from the original axial velocity field under the same conditions. In this situation, 90 % of the data points lie in the vicinity of an absolute standard deviation equal to 1.5 which is 3 times worse than that of the reconstructed axial velocity of the first experimental setup. This is solid proof that the exact DMD method is biased toward the noise and that the method fails when treating more complex data fields.
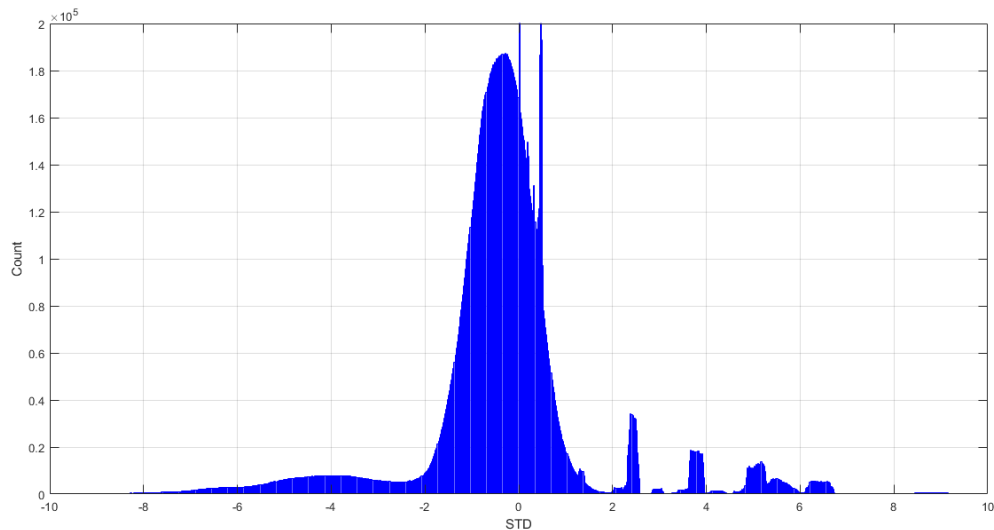
Figure 5.16: Standard Deviation of the Reconstructed Axial Velocity from the Original Field (fourth experimental setup).

5.2.2. DMD of other fields

The application of the DMD as a data reconstruction technique was extended to include other fields like *transversal velocity*, *vorticity*, and *turbulent kinetic energy*. All three fields are highly random and exhibit larger fluctuations than those of the axial velocity field, even though when studying those fields under the experimental setup with the lowest upsetting conditions (0.5 mm at 3 Hz). The reason behind this complexity is in the nature of those fields, take for example vorticity, which describes the local rotation (spinning) of the flow field. For an unforced flow under stable conditions, the vorticity field

would still be complicated, and in our case, with the added complexity due to the forcing conditions and the seismic ones, the complexity of the field would significantly increase. The real challenge in studying those fields is in finding the right number of modes that can accurately describe the system. Naturally, such fields would need a higher number of modes than those of simpler ones (e.x. axial velocity of the first experimental setup). With all this in mind, the DMD technique was applied and the results are displayed below for completeness.

Starting from the transversal velocity field under excitation conditions of 0.5 mm and 3 Hz, the results are displayed in figure 5.17 and 5.18 we can see that some of the system dynamics are captured at the initial time step, however, moving forward in time, we can see that the reconstructed field completely dies out.

Figure 5.17: 2D Representation of the Real Transversal Velocity Field (Blue) and the Reconstructed one (Red) at T=1, T=100.

Figure 5.18: 1D Representation of the Real Transversal Velocity Field (Blue) and the Reconstructed one (Red) at X=20 for T=1, T=100.

With the vorticity field under the same experimental condition, we can see in figure 5.19 and 5.20 that fluctuations are even higher. In some regions, the reconstructed field at the initial time step highly agreed with the original field, however, at only T=100 the reconstructed field is null.

Figure 5.19: 2D Representation of the Real Vorticity Field (Blue) and the Reconstructed one (Red) at T=1, T=100.

Figure 5.20: 1D Representation of the Real Vorticity Field (Blue) and the Reconstructed one (Red) at X=20 for T=1, T=100.
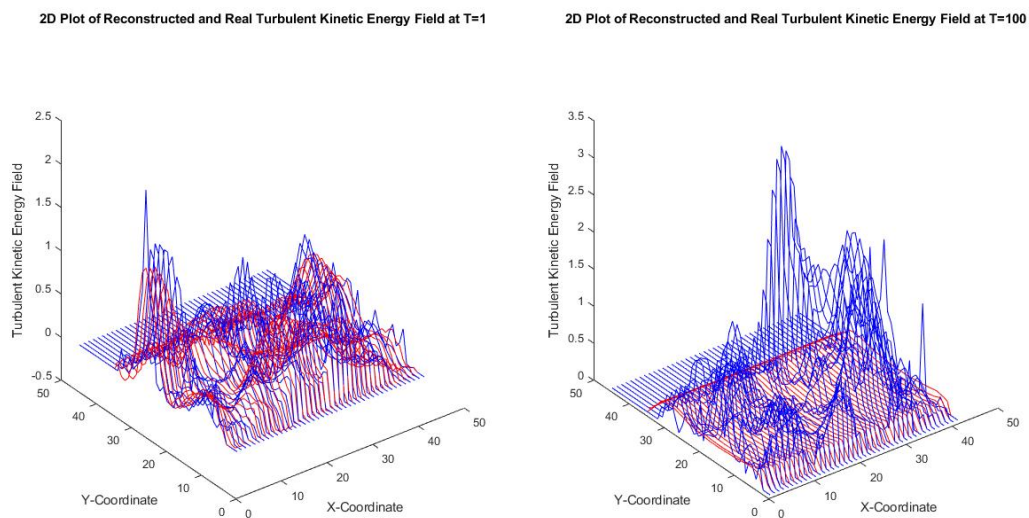
Figure 5.21: 2D Representation of the Turbulent Kinetic Energy Field (Blue) and the Reconstructed one (Red) at T=1, T=100.
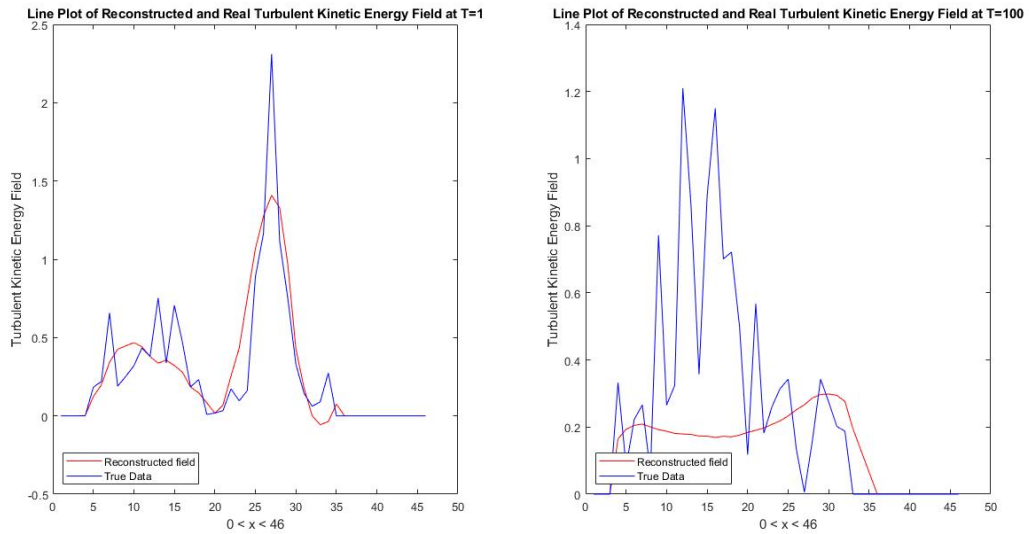
Figure 5.22: 1D Representation of the Real Turbulent Kinetic Energy Field (Blue) and the Reconstructed one (Red) at X=20 for T=1, T=100.

For the turbulent kinetic energy shown in figure 5.21 and 5.22, the results are somewhat similar to the vorticity and transversal velocity fields. However, it should be noted that moving forward in time, the reconstructed field does not die out, however, it lands on a value that is not at all representative of the original field.

It was only expected that upon studying highly complex fields the results will be similar to that drawn from the simple axial velocity field under severe excitation conditions. This is in agreement with what was found in the literature about the limitation of DMD as a DDM technique. The above results confirm that DMD is highly sensitive to the system's noise and data fluctuations, the technique completely fails to capture the system dynamics under such conditions and hence, an adjustment is essential.

5.2.3. Attempts to enhance the DMD findings

Several trials were carried out in an effort to improve the code and the results. These attempts tried to optimize the analysis and account for unique data considerations. Four options were investigated: scaling all data points by a factor, creating a new data matrix by adding intermediate data points, sectioning the present data matrix, and multiplying it by a bias. In the first trial, all data points were scaled with a factor. When the magnitudes of different variables or features vary greatly, scaling data might be valuable. Scaling involves multiplying each data point by a factor that normalizes its magnitude in relation to the other data points. This method assures that all variables contribute

equally to the study, removing any potential bias induced by bigger magnitude variables. By decreasing the impact of magnitude inconsistencies, scaling the data enables a more robust and reliable analysis. A fresh data matrix was created in the second trial by adding intermediate data points. This method attempted to improve resolution and capture finer details in the data. The temporal or spatial resolution of the data is improved by inserting extra data points between the existing ones. This higher resolution can provide more accurate and thorough information about the system's underlying dynamics. The analysis gets more accurate by integrating intermediate data points, allowing for greater detection and characterization of patterns and structures within the data. The third attempt involved dividing the present data matrix into sections. The process of separating a data matrix into smaller, more manageable portions is referred to as sectioning. This method is especially beneficial when dealing with enormous datasets or extended time series. The computing burden is minimized by separating the data into sections, and the analysis can be conducted on smaller subsets of the data. This can boost computational efficiency and make it easier to analyze the results. Sectioning also allows for the investigation of certain data segments, providing for a more targeted analysis of specific locations or time intervals. The fourth attempt was based on multiplying the data matrix with a bias. This method attempted to create a bias or weighting factor to specific data points, variables, or areas of interest. The emphasis or relevance of various data components can be altered by using a bias. This is especially useful when specific variables or regions are recognized to be more important or relevant to the study. When the data matrix is multiplied by a bias, a customized weighting scheme is created, allowing for the priority of specific parts of the data and improving the analysis in accordance with the study objectives.

Despite the efforts expended in carrying out the aforementioned trials, it is crucial to highlight that none of them resulted in a discernible improvement in the outcomes. While these trials were designed to improve the analysis, it is likely that the nature of the data or the study's specific context restricted the usefulness of these approaches. It is not rare to come across circumstances in which specific changes or alterations do not result in considerable improvements, showing the intricacy and uniqueness of each analysis. Nonetheless, the investigation of these trials yielded useful insights into the constraints and challenges connected with the data and the code, informing future research efforts and leading viable alternative techniques. Because the aforementioned trials had limited success in improving the outcomes, an alternate algorithm known as Bagging Optimized Dynamic Mode Decomposition (BOP DMD), explained earlier, was employed. Recognizing the need for a new approach, BOP DMD proposed a viable solution to the problems identified. The results obtained from BOP-DMD are displayed in the next section.

5.2.4. Field Reconstruction and Validation Using BOP-DMD

The use of the BOP-DMD method described earlier in 2.3 was only necessary to overcome the obstacles faced by the exact DMD method. Since the flow field of a PWR coolant under seismic conditions is characterized by large data fluctuations, and since there could be some arbitrary system noise from the experimental measurements constraints, the application of BOP-DMD as a data reconstruction technique was of high suitability. The technique, as was mentioned earlier, leverages the statistical method of bagging to improve the DMD performance and overcome the sensitivity to noise. We will first start with the analysis of the axial velocity field from the first experimental setup, then we will extend the analysis to include other fields of higher noise. Also, some minor modifications were applied to enhance the results even further.

Similar to the exact DMD method, we first started by calculating the number of modes to which the system will be reduced, for the axial velocity field, this is shown in figure 4.1 to be 3 modes. Following the BOP-DMD algorithm described in 2.1, the reconstructed field satisfies equation 2.6. Here the DMD eigenvalues, DMD modes, and their loadings are taken to be the mean values over the single DMD eigenvalues, DMD modes, and their loadings obtained from each cycle. It should be noted here that the reconstructed field can later be used as a training data matrix for achieving accurate forecasting. Validation is done by comparing the reconstructed field to the original field of axial velocity. The comparison was performed in 2D and line plots as shown in figure 5.23 and 5.24 respectively. The plots show the axial velocity field taken at a fixed time point (T=1). The blue lines represent the original data field, while the red lines represent the reconstructed one using BOP-DMD.

The 2D plot shown in figure 5.23 allows for a global visualization of the reconstructed field compared to the original one at all positions. It is evident that the reconstructed field using BOP-DMD agrees more with the original field than the one reconstructed using exact DMD. The fabricated field now is not only capable of representing the average behavior of the original field but also capable of capturing field variations. To study the excellence of the method, figure 5.24 shows a line plot of the reconstructed axial velocity compared to the original field taken at a fixed axial position (Y=20) and fixed time point (T=1), we now can see that the reconstructed field follows the original one to a great extend. However, for some minor points, we can see that the reconstructed field slightly deviates from the original, those points are thought to be systematic noise.
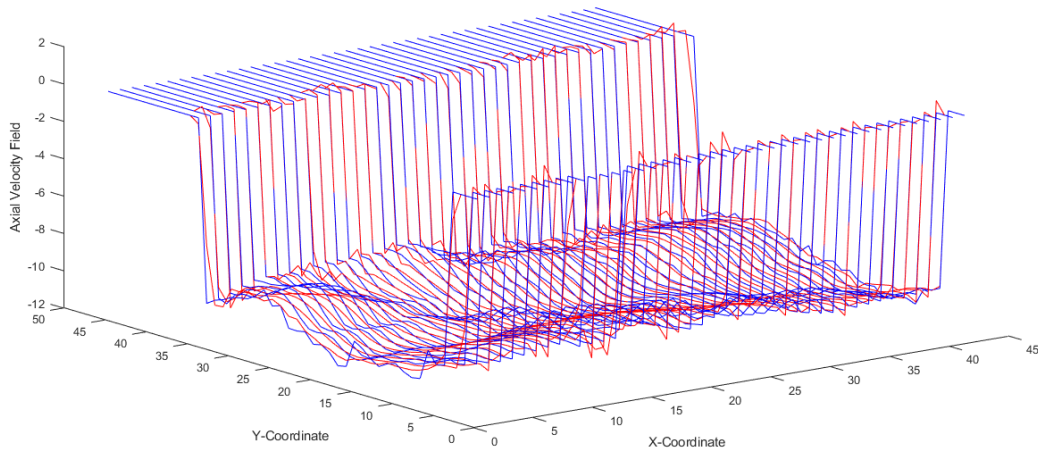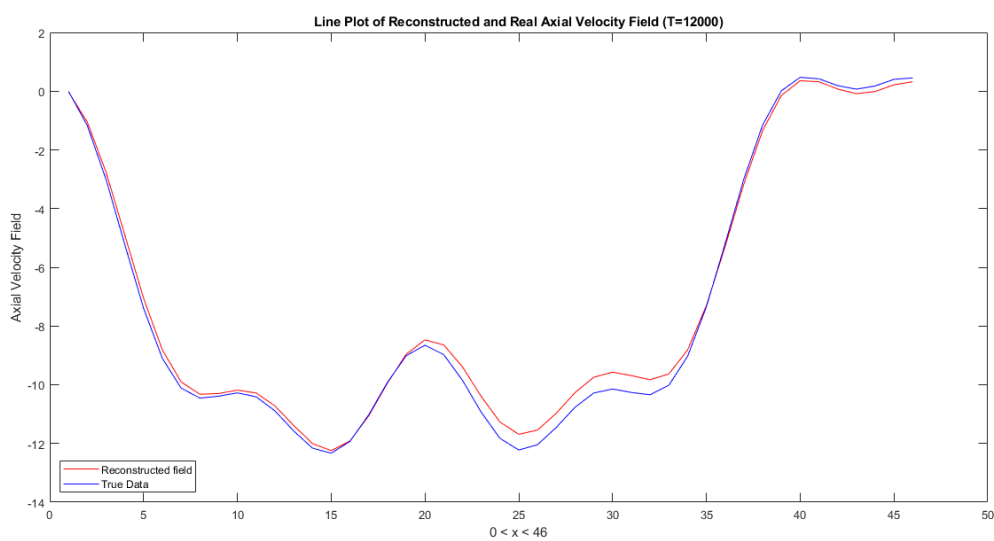
Figure 5.23: 2D Representation of the Real Axial Velocity Field (Blue) and the Reconstructed one (Red) Using BOP-DMD at T=1.
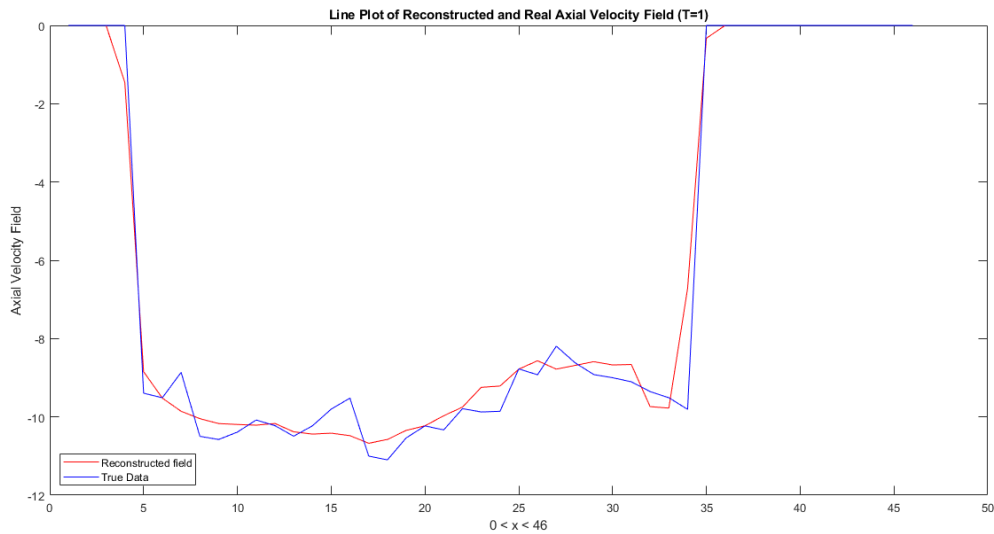
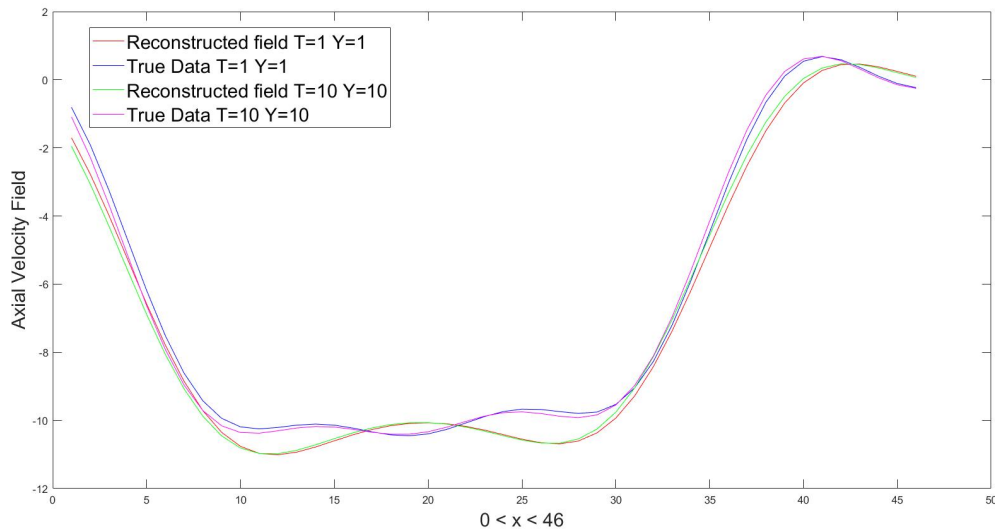Figure 5.24: 1D Representation of the Real Axial Velocity Field (Blue) and the Reconstructed one (Red) Using BOP-DMD at T=1.

Knowing the fact that BOP-DMD is insensitive to systematic noise, it was acceptable to witness the reconstructed field slightly deviating from the original field. These variations ranged from 0.67 % up to 12.5 %. It was noticed that, upon the analysis of fields with higher noise, the variations became evidently larger, and hence, de-noising was necessary to study the effect of noise on the reconstructed fields.

To achieve a solid validation of the BOP-DMD method, noise filtering techniques were applied to the original field to remove the unnecessary systematic noise. Those techniques shall be extensively described in a later section. After denoising the original axial velocity field, the BOP-DMD method was applied to produce a fabricated axial velocity field. Both fields were again compared graphically.
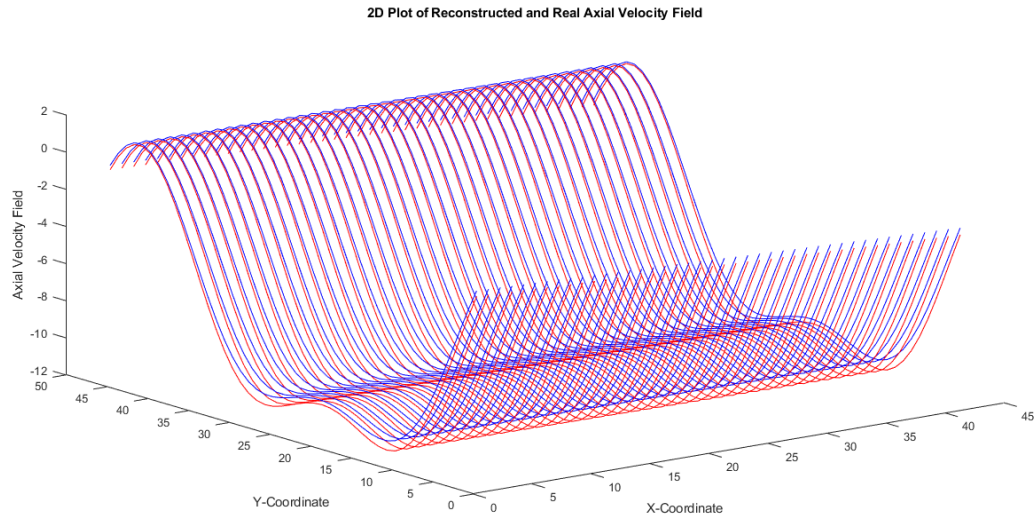
Figure 5.25: 2D Representation of the Real (denoised) Axial Velocity Field (Blue) and the Reconstructed one (Red) Using BOP-DMD at T=1.

Figure 5.25 shows a global 2D visualization of both fields, it is evident that now, after removing the unnecessary noise components, the reconstructed fields almost completely agree with the original one. Figure 5.26 shows a line plot of both fields taken at the same time point and the axial mid-plane, we can see that variations are now reduced to as low as 0.05 %
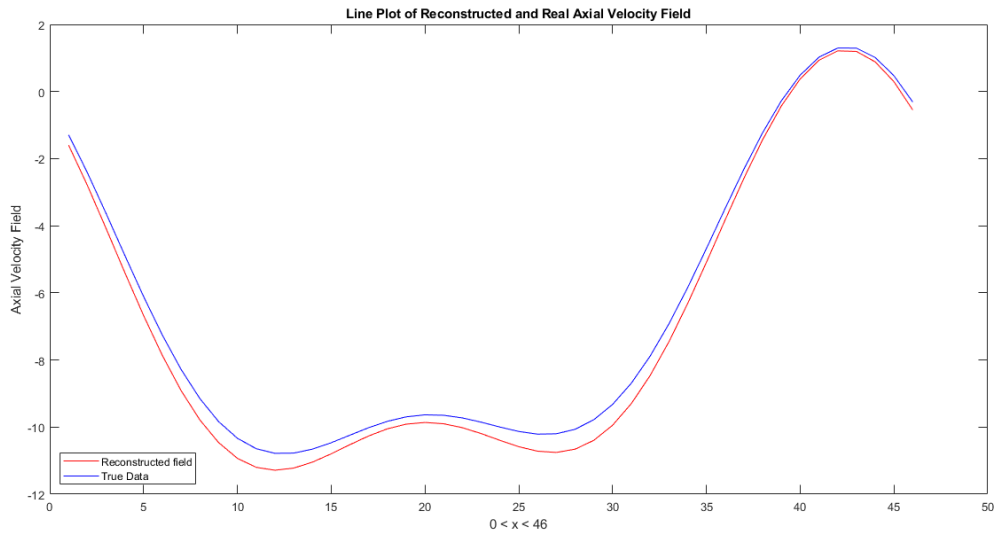
Figure 5.26: 1D Representation of the Real (denoised) Axial Velocity Field (Blue) and the Reconstructed one (Red) Using BOP-DMD at T=1.

One of the limitations of the exact DMD method is that it failed to capture the system dynamics, i.e., it failed to provide accurate field reconstruction at future time points. This was tested using BOP-DMD, figure 5.27 shows both the reconstructed and the original fields at T=12000. Variations between both fields are now in the range of 2% up to 5%, and it is evident that the original field behavior is no longer constant at the mid-regions since the flow has gained enough momentum to show variations in the axial velocity.

Figure 5.27: 1D Representation of the Real (denoised) Axial Velocity Field (Blue) and the Reconstructed one (Red) Using BOP-DMD at T=12000.

Figure 5.28 shows the reconstructed field and the original field after removing the noise compared at different, randomly chosen, time steps and positions (T=1, Y=1 and T=10, Y=10). This shows that the BOP-DMD reconstructed field agrees with the original one at almost all positions and time points to a great extent.

Figure 5.28: 1D Representation of the Real (denoised) Axial Velocity Field (Blue) and the Reconstructed one (Red) Using BOP-DMD.

The study of the axial velocity fields from other experimental setups (different excitation conditions) was necessary to test the validity of the BOP-DMD method for more complex fields.
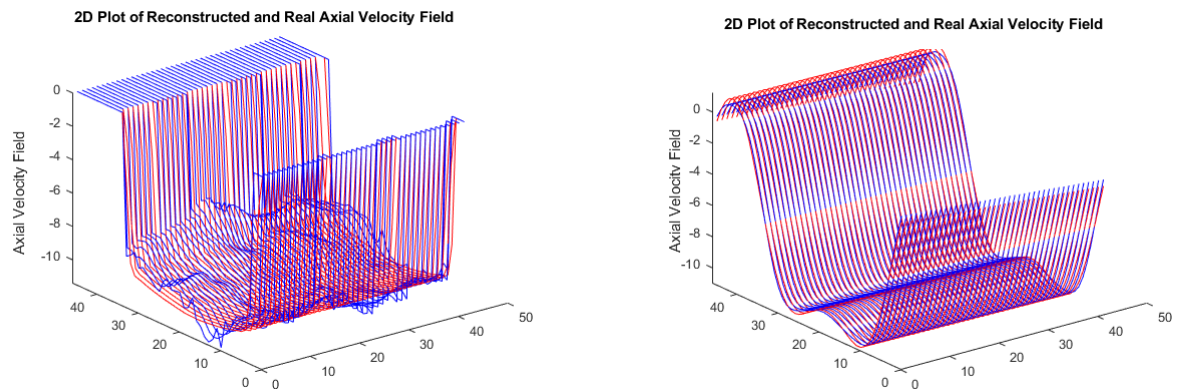
Figure 5.29: Real Axial Velocity Field from the Second Experimental Setup (Blue) and the Reconstructed one (Red) Using BOP-DM with noise and denoised

Figure 5.29 shows the reconstructed field of the axial velocity field from the second experimental setup compared to the original field in the presence of noise and after denoising. The results are similar to that obtained from the first experimental setup, since both fields are almost similar, in terms of fluctuations and systematic noise.
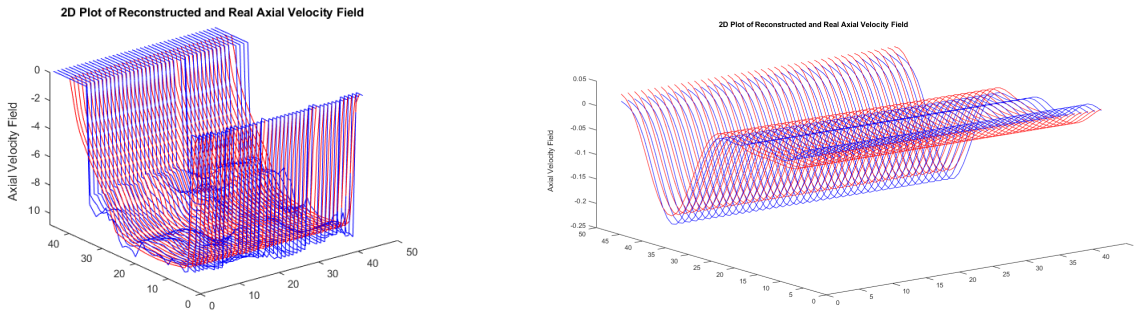
Figure 5.30: Real Axial Velocity Field from the Third Experimental Setup (Blue) and the Reconstructed one (Red) Using BOP-DM with noise and denoised

Figure 5.30 shows the reconstructed field of the axial velocity field from the third experimental setup compared to the original field also in the presence of noise and after denoising. At such excitation conditions, fluctuations are considered to be moderate, and the BOP-DMD successfully captures the system dynamics.
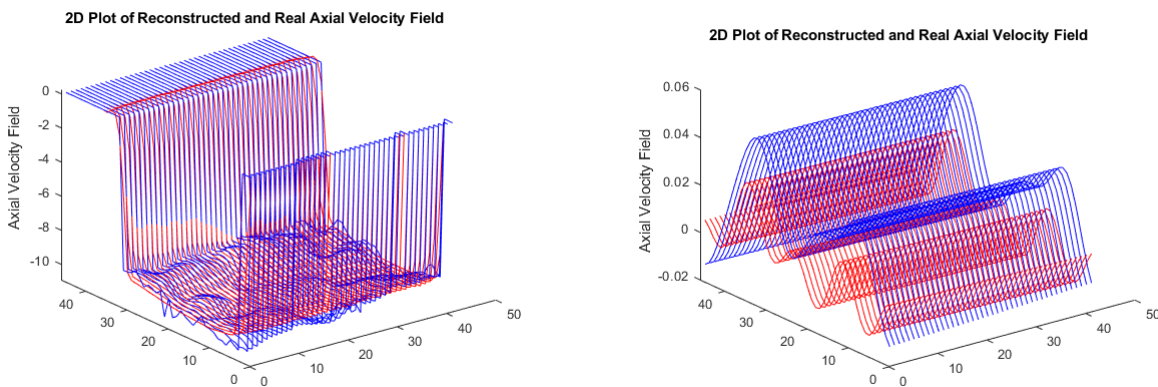
Figure 5.31: Real Axial Velocity Field from the Fourth Experimental Setup (Blue) and the Reconstructed one (Red) Using BOP-DM with noise and denoised

Moving forward to the axial velocity of the fourth, and final, experimental setup shown in figure 5.31, the variations between the reconstructed and original field notably increase due to the increased fluctuations under such strong excitation conditions, nevertheless, those variations still lie within an acceptable limit.

5.2.5. Comparing BOP-DMD to Exact DMD

To properly demonstrate the good performance of BOP-DMD and the need of using such a technique, we compare its results with the standard DMD, the axial velocity field previously analyzed using the exact DMD method is compared to the one reconstructed using BOP-DMD.
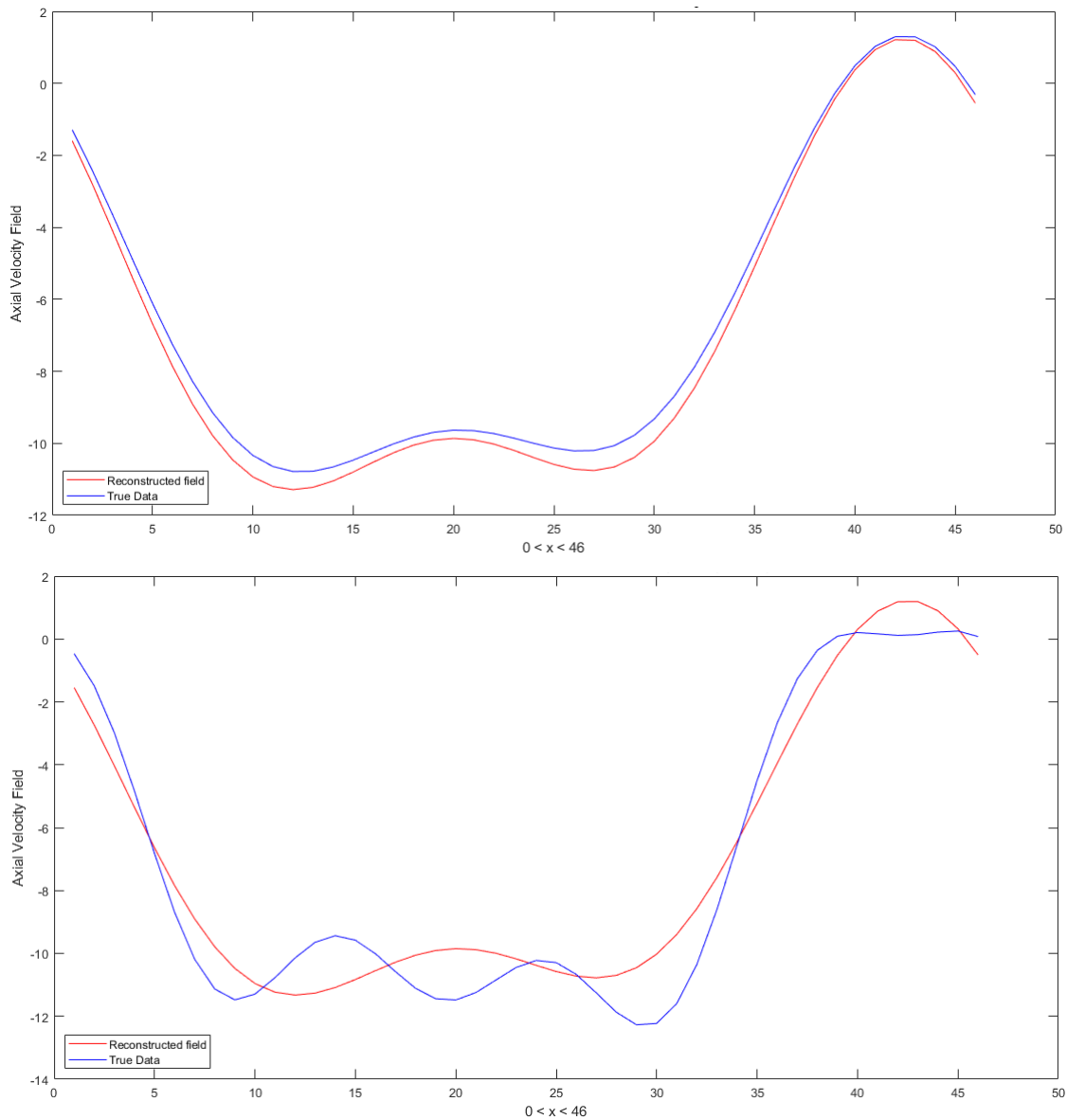
Figure 5.32: Comparison between the exact DMD method and the BOP-DMD method for axial velocity reconstruction

Figure 5.32 shows the reconstruction of the axial velocity field obtained from the first excitation condition using BOP-DMD (Top) and exact DMD (Bottom) at Y=20 and

T=1000 both being denoised. It was already shown that as time passes, the reconstructed field using exact DMD fails to capture the system dynamics and shows a flat behavior. Denoising the original field before applying the exact DMD method helped avoid a rather flat behavior, however, the variations at initial time points ranged from 1% up to 10.5%, while for later time instants in the experiment, variations reached a value as high as 19%. These values are many times higher than those obtained with BOP-DMD.

5.3.   Effect of Noise and Denoising

The presence of noise in the treated data fields can highly affect the accuracy of the recon- structed field. For the exact DMD, the algorithm fails to capture system dynamics at final time points, while for BOP-DMD the presence of noise increased variations between both reconstructed and original fields to two times its value without noise. Hence, this thesis work must include the effect of noise on the analysis and the used denoising techniques.

5.3.1.   Effect of Noise
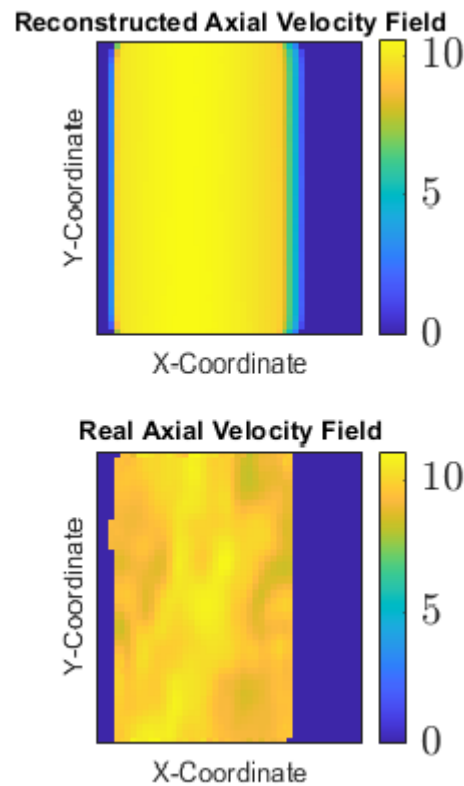
Figure 5.33: Reconstructed and original fields in the presence of noise

Considering the reconstructed field using BOP-DMD, since it is the technique of choice in this analysis, figure 5.33 shows reconstructed and original fields in the presence of noise. One can see that the reconstructed field is insensitive to systematic noise which could benefit applications like forecasting, during which the interest is drawn to the actual field values in future incidents. Variations between both fields are present in the peripheral and mid-field regions and are thought to be noise loadings. To confirm this deduction, denoising was applied to eliminate unnecessary fluctuations that are, in fact, unrepresentative of the actual field values. This is shown in figure 5.34 we can see that variations are almost absent and both original and fabricated fields are quite identical after eliminating noise effects.
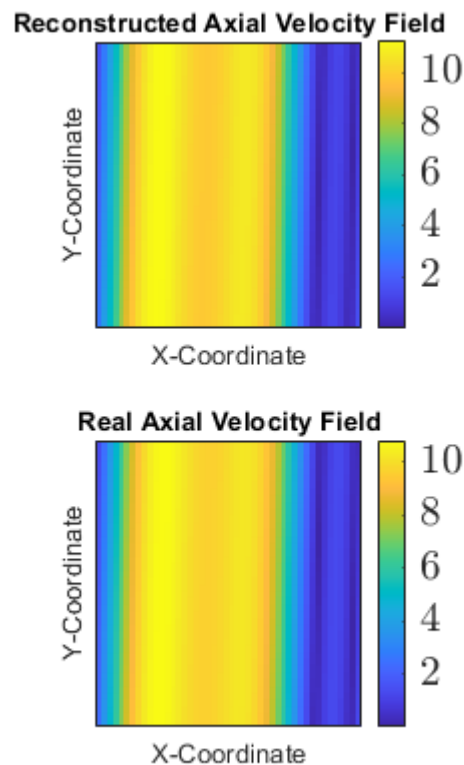
Figure 5.34: Reconstructed and original fields after denoising

Although BOP-DMD shows an evident improvement over the exact DMD method, the study of the effect of noise was necessary. Figure 5.35 shows a fabricated simple field (mixed sine and cosine signals) with additive noise, where the red plot represents the original field and the blue one represents the reconstructed field. The figure shows reconstruction done in the presence of 5% noise (Top) and 50% noise (Bottom) respectively.
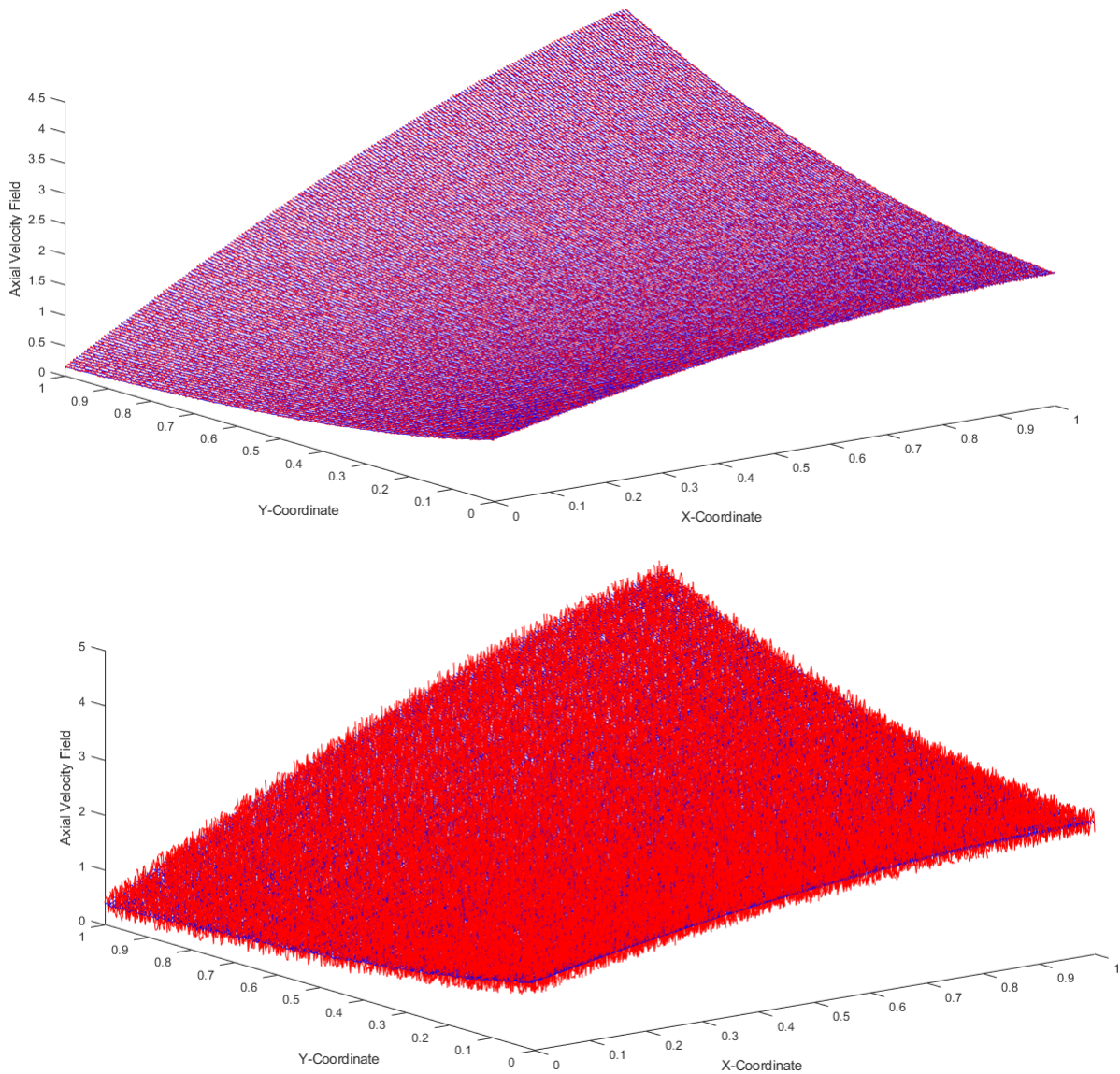
Figure 5.35: Effect of noise on the reconstructed fields using BOP-DMD

The BOP-DMD method is capable of representing the original field as it is, disregarding the value of the noise-to-signal ratio. This is a shred of solid evidence that the BOP-DMD method successfully overcomes the limitations of the exact DMD method and its sensitivity to noise, and justifies the leaning of this study towards the use of this method for the data-driven modeling of complex PWR flow fields under different seismic conditions.

5.3.2.   Denoising Techniques

For the treated data in this study, the noise is either systematic from the measuring equipment or arbitrary due to the lack of use of a calibration target during the experiment as discussed in 3.1. In all cases, the reconstructed fields were denoised using FFT (fast-Fourier transform), and the results were confirmed using wavelets analysis, both were discussed earlier in 4.4, here, we will only display the results obtained from both denoising techniques.

Figure 5.36 shows the PSD (power spectral density) plotted against the frequencies for the axial velocity field, we can see the minor peaks following the central peak, those small peaks represented noise and were cut out.
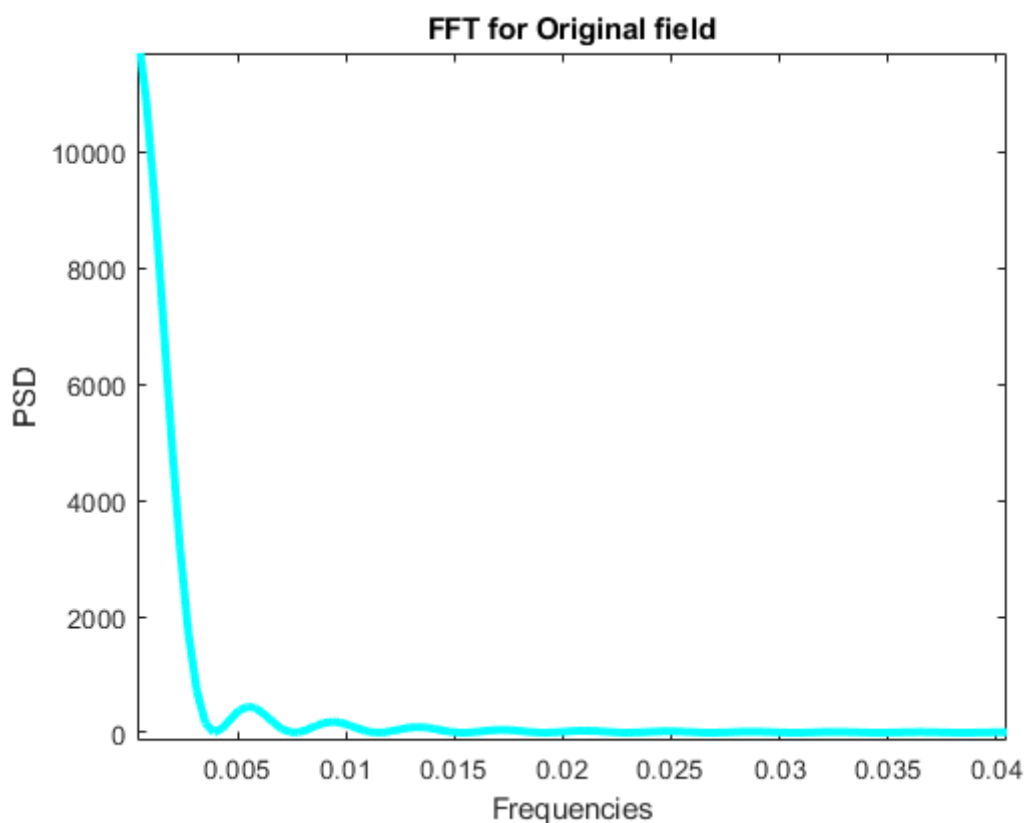
Figure 5.36: PSD vs. Frequencies for the Axial Velocity Field

Naturally, the axial velocity field is the field of minimum noise, i.e., noise components are of the least relevance. However, for more complex fields like transversal velocity, the situation is a bit different. Looking at Figure 5.37 showing the PSD plotted against the frequencies associating the transversal velocity fields, we can see that noise components now build up to peaks that are comparable to the data peaks. Filtering out such noise

points can only mean that part of the data is lost. Hence, normally a limit is set to the noise filtering process above which filtering causes serious loss of data. In our case, this limit was set to 10% of the data points.
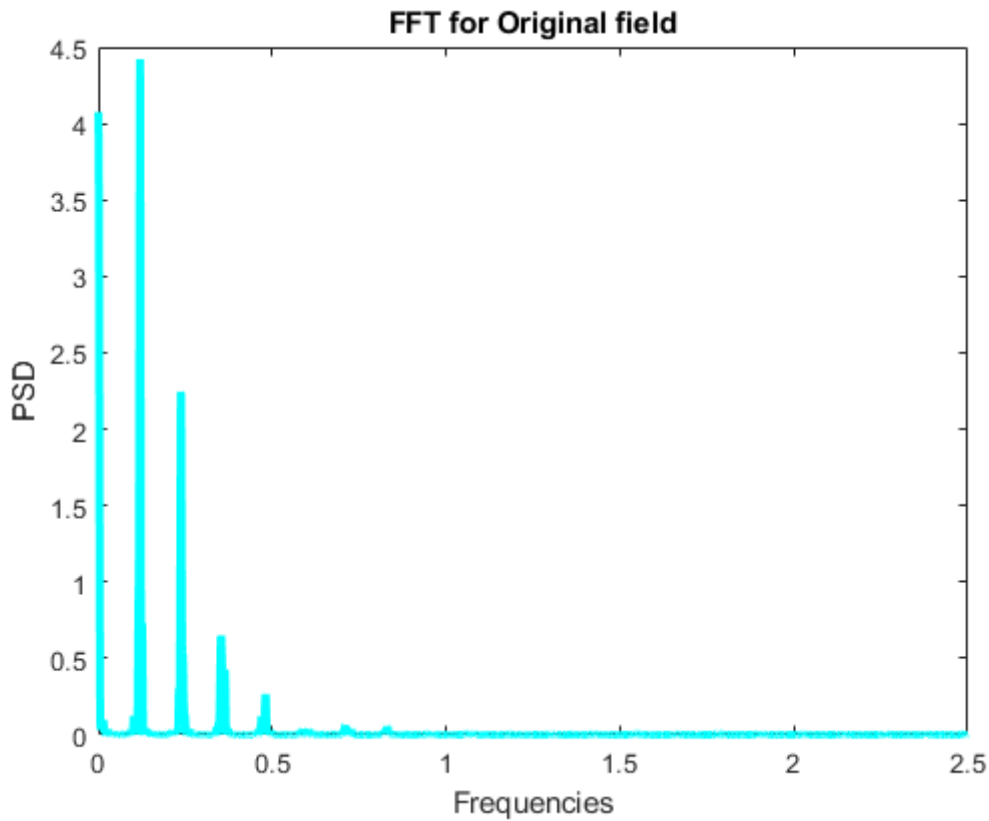
Figure 5.37: PSD vs. Frequencies for the Transversal Velocity Field.

The results were confirmed also using wavelets analysis discussed in 4.4. Figure 5.38 compares denoising using FFT to that using wavelets analysis, where the blue plot is the original axial velocity field and the red plot is the de-noised one. De-noising using wavelet analysis shows typical results to that performed using FFT, which makes using FFT for de-noising reasonable.

2D Plot of Axial Velocity Field denoised with wavelets   **2D Plot of Axial Velocity Field denoised with fourier**
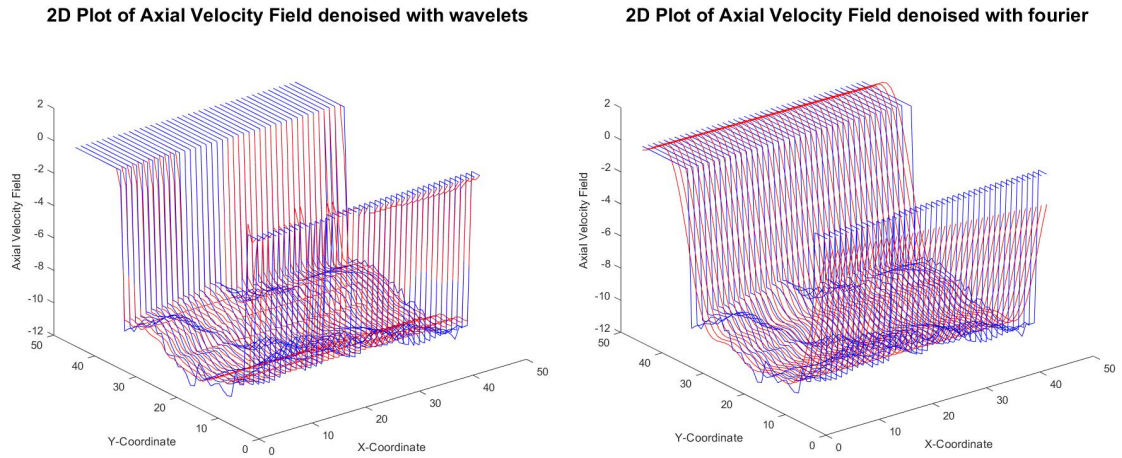
Figure 5.38: De-noised Axial Velocity Field using wavelets analysis (Left) and FFT (right).

5.4. Findings from other fields

After validating the BOP-DMD technique and applying it to reconstruct the axial veloc-
ity field, the analysis was extended to include other fields, for example, the transversal
instantaneous velocity was studied and is shown in Figure 5.39 where the reconstructed
field is plotted against the original field at T=1000 and after denoising using FFT. It
is evident that the reconstruction of such a complex field using BOP-DMD is improved
greatly when compared to the reconstruction of the same field using the exact DMD
method shown earlier in Figure 5.17.
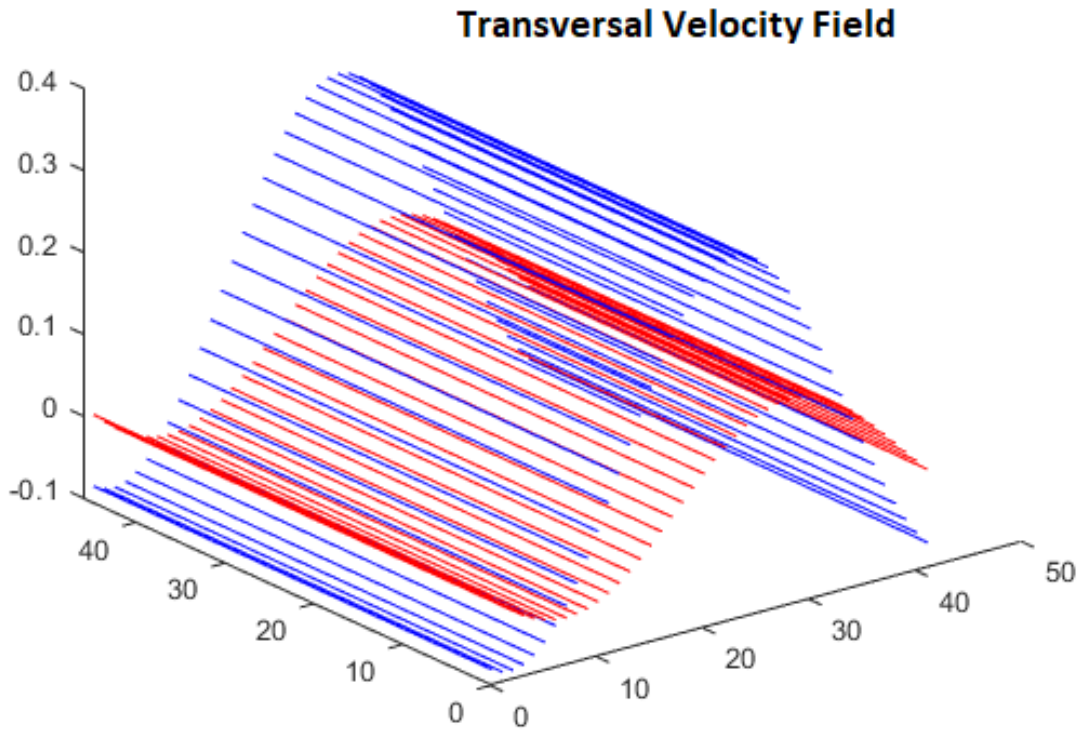
Figure 5.39: Reconstructed and Original Transversal Velocity Field Using BOP-DMD.

Variations between fabricated and original fields are greatly reduced which makes the reconstruction process a success. When closely studying the 1D plot shown in Figure 5.40 taken of both fields at Y=20 and T=1000 we can see that both fields are highly identical in the peripheral regions, while in the mid planes, exactly from X=20 to X=30, variations are as low as 1%. This is solid proof of the advancement of the BOP-DMD method over the conventional DMD method.
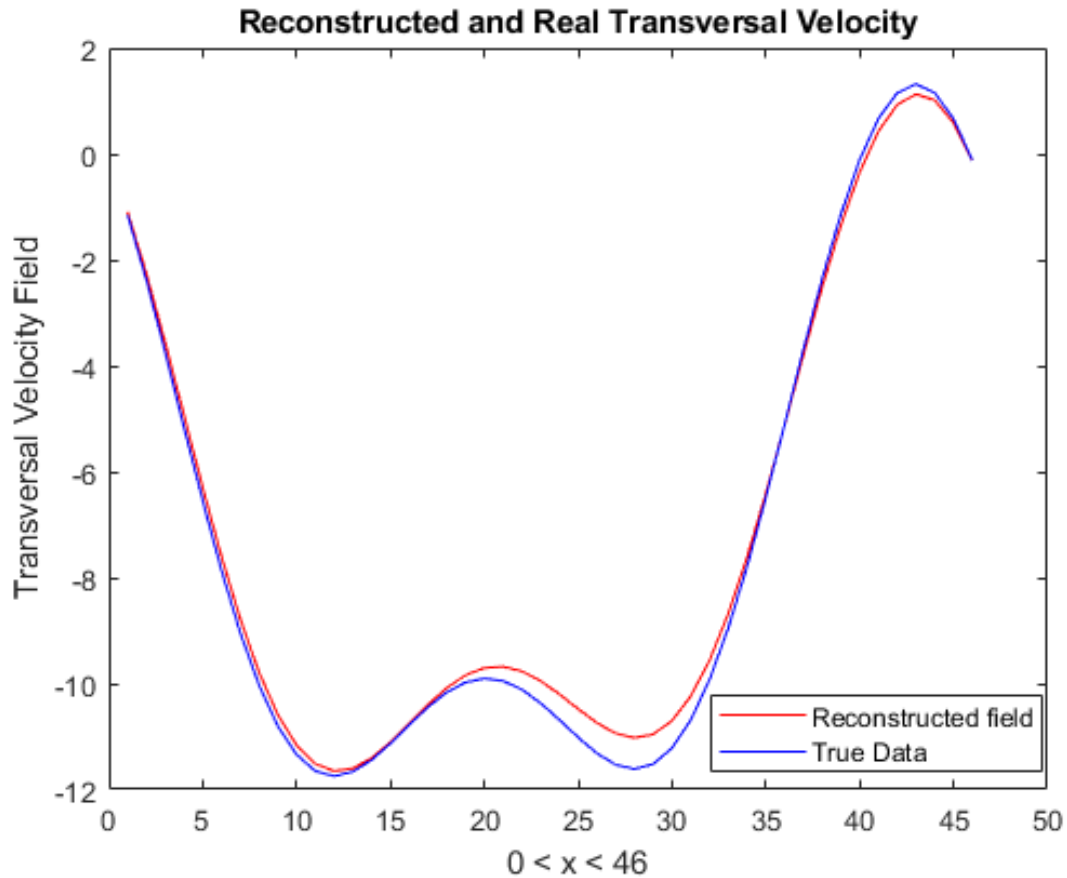
Figure 5.40: 1D Plot of the Reconstructed and Original Transversal Velocity Field Using BOP-DMD.

5.5.   Vorticity Reconstruction

In addition to the previously discussed results involving the application of BOP-DMD as a successful field reconstruction tool, an opportunity presented itself for a deeper analysis of the flow field understudy. As an interesting application to the reconstruction of data fields using BOP-DMD, this study included the reconstruction of the vorticity field from the axial and transversal velocity fields. The importance of such an application lies in the crucial insights into the dynamics of flow fields provided by field vorticity. Such an interesting finding opens the door to a better understanding of flow field behavior. Using BOp-DMD as a DDM technique, one can now obtain an accurate future prediction of complex flow dynamics using basic field parameters like velocity fields that are rather simpler to be measured.

The vorticity reconstruction process involved using the fabricated axial and transversal velocity fields obtained from the BOP-DMD reconstruction algorithm. Following equation 5.1 the vorticity field Ω is given by the curl of the velocity field U.

$$\Omega = \nabla \times U \tag{5.1}$$

The reconstructed vorticity was compared to the original vorticity field obtained from direct measurement both after denoising and are shown in Figure 5.41. A general agreement in the trend of the original field and the reconstructed one is observed, however, the noticeable variation in the magnitudes of both fields is due to the limitations imposed on the denoising process, in the sense that further denoising could lead to a highly distorted signal.
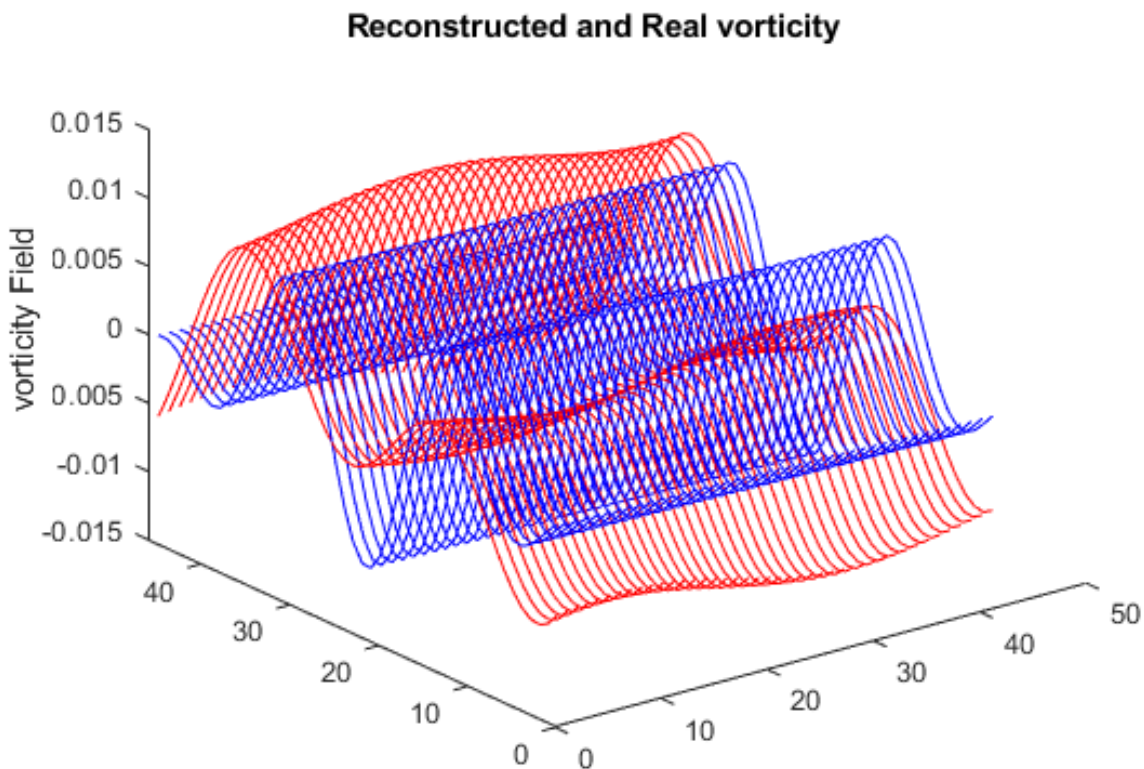
Figure 5.41: : Reconstructed and Original Vorticity Field Using BOP-DMD.

The promising reconstruction of the vorticity field can be highlighted in Figure 5.42.

The figure shows the 1D plot taken at Y=20 and T= 100, minor variations between the reconstructed vorticity field and the original one are present in some regions, however, those variations are almost as low as 2.5%. This is considered a revolutionary finding in both fields of fluid dynamics and data-driven modeling.
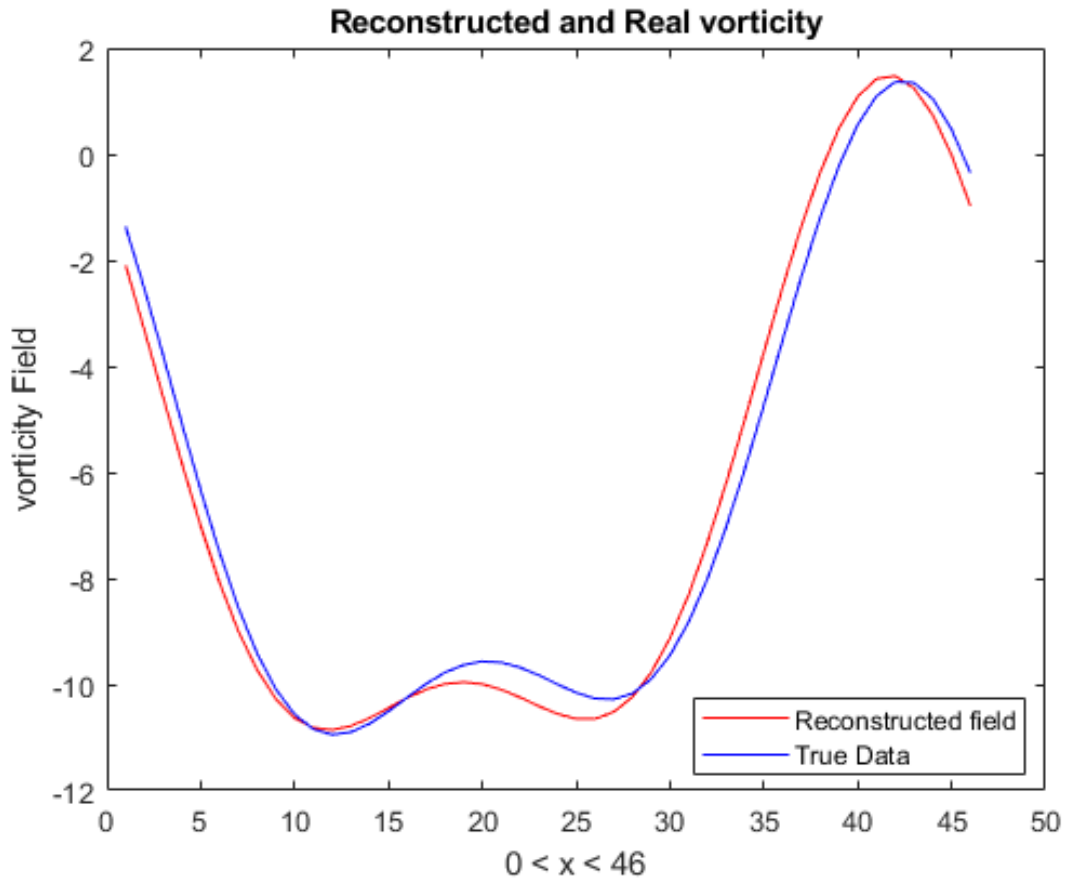
Figure 5.42: 1D Plot of the Reconstructed and Original Vorticity Field Using BOP-DMD.

5.6.   Conclusion

The BOP-DMD method when used for data reconstruction of high-dimensional fields shows a high level of accuracy. In this study, the method was tested on high-dimensional and highly noised fields and has proven its superiority over the exact DMD method. Also, the method is relevant for any high-dimensional field and does not require tedious hyperparameter tuning, it can be used for future data prediction and can highly reduce the computational cost when treating high-dimensional complex fields. The use of a noise filtering technique on the reconstructed fields (FFT or wavelets analysis) can highly enhance reconstruction accuracy, especially when dealing with systematic noise.

6 | Conclusion

In this thesis work, the main goal was to apply a data-driven modeling approach for the study of the flow field of a Pressurized Water Reactor (PWR) under seismic conditions. Field measurements were obtained from an experiment performed at the ICARE facility through which particle image velocimetry (PIV) was applied to measure essential flow parameters. The study adopted bagging-optimized dynamic mode decomposition (BOP-DMD) as the data-driven modeling technique which is applied to the flow fields in hand to gain important insights into the complex fluid dynamics. Applying BOP-DMD, an important coherent spatiotemporal flow structure was extracted from the original flow field, which paves the way for field forecasting. Such technique was carefully chosen over its precedent (*exact DMD*) due to its insensitivity to arbitrary noise that characterized the fluid fields understudy, and due to its enhanced capabilities of providing stable forecasts of complex fluid fields. The primary research objectives were successfully achieved by our study. We were able to accurately analyze and anticipate the flow behavior between two PWR surrogate bundles under seismic conditions by using the BOP-DMD approach. The detected modes gave useful insights into flow mechanics and enabled a thorough knowledge of the system's dynamics. The conclusions of this thesis have profound implications for nuclear engineering and reactor safety. The adopted data-driven modeling methodology, which employs BOP-DMD, provides an innovative and efficient method for analyzing and forecasting flow behavior in complex systems. This methodology has the potential to improve the safety and performance evaluation of nuclear reactor systems, particularly in seismic situations.

6.1. Summary of Findings

The BOP-DMD method was thoroughly used in high-dimensional and very complicated fields such as axial velocity, transversal velocity, vorticity, and turbulent kinetic energy in this thorough study. Because of the presence of noise components caused by experimental restrictions and system complexities, these fields exhibited complex and dynamic behavior. The major goal was to use the BOP-DMD algorithm to break down the examined

fields into their underlying dynamical components, then reconstruct the fields from these components. The fabricated fields were then compared to the original fields to assess the BOP-DMD method's accuracy and fidelity. Results obtained from the reconstruction process were outstanding, reconstructed and original fields were, to a great extent, identical. Variations between both fields were as low as 1% for some fields of minimum noise components like axial velocity, while it was no more than 3% for more complex fields like vorticity.

The study also included the reconstruction of the vorticity field from the fabricated axial and transversal velocity components. Although the reconstruction process followed simple mathematics, such an interesting finding opens the door to a better understanding of flow field behavior. Using BOp-DMD as a DDM technique, one can now obtain an accurate future prediction of complex flow dynamics carried by the vorticity field, using only forecasted basic fields like velocity fields that are rather simpler to be measured.

Furthermore, the findings of the BOP-DMD approach were compared to those of the standard DMD method. The comparison revealed the tremendous breakthroughs and improvements that the BOP-DMD strategy provided over its predecessor. In regards to accuracy, noise tolerance, and its capacity to capture hidden dynamics within the examined fields, the BOP-DMD approach exceeded the exact DMD method. In general, the results of this study highlight the BOP-DMD method's usefulness and potential as a robust data-driven modeling methodology for complicated fields. The capacity of BOP-DMD to properly reconstruct fields, minimize the effects of noise, and overcome the limits of existing approaches makes it a powerful tool in a variety of scientific and engineering applications.

6.2.   Future Perspectives

To my knowledge, the results obtained in this study from the application of the BOP-DMD to complex flow fields are the first of their kind. This study provides important findings for many fields of science and engineering, specifically in the fields of fluid dynamics and reactor safety.

In this work, noise presented in the analyzed data fields was eliminated through the use of noise filtering techniques. This was done to enhance the robustness of BOP-DMD when applied to fields drawn from experimental measurements where noise components are of great significance. Another approach that presents an opportunity for future research is to integrate BOP-DMD with control theory. The topic *DMD with control* was first introduced by Proctor, Brunton, and Kutz [20] and it introduces control theory to the

DMD framework which could be applied to control unwanted signal components like noise. This concept, if integrated with the BOP-DMD approach adopted in the current study, could potentially provide valuable insights into the world of complex field modeling.

Another approach to studying complex flow fields around PWR surrogate bundles under seismic conditions is to make use of the capability of the BOP-DMD as a model reduction data-driven modeling technique with the deterministic computationally expensive CFD analysis techniques. Such a combination of two powerful techniques could result in a highly accurate and significantly enhanced study of the nature of complex flow fields around PWR surrogate bundles under seismic conditions.

Bibliography

[1] *Nuclear Power Reactors in the World.* Number 2 in Reference Data Series. INTERNATIONAL ATOMIC ENERGY AGENCY, Vienna, 2022. ISBN 978-92-0-125122-0. URL `https://www.iaea.org/publications/15211/nuclear-power-reactors-in-the-world`.

[2] R. J. Adrian and J. Westerweel. *Particle image velocimetry.* Number 30. Cambridge university press, 2011.

[3] T. Askham and J. N. Kutz. Variable projection methods for an optimized dynamic mode decomposition. *SIAM Journal on Applied Dynamical Systems*, 17(1):380–416, 2018.

[4] P. Bühlmann. *Bagging, boosting and ensemble methods.* Springer, 2012.

[5] R. Capanna, L. Longo, F. Bazin, G. Ricciardi, and P. M. Bardet. Deployment of time-resolved particle image velocimetry between two pwr surrogate bundles. *Nuclear Engineering and Design*, 382:111375, 2021.

[6] L. A. C. De Filippis, L. M. Serio, F. Facchini, and G. Mummolo. Ann modelling to optimize manufacturing process. *Advanced applications for artificial neural networks*, pages 201–226, 2018.

[7] A. Di Ronco, C. Introini, E. Cervi, S. Lorenzi, Y. S. Jeong, S. B. Seo, I. C. Bang, F. Giacobbo, and A. Cammi. Dynamic mode decomposition for the stability analysis of the molten salt fast reactor core. *Nuclear Engineering and Design*, 362:110529, 2020.

[8] D. D'Agostino, M. Andre, P. Bardet, A. Serani, M. Felli, and M. Diez. Observing piv measurements through the lens of data clustering. In *Proceedings of the 33rd Symposium on Naval Hydrodynamics, Osaka, Japan*, pages 18–23, 2020.

[9] N. B. Erichson, L. Mathelin, J. N. Kutz, and S. L. Brunton. Randomized dynamic mode decomposition. *SIAM Journal on Applied Dynamical Systems*, 18(4):1867–1891, 2019.

[10] A. Fischer. Imaging flow velocimetry with laser mie scattering. *Applied Sciences*, 7 (12):1298, 2017.

[11] Y. He, X. Ye, J. Z. Huang, and P. Fournier-Viger. Bayesian attribute bagging-based extreme learning machine for high-dimensional classification and regression. *ACM Transactions on Intelligent Systems and Technology (TIST)*, 13(2):1–26, 2022.

[12] J. Heiland, P. Benner, and R. Bahmani. Convolutional neural networks for very low-dimensional lpv approximations of incompressible navier-stokes equations. *Frontiers in Applied Mathematics and Statistics*, 8:35, 2022.

[13] K.-l. Hsu, H. V. Gupta, and S. Sorooshian. Artificial neural network modeling of the rainfall-runoff process. *Water resources research*, 31(10):2517–2530, 1995.

[14] H. Ibrahim, C. Intorini, R. Capanna, A. Cammi, P. Bardet, and G. Ricciardi. Data-driven modeling of the flow field between two pwr surrogate bundles under seismic conditions using bagging-optimized dynamic mode decomposition (bop-dmd). In *Proceedings of the 20th International Topical Meeting on Nuclear Reactor Thermal Hydraulics (NURETH-20), Washington, D.C., USA*, 2023.

[15] K. Ikeda and M. Hoshi. Development of rod-embedded fiber ldv to measure velocity in fuel rod bundles. *Journal of nuclear science and technology*, 43(2):150–158, 2006.

[16] M. Jehanzaib, M. Bilal Idrees, D. Kim, and T.-W. Kim. Comprehensive evaluation of machine learning techniques for hydrological drought forecasting. *Journal of Irrigation and Drainage Engineering*, 147(7):04021022, 2021.

[17] J. H. Jeong and B.-S. Han. Coolant flow field in a real geometry of pwr downcomer and lower plenum. *Annals of Nuclear Energy*, 35(4):610–619, 2008.

[18] J. N. Kutz. *Data-driven modeling & scientific computation: methods for complex systems & big data*. Oxford University Press, 2013.

[19] J. N. Kutz, S. L. Brunton, B. W. Brunton, and J. L. Proctor. *Dynamic mode decomposition: data-driven modeling of complex systems*. SIAM, 2016.

[20] J. N. Kutz, S. L. Brunton, B. W. Brunton, and J. L. Proctor. *Dynamic mode decomposition: data-driven modeling of complex systems*. SIAM, 2016.

[21] J. N. Kutz, A. Nachbin, P. J. Baddoo, and J. W. Bush. Pilot-wave dynamics: Using dynamic mode decomposition to characterize bifurcations, routes to chaos and emergent statistics. *arXiv preprint arXiv:2210.07097*, 2022.

[22] S. Le Clainche and J. M. Vega. Higher order dynamic mode decomposition. *SIAM Journal on Applied Dynamical Systems*, 16(2):882–925, 2017.

[23] A. Lobbrecht and D. Solomatine. Control of water levels in polder areas using neural networks and fuzzy adaptive systems. *Water industry systems: modelling and optimization applications. Research Studies Press Ltd., Baldock*, pages 509–518, 1999.

[24] H. T. Luong, Y. Wang, H.-G. Sung, and C. H. Sohn. A comparative study of dynamic mode decomposition methods for mode identification in a cryogenic swirl injector. *Journal of Sound and Vibration*, 503:116108, 2021. ISSN 0022-460X. doi: https://doi.org/10.1016/j.jsv.2021.116108. URL `https://www.sciencedirect.com/science/article/pii/S0022460X21001802`.

[25] Z. Ma, J. Yu, and R. Xiao. Data-driven reduced order modeling for parametrized time-dependent flow problems. *Physics of Fluids*, 34(7):075109, 2022.

[26] A. Miller, B. Blott, and T. Hames. Review of neural network applications in medical imaging and signal processing. *Medical and Biological Engineering and Computing*, 30:449–464, 1992.

[27] F. J. Montáns, F. Chinesta, R. Gómez-Bombarelli, and J. N. Kutz. Data-driven modeling and learning in science and engineering. *Comptes Rendus Mécanique*, 347 (11):845–855, 2019.

[28] P. Nakamoto. *Neural Networks & Deep Learning*. Machine Learning Series. Createspace Independent Publishing, 2017. ISBN 9781981614066. URL `https://books.google.it/books?id=PYcLtAEACAAJ`.

[29] H. M. Nazir, I. Hussain, M. Faisal, E. E. Elashkar, and A. M. Shoukry. Improving the prediction accuracy of river inflow using two data pre-processing techniques coupled with data-driven model. *PeerJ*, 7:e8043, 2019.

[30] NRC. Typical pressurized-water reactor, 2023. URL `https://www.nrc.gov/reactors/power/pwrs.html`.

[31] K. Okamoto, S. Nishio, T. Saga, and T. Kobayashi. Standard images for particle-image velocimetry. *Measurement Science and Technology*, 11(6):685, 2000.

[32] T. Persoons. Chapter two - measuring flow velocity and turbulence fields in thermal sciences using particle image velocimetry: A best practice guide. volume 54 of *Advances in Heat Transfer*, pages 37–87. Elsevier, 2022. doi: https://doi.org/10.1016/bs.aiht.2022.07.001. URL `https://www.sciencedirect.com/science/article/pii/S0065271722000016`.

[33] J. L. Proctor, S. L. Brunton, and J. N. Kutz. Dynamic mode decomposition with control. *SIAM Journal on Applied Dynamical Systems*, 15(1):142–161, 2016.

[34] K. Qaderi, V. Jalali, S. Etminan, M. Masoumi Shahr-babak, and M. Homaee. Estimating soil hydraulic conductivity using different data-driven models of ann, gmdh and gmdh-hs. *Paddy and Water Environment*, 16(4):823–833, 2018.

[35] M. Raffel, C. E. Willert, J. Kompenhans, et al. *Particle image velocimetry: a practical guide*, volume 2. Springer, 1998.

[36] M. Raffel, C. E. Willert, F. Scarano, C. J. Kähler, S. T. Wereley, J. Kompenhans, M. Raffel, C. E. Willert, F. Scarano, C. J. Kähler, et al. Image evaluation methods for piv. *Particle image velocimetry: a practical guide*, pages 145–202, 2018.

[37] L. S. Riza et al. Data science and big data processing in r: Representations and software. 2016.

[38] D. Sashidhar and J. N. Kutz. Bagging, optimized dynamic mode decomposition for robust, stable forecasting with spatial and temporal uncertainty quantification. *Philosophical Transactions of the Royal Society A*, 380(2229):20210199, 2022.

[39] P. J. Schmid. Dynamic mode decomposition and its variants. *Annual Review of Fluid Mechanics*, 54:225–254, 2022.

[40] D. Solomatine, C. Rojas, S. Velickov, and H. Wust. Chaos theory in predicting surge water levels in the north sea. In *Proc. 4th Int. Conference on Hydroinformatics, Cedar-Rapids*, 2000.

[41] D. Solomatine, L. See, and R. Abrahart. *Data-Driven Modelling: Concepts, Approaches and Experiences*, pages 17–30. Springer Berlin Heidelberg, Berlin, Heidelberg, 2008. ISBN 978-3-540-79881-1. doi: 10.1007/978-3-540-79881-1_2. URL https://doi.org/10.1007/978-3-540-79881-1_2.

[42] D. Solomatine, L. M. See, and R. Abrahart. Data-driven modelling: concepts, approaches and experiences. *Practical hydroinformatics: Computational intelligence and technological developments in water applications*, pages 17–30, 2008.

[43] K. Stergiou and T. E. Karakasidis. Application of deep learning and chaos theory for load forecasting in greece. *Neural Computing and Applications*, 33:16713–16731, 2021.

[44] W. Sun. Sports performance prediction based on chaos theory and machine learning. *Wireless Communications and Mobile Computing*, 2022, 2022.

[45] C. D. Sutton. Classification and regression trees, bagging, and boosting. *Handbook of statistics*, 24:303–329, 2005.

[46] Z. Tian, L. Yang, S. Han, X. Yuan, H. Lu, S. Li, and L. Liu. Numerical investigation on the flow characteristics in a 17× 17 full-scale fuel assembly. *Energies*, 13(2):397, 2020.

[47] G. Tissot, L. Cordier, N. Benard, and B. R. Noack. Model reduction using dynamic mode decomposition. *Comptes Rendus Mécanique*, 342(6-7):410–416, 2014.

[48] O. Tornblom. Introduction course in particle image velocimetry. *Course Introductory Material: STEM Project, KTH, Department of Mechanics, Stockholm Sweden*, 2004.

[49] J. H. Tu. *Dynamic mode decomposition: Theory and applications*. PhD thesis, Princeton University, 2013.

[50] N. A. Weichselbaum. *Non-intrusive experimental study on nuclear fuel assembly response to seismic loads*. PhD thesis, The George Washington University, 2016.

[51] A. Weiner and R. Semaan. A robust dynamic mode decomposition methodology for an airfoil undergoing transonic shock buffet. *arXiv preprint arXiv:2212.10250*, 2022.

[52] J. Xiong, Y. Yu, N. Yu, X. Fu, H. Wang, X. Cheng, and Y. Yang. Laser doppler measurement and cfd validation in 3× 3 bundle flow. *Nuclear Engineering and Design*, 270:396–403, 2014.

[53] L. Zadeh. Fuzzy sets. *Inform Control*, 8:338–353, 1965.

[54] C. Zhang, H. Ju, D. Zhang, S. Wu, Y. Xu, Y. Wu, S. Qiu, and G. Su. Piv measurement and numerical investigation on flow characteristics of simulated fast reactor fuel subassembly. *Nuclear Engineering and Technology*, 52(5):897–907, 2020.

[55] H. Zhang. *Data-driven modeling for fluid dynamics and control*. PhD thesis, Princeton University, 2020.

A | Appendix: Singular value decomposition (SVD)

In this Appendix, we describe Singular Value Decomposition (SVD), which is a fundamental mathematical technique utilized in a wide range of disciplines such as data analysis, signal processing, and linear algebra. SVD is significant in the context of this thesis work since it provides the mathematical foundation for the used data-driven methodology. Briefly speaking, the SVD technique decomposes any matrix into some fundamental components known as singular values and vectors. Given the m-by-n data matrix A, its SVD is as follows:

$$A = U\Sigma V^*$$

where U is an m-by-m orthogonal matrix, Σ is an m-by-n diagonal matrix containing non-negative values known as singular values and V^* denotes the conjugate transpose of the n-by-n orthogonal matrix V.

The singular values in Σ are in decreasing order, which means that the first diagonal element corresponds to the largest single value, the second diagonal element corresponds to the second largest singular value, and so on. The singular values reveal important information about the importance of each mode or component in the decomposition collected in the matrices U and V^*, which contain the left and right singular vectors, respectively. These vectors define the original data space directions or axis along which matrix A exhibits the greatest notable variability or structure.

SVD has many applications; in this study, the method is used as the basis of both exact and BOP-DMD. SVD is applied to the data matrices under analysis to achieve low dimensionality reduction of the high dimensional space.

List of Figures

List of Tables

List of Symbols

Variable	Description
t_k	K^{t^h} point of time
Δt	Time spacing between two snapshot
$\hat{X}$	Data matrix
ϕ_k	Eigenvectors of the matrix A
ω_k	Eigenvalues of the matrix A
b_k	Loading of the initial data matrix X_0
$\mathcal{A}$	DMD mapping matrix
U	m by m orthogonal singular vectors matrix
Σ	m by n diagonal singular values matrix
V	m by m orthogonal right singular values matrix
V^*	Conjugate transpose of V
k	BOP-DMD number of trials
p	BOP-DMD randomly selected indices
λ_{Kopt}	Optimised eigenvalues
$\mathcal{V}$	PIV particle velocity
d	PIV particle displacement
M	PIV image magnification
W_o	Initial beam half waist before the focusing of the lens
f	Lens focal point

Variable	Description
h_{gap}	Gap width
n	Refractive index
Z_R	Raleigh range
W_f	Beam width after the focal point
R_e	Reynold's number
r	Reduced matrix rank
T	Time vector
X	Transversal spatial vector
Y	Axial spatial vector
V_y	Axial velocity
V_x	Transversal velocity
Ω	Vorticity field

Acknowledgements

I am deeply grateful to my advisors, Professor Antonio Cammi and Doctor Carolina Introini, for their unwavering support and guidance throughout my thesis work. Their expertise and patience have been invaluable to me and have played a crucial role in the success of this thesis.

I am also very grateful to Professor Roberto Capanna from George Washington University, who went above and beyond to help me with my work and continuously provided his valuable assistance.

Special thanks to the ICARE experimental facility and Professor Guillaume Ricciardi who provided the experimental data used in this thesis work.

Finally, I am deeply thankful to my friends and family for their love and support during this process. Without their encouragement and motivation, I would not have been able to complete this journey.